Development and Application of Molecular Orbital Theories

Michael Charles Wrinn
Department of Chemistry
McGill University, Montreal
May, 1991

A Thesis submitted to Faculty of Graduate Studies and Research in partial fulfillment of the requirements for the degree of Ph.D.

This thesis has been prepared in the format of published or to be published papers, according to the procedure described in the McGill University Faculty of Graduate Studies and Research *Guidelines Concerning Thesis Preparation*:

The candidate has the option, subject to the approval of the Department, of including as part of the thesis the text, or duplicated published text (see below), of an original paper, or papers. In this case the thesis must still conform to all other requirements explained in Guidelines Concerning Thesis Preparation. Additional material (procedural and design data as well as descriptions of equipment) must be provided in sufficient detail (e.g. in appendices) to allow a clear and precise judgement to be make of the importance and originality of the research reported. The thesis should be more than a mere collection of manuscripts published or to be published. It must include a general abstract, a full introduction and literature review and a final overall conclusion. Connecting texts which provide logical bridges between different manuscripts are usually desirable in the interests of cohesion.

It is acceptable for theses to include as chapters authentic copies of papers already published, provided these are duplicated clearly on regulation thesis stationery and bound as an integral part of the thesis. Photographs or other materials which do not duplicate well must be included in their original form. In such instances, connecting texts are mandatory and supplementary explanatory material is almost always necessary.

The inclusion of manuscripts co-authored by the candidate and others is acceptable but the candidate is required to make an explicit statement on who contributed to such work, and to what extent, and supervisors must attest to the accuracy of the claims, e.g. before the Oral Committee. Since the task of the Examiners is make more difficult in these cases, it is in the candidate's interest to make the responsibilities of authors perfectly clear. Candidates following this option must inform the Department before it submits the thesis for review.

Abstract

Electronic structure calculations were performed with the Multiple-Scattering Local-Density-Approximation (MS-LDA) theory on the heterocycles 2-imidazolidinenone and 2,1,3-benzoxadiazole, and the sulphur and selenium analogues. Correlation effects in these compounds were examined by systematically comparing properties; ionization potentials (IP), nuclear quadrupole resonances, and electron density differences with and without inclusion of the correlation energy functional. The differential relaxation effect within Slater transition–state calculations for IP was more important than generally thought. A MS-LDA calculation was performed on the compound 2,1,3-benzoxadiazole$[Cr(CO)_5]_2$, and the resulting electronic structure compared to that of the free heterocycle; in the ligand, the ring adopted a benzenoid structure.

The Generalized-Exchange Self-Interaction-Corrected (GX-SIC) orbital-density functional was implemented for the first time into a molecular program, the linear combination of Gaussian–type orbital local–density–approximation (LCGTO-LDA) code, and was tested by calculating the equilibrium geometry of water; the GX-SIC results were significantly better than conventional LDA results.

Calculations were made with the Perturbative Configuration Interaction over Localized Orbitals (PCILO) theory to investigate the importance of hybridization of the atomic orbitals. Previously thought unimportant, the choice noticeably changes the predicted equilibrium geometry, through 3rd order in the perturbation series.

Résumé

Les calculs de structure électronique ont été effectués avec la théorie "Multiple-Scattering Local-Density-Approximation (MS–LDA) sur les hétérocycles imidazolidinenone-2 et benzoxadiazole-2,1,3, et sur les analogues du soufre et du silicium. Les effets de corrélation chez ces composés ont été examinés par une comparaison systématique de quelques propriétés; potentiel d'ionisation (PI), résonance nucléaire quadrupolaire, et différence de densité électronique avec et sans inclusion du "correlation energy functional". L'effet de relaxation différentielle à l'intérieur des calculs de transition d'état de Slater pour les potentiels d'ionisation s'est avéré plus important que ce qui est généralement admis. Un calcul MS-LDA a été effectué pour le composé benzoxadiazole-2,1,3 $[Cr(CO)_5]_2$ et la structure électronique résultante a été comparée avec celle de l'hétérocycle libre; en présence du ligand, l'anneau a adopté une structure benzénoïde.

La méthode "Generalized-Exchange Self-Interaction-Corrected (GX-SIC) orbital-density functional" a été inclue pour la première fois dans une programmation moléculaire, soit le code "linear combination of Gaussian-type orbital local-density-approximation (LCGTO-LDA)", et fut mise à l'épreuve dans les calculs d'équilibre géométrique de l'eau. Les résultats du GX-SIC ont été beaucoup plus précis que les résultats traditionnels du LDA.

Des calculs utilisant la méthode PCILO (Perturbative Configuration Interaction over Localized Orbitals) ont été effectués afin d'examiner l'importance du choix des orbitales atomiques hybrides; contrairement à ce que l'on admettait jusqu'ici, ce choix modifie sensiblement la géométrie d'équilibre prévue, et ce, jusqu'au troisième ordre de perturbation.

Acknowledgements

I extend sincere thanks to my thesis supervisor, Professor M. A. Whitehead, for his help, badgering and encouragement through the years.

Thanks are extended also to my colleagues in Professor Whitehead's research group: Drs. Soheil Manoli, Mualla Berksoy-Boluk, Yufei Guo, Roland Treppanier, and Alex Koukoulas, Mr. Fortunato Villamagna, Mr. Slaven Suba, and Ms. Nuria Gallego, for many challenging conversations and group meetings.

Contents

I. *Density Functional Theory*

I.1 Introduction and Background

Density Functional Theory states that the ground state energy for N electrons in an external potential is uniquely determined by the electron density:

$$E = E[\rho(\mathbf{r})] \tag{1}$$

This result was intuitively derived by Thomas (1926) and Fermi(1928); the resulting Thomas-Fermi theory approximated the ground state density by that of a homogeneous electron gas. This semiclassical theory was hampered by a crude approximation to the kinetic energy term T:

$$T = C_k \int [\rho(\mathbf{r})]^{5/3}\, d\mathbf{r}, \tag{2}$$

derived from the kinetic energy density of a uniform electron gas (March, 1981); also, exchange was not considered.

Dirac (1930), also assuming a uniform electron gas, introduced an exchange term to Thomas-Fermi theory derived from a uniform electron gas, which gave an exchange potential proportional to the cube root of the electron density:

$$v_{TFD} = -(\frac{3}{\pi})^{1/3}[\rho(\mathbf{r})]^{1/3} \tag{3}$$

in atomic units. This theory is called the Thomas-Fermi-Dirac (TFD) theory. It does not correctly predict outer-valence electron properties, such as ionization potentials (Bethe and Jackiw, 1968); the major weakness is the statistical treatment of the kinetic energy term in eq.(2) (Teller, 1962).

Slater (1951) using statistical arguments, replaced the nonlocal exchange term v_{ex} in the Hartree-Fock one-electron equations

$$\left\{ h(\mathbf{r}) + v_{Coulomb}(\mathbf{r}) + v_{ex}(\mathbf{r}) \right\} \phi_i(\mathbf{r}) = \epsilon_i\, \phi_i(\mathbf{r}) \tag{4}$$

where

$$v_{ex}(\mathbf{r})\,\phi_i(\mathbf{r}) = \left\{ \int \frac{\phi^*(\mathbf{r}')\phi_i(\mathbf{r}')}{|\mathbf{r}-\mathbf{r}'|}\, d(\mathbf{r}') \right\} \phi_i(\mathbf{r}) \tag{5}$$

with a uniform-gas exchange potential v_{HFS}:

$$v_{HFS} = -\frac{3}{2}\left(\frac{3}{\pi}\right)^{1/3} [\rho(\mathbf{r})]^{1/3} \tag{6}$$

where HFS stands for Hartree-Fock-Slater, as this theory is called; it closely resembles modern density functional theories which make use of a local (electron gas derived) exchange potential.

A proof of eq.(1) did not appear until Hohenberg and Kohn (1964) showed that for a given external potential v (for the case of atoms and molecules, v is the potential generated by the nuclei), there can be only one charge density. They showed further that the total energy E could be partitioned among expectation values of the kinetic, nuclear-nuclear, Coulomb, and an (unspecified) exchange-correlation energy:

$$E[\rho(\mathbf{r})] = \Big\langle kinetic + nuclear + Coulomb \Big\rangle + E_{xc} \tag{7}$$

This result was used in a variational treatment by Kohn and Sham (1965), to derive the one-electron equations

$$\left\{ kinetic + nuclear + Coulomb + \frac{\delta}{\delta\rho} E_{xc} \right\} \psi_i = \epsilon_i \psi_i \tag{8}$$

What is remarkable about equations (7) and (8) is that the kinetic energy operator can be rigorously assigned a single-particle form; the problem of finding the kinetic energy of correlated electrons is shifted to the E_{xc} term, obviating that particular weakness of TFD theory. Eq.(7) is not limited to exchange-only formulations as is the Hartree-Fock theory; correlation effects can be accounted for by E_{xc}.

Hohenberg-Kohn-Sham density functional theory assumed that the density *can* be produced from, or represented by, a ground state antisymmetric wavefunction and

an external potential v. Counter examples have been found (Levy, 1982) which show that not every density is "v-representable". It has been shown (Parr,1989, and references therein), however, that the v-representable condition is more stringent than necessary. A weaker, N-representable condition is sufficient: the density $\rho(\mathbf{r})$ must be obtainable from an antisymmetric wavefunction. This removes the condition on the external potential v; the N-representable conditions, i.e. the density is non-negative, continuous, and

$$\int \rho(\mathbf{r})\, d\mathbf{r} = N \tag{9}$$

is met by any reasonable physical density.

In practice, the exchange energy from the uniform electron gas is used in equation (8), which yields an exchange energy equal to that in equation (3). To reconcile the difference between forms (3) and (6) (v_{TFD} and v_{HFS}), Slater(1972) proposed an adjustable parameter α:

$$v_x = -\frac{3}{2}\,\alpha\,(\frac{3}{\pi})^{1/3}[\rho(\mathbf{r})]^{1/3} \tag{10}$$

where α takes values between $\frac{2}{3}$ and 1, respectively, for the TFD and HFS forms of the exchange potential; this is the $X\alpha$ form of density functional theory. The most commonly used α values were determined by Schwartz (1972), who found the value for each element which equalized the total energies of atomic $X\alpha$ and Hartree-Fock calculations.

The electron gas correlation energy was obtained from Monte Carlo calculations by Ceperley and Alder (1980); Vosko, Wilk and Nusair (1980) fitted the Monte Carlo data to the functional form

$$v_c(r_s) = A\Bigg\{ ln\frac{r_s}{r_s + b\sqrt{r_s} + c}$$

$$+ \frac{2b}{\sqrt{(4c - b^2)}} tan^{-1}\frac{\sqrt{(4c - b^2)}}{2\sqrt{r_s} + b}$$

$$- \frac{bx_0}{x_0^2 + bx_0 + c}\left[ln\frac{(\sqrt{r_s} - x_0)^2}{r_s + b\sqrt{r_s} + c}\right.$$

$$\left. + \frac{2(b + 2x_0)}{\sqrt{(4c - b^2)}} tan^{-1}\frac{\sqrt{(4c - b^2)}}{2\sqrt{r_s} + b}\right]\Bigg\} \qquad (11)$$

where

$$r_s = \rho^{-\frac{1}{3}}(\mathbf{r}) \qquad (12)$$

and the remaining constants are used for fitting.

Expression (10) correctly reproduces the high ($r_s << 1$) and low density limits for the electron gas correlation; it is referred to as the VWN correlation functional, and is the most commonly used form.

The exchange and correlation functionals derived from the electron gas assume that over a small, local volume of space, the density $\rho(\mathbf{r})$ is homogeneous; such functional forms are called Local Density Functionals (LDF). There is no known rigorous, systematic way to improve the LDF approximation; nevertheless, research on "nonlocal" functionals has proceeded in two distinct directions. One investigates functionals of the gradient of the density, $F[\nabla\rho]$; the other uses orbital-dependent functionals, $F[\rho_i]$. Gradient methods will not be addressed in this thesis.

Orbital-dependent methods: The Self-interaction Correction

The LDF approximation contains self-interaction energy which is not cancelled exactly (in contrast to Hartree-Fock methods) by the Coulomb self-interaction term. A practice introduced by Slater (1974), of removing half an electron from an orbital, then identifying that orbital energy with the (Koopman's theorem) ionization energy, was shown by Gopinathan (1979) to be a partial removal of the spurious self-interaction energy,

Perdew and Zunger (1981) formally derived the one-electron equations which include a self-interaction correction term. The derivation proceeded from the fact that the total electron self-interaction energy must be zero,

$$J[\rho_i] + E_x[\rho_i, 0] = 0 \tag{13}$$

where J and E_x are the Coulomb and exchange energies, respectively, and ρ_i is the density of the ith particle. The sum of equation (13) over all i particles was the correction to the total energy; when the variational method was applied, this led to an orbital-dependent exchange functional v_x^i.

Because there is a different v_x^i potential for each one-electron wavefunction, the resulting wavefunctions are not orthogonal to one another. Further, since the orbital density ρ_i is not invariant to a unitary transform, then neither is the total energy; a localization transform, for example, will maximize the single particle self-interaction energy. Heaton (1982) and Pederson *et al.* (1983, 1984) proposed to make a virtue out of this feature by choosing the basis which produces the lowest total energy, but their approach has not been widely used or tested.

Orbital-dependent methods: The Generalized Exchange

Manoli and Whitehead (1988a, 1988b) derived an orbital-dependent exchange functional, including a self-interaction correction, from density-matrix formalism; it was called the "Generalized Exchange" (GX) because standard LDF forms could be derived as a limiting cases of the GX. The method was tested, for a variety of Fermi hole models, on calculations of atoms.

The electron-electron interaction may be expressed in terms of one- and two-particle density matrices. The single-particle density matrix $\rho(\mathbf{r})$ is defined as

$$\rho(\mathbf{r}) = N \int |\Psi(\mathbf{r_1}, \mathbf{r_2}, ..., \mathbf{r_N})|^2 \, d\mathbf{r_2} ... \, d\mathbf{r_N} \tag{14}$$

and the two-particle density matrix as

$$\rho(\mathbf{r}, \mathbf{r}') = N(N-1) \int |\Psi(\mathbf{r_1}, \mathbf{r_2}, ..., \mathbf{r_N})|^2 \, d\mathbf{r_3} ... \, d\mathbf{r_N}, \tag{15}$$

where Ψ is the total wavefunction for N electrons. The normalization conditions are

$$\int \rho(\mathbf{r}) \, d\mathbf{r} = N \tag{16}$$

and

$$\int \rho(\mathbf{r}, \mathbf{r}') \, d\mathbf{r} \, d\mathbf{r}' = N(N-1) \tag{17}$$

while

$$\int \rho(\mathbf{r}, \mathbf{r}') \, d\mathbf{r}' = (N-1) \, \rho(\mathbf{r}) \tag{18}$$

The quantity $\rho(\mathbf{r}, \mathbf{r}')$ is the probability of finding a particle at $\mathbf{r}'$ when another is at $\mathbf{r}$; when integrated, it gives the number of two-particle interactions. Equation (18) is the interaction between the electron density at $\mathbf{r}, \rho(\mathbf{r})$, and the other $(N-1)$ electrons.

The two-particle density matrix, allowing explicitly for spin, is

$$\rho_{ss}(\mathbf{r},\mathbf{r}') = \rho_s(\mathbf{r})\rho_s(\mathbf{r}') + \rho_s(\mathbf{r})\rho_s(\mathbf{r}')f_{ss}(\mathbf{r},\mathbf{r}') \tag{19}$$

for two electons of like spin s. The first term on the right-hand side is the Coulomb interaction between the densities at $\mathbf{r}$ and $\mathbf{r}'$; the second term is the exchange-correlation function $f_{ss}(\mathbf{r},\mathbf{r}')$, as yet unspecified.

Manoli postulated an orbital dependent exchange-correlation function, $f^i_{ss}(\mathbf{r},\mathbf{r}')$, which was related to the total exchange-correlation by

$$\sum_i f^i_{ss}(\mathbf{r},\mathbf{r}') = f_{ss}(\mathbf{r},\mathbf{r}') \tag{20}$$

Integrating the right-hand side of eq.(19), and substituting eq.(18), and f^i_{ss} from eq.(20) gives,

$$\int \rho_s(\mathbf{r}')\,d\mathbf{r}' + \int \rho_s(\mathbf{r}')\sum_i f^i_{ss}(\mathbf{r},\mathbf{r}')\,d\mathbf{r}' = N_s - 1. \tag{21}$$

The one-electron density sum rule is

$$\int \rho_i(\mathbf{r}')\,d\mathbf{r}' = 1. \tag{22}$$

Substituting this value for 1 on the right-hand side of eq.(21), substituting from eq.(16) the value for N, and rearranging, gives

$$\int \rho_s(\mathbf{r}')\sum_i f^i_{ss}(\mathbf{r},\mathbf{r}')\,d\mathbf{r}' + \int \rho_i(\mathbf{r}')\,d\mathbf{r}' = 0. \tag{23}$$

Multiplying and dividing the second term in eq.(23) by

$$\rho_s(\mathbf{r}) = \sum_i \rho_i(\mathbf{r}) \tag{24}$$

gives

$$\int \sum_i \left\{ \rho_s(\mathbf{r}')f^i_{ss}(\mathbf{r},\mathbf{r}') + \frac{\rho_i(\mathbf{r})\rho_i(\mathbf{r}')}{\rho_s(\mathbf{r}')} \right\} d\mathbf{r}' = 0. \tag{25}$$

A single-particle sum rule may be deduced immediately by rearranging of eq.(25):

$$\int \rho_s(\mathbf{r}')f^i_{ss}(\mathbf{r},\mathbf{r}')\,d\mathbf{r}' = \frac{\rho_i(\mathbf{r})}{\rho_s(\mathbf{r})} \tag{26}$$

Although f_{ss} and f^i_{ss} have not been given explicit forms, certain limits impose constraints on these functions limiting behaviour.

In the limit when $|\mathbf{r}-\mathbf{r}'| \to 0$,

$$\begin{aligned}\rho_{ss}(\mathbf{r},\mathbf{r}') &= \rho_s(\mathbf{r})\rho_s(\mathbf{r}') + \rho_s(\mathbf{r})\rho_s(\mathbf{r}')\sum_i f^i_{ss}(\mathbf{r},\mathbf{r}') \\ &= 0\end{aligned} \tag{27}$$

which implies

$$\begin{aligned}\sum_i f^i_{ss}(\mathbf{r},\mathbf{r}') &= -1 \\ &= -\frac{\sum_i \rho_i(\mathbf{r})}{\rho_s(\mathbf{r})}\end{aligned} \tag{28}$$

that is

$$f^i_{ss}(\mathbf{r},\mathbf{r}') = -\frac{\rho_i(\mathbf{r})}{\rho_s(\mathbf{r})} \tag{29}$$

Eq.(27) also implies that

$$f^{ss}(\mathbf{r},\mathbf{r}') \to -1 \tag{30}$$

in the limit as the electrons coalesce.

At the large separation limit, as $|\mathbf{r}-\mathbf{r}'| \to \infty$, the electron interaction does not change, and the exchange-correlation function f^{ss} goes to a constant value. While it is intuitively evident that the large-separation limit of the two particle density matrix is

$$\rho(\mathbf{r},\mathbf{r}') \to \rho_s(\mathbf{r})\rho_s(\mathbf{r}') \tag{31}$$

so that only the Coulomb interaction remains, Kutzelnigg *et al.* (1968) have shown that the proper limit is

$$\rho(\mathbf{r},\mathbf{r}') \rightarrow \rho_s(\mathbf{r})\rho_s(\mathbf{r}') - \frac{1}{N_s}\rho_s(\mathbf{r})\rho_s(\mathbf{r}') \tag{32}$$

i.e.

$$f^{ss}(\mathbf{r},\mathbf{r}') \rightarrow -\frac{1}{N_s} \tag{33}$$

rather than 0.

This same large-separation limit applies to f_i^{ss}, because the sum over all i must satisfy eq.(33). However, a crucial step in the derivation of the GX theory was setting each of the integrands of eq.(25), individually, to 0, which led to

$$f_i^{ss} \rightarrow -\frac{\rho_i(\mathbf{r})\rho_i(\mathbf{r}')}{\rho_s(\mathbf{r})\rho_s(\mathbf{r}')} \tag{34}$$

which is consistent with eq.(33) only when

$$\frac{\rho_i(\mathbf{r}')}{\rho_s(\mathbf{r}')} = \frac{1}{N_s} \tag{35}$$

Eq.(35) is valid for classical point charges only, and represents the primary approximation of the GX theory.

Because there was contention over this point in the original work (Manoli, 1986), it is useful to compare the GX exchange functional with the exact, Hartree-Fock form.

The Generalized Exchange in the Hartree-Fock Limit

The nature of Manoli's orbital-dependent exchange approximation may be illustrated by specifically using the Hartree-Fock exchange energy, for which the result is known. Consequently,

$$E_{ex}^{HF} = -\frac{1}{2}\sum_{i,j} n_i n_j \int \phi_i^*(\mathbf{r})\phi_j^*(\mathbf{r}')g_{\mathbf{r}\mathbf{r}'}\phi_j(\mathbf{r})\phi_i(\mathbf{r}')\,d\mathbf{r}\,d\mathbf{r}' \tag{36}$$

where

$$g_{\mathbf{r}\mathbf{r}'} = \frac{1}{\mathbf{r} - \mathbf{r}'}$$

Equation (36) can be expanded (Slater, 1960), so that an exchange density U_{ex}^{HF} can be explicitly obtained:

$$E_{ex}^{HF} = -\frac{1}{2}\sum_{i,j} n_i n_j \int \frac{\sum_k \phi_k^*(\mathbf{r})\phi_k(\mathbf{r})}{\sum_k \phi_k^*(\mathbf{r})\phi_k(\mathbf{r})} \phi_i^*(\mathbf{r})\phi_j^*(\mathbf{r}')g_{\mathbf{r}\mathbf{r}'}\phi_j(\mathbf{r})\phi_i(\mathbf{r}')\,d\mathbf{r}\,d\mathbf{r}' \quad (37)$$

$$= -\frac{1}{2}\int \rho(\mathbf{r})\left\{\frac{\sum_{i,j} n_i n_j \phi_i^*(\mathbf{r})\phi_j^*(\mathbf{r}')g_{\mathbf{r}\mathbf{r}'}\phi_j(\mathbf{r})\phi_i(\mathbf{r}')}{\sum_k \phi_k^*(\mathbf{r})\phi_k(\mathbf{r})}\,d\mathbf{r}'\right\} d\mathbf{r} \quad (38)$$

$$= -\frac{1}{2}\int \rho(\mathbf{r})\,U_{ex}^{HF}(\mathbf{r})\,d\mathbf{r} \quad (39)$$

where the quantity in braces in eq.(37) is identified with a Hartree-Fock exchange density term U_{ex}^{HF}.

Treating the exchange energy by means of the two-particle density matrix yields:

$$E_{ex} = \frac{1}{2}\int \rho(\mathbf{r})\left\{\int \rho(\mathbf{r}')g_{\mathbf{r}\mathbf{r}'}f_{ss}(\mathbf{r},\mathbf{r}')\,d\mathbf{r}\right\} d\mathbf{r}' \quad (40)$$

from which

$$U_{ex}^{HF}(\mathbf{r}) = \int \rho(\mathbf{r})g_{\mathbf{r}\mathbf{r}'}f_{ss}(\mathbf{r},\mathbf{r}')\,d\mathbf{r} \quad (41)$$

and

$$f_{ss}^{HF}(\mathbf{r},\mathbf{r}') = -\frac{\sum_i n_i\phi_i^*(\mathbf{r})\phi_i(\mathbf{r}')\sum_j n_j\phi_j^*(\mathbf{r}')\phi_j(\mathbf{r})}{\rho(\mathbf{r})\rho(\mathbf{r}')} \quad (42)$$

The limiting cases examined previously must hold for f_{ss}^{HF}. In the limit of small separations, $\mathbf{r} \to \mathbf{r}'$, thus

$$\sum_i \phi_i^*(\mathbf{r})\phi_i(\mathbf{r}') \to \rho(\mathbf{r}) \quad (43)$$

and

$$f_{ss}^{HF}(\mathbf{r},\mathbf{r}') \to -1 \quad (44)$$

which is consistent with eq.(30).

The total pair correlation function $f_{ss}^{HF}(\mathbf{r})$ may be partitioned into orbital-dependent functions

$$f_{ss}^{HF}(\mathbf{r}) = \sum_i f_{ss}^{HF,i}(\mathbf{r}) \tag{45}$$

by making the identification

$$f_{ss}^{HF,i}(\mathbf{r},\mathbf{r}') = -\phi_i^*(\mathbf{r})\phi_i(\mathbf{r}')\frac{\sum_j n_j\phi_j^*(\mathbf{r}')\phi_j(\mathbf{r})}{\rho(\mathbf{r})\rho(\mathbf{r}')} \tag{46}$$

As $\mathbf{r} \rightarrow \mathbf{r}'$,

$$f_{ss}^{HF,i}(\mathbf{r},\mathbf{r}) \rightarrow -\frac{\rho_i(\mathbf{r})}{\rho(\mathbf{r})} \tag{47}$$

as in the GX derivation, eq.(29); summation over i recovers eq.(30) (or equivalently eq.(44)).

The large separation limit postulated by eq.(34) must also hold for $f_{ss}^{HF,i}$:

$$-\phi_i^*(\mathbf{r})\phi_i(\mathbf{r}')\,\frac{\sum_j n_j\phi_j^*(\mathbf{r}')\phi_j(\mathbf{r}')}{\rho(\mathbf{r})\rho(\mathbf{r}')} \;\rightarrow\; -\frac{\rho_i(\mathbf{r})\rho_i(\mathbf{r})}{\rho(\mathbf{r})\rho(\mathbf{r}')} \tag{47}$$

as $|\mathbf{r}-\mathbf{r}'| \rightarrow \infty$.

This implies

$$-\phi_i^*(\mathbf{r})\phi_i(\mathbf{r}')\sum_j n_j\phi_j^*(\mathbf{r}')\phi_j(\mathbf{r}) \rightarrow -\rho_i(\mathbf{r})\rho_i(\mathbf{r}') \tag{48}$$

as $|\mathbf{r}-\mathbf{r}'| \rightarrow \infty$, which is not the case.

The form of $f_{ss}^{HF,i}$ may be manipulated by multiplying the top and bottom of eq.(46) by $\phi_i^*(\mathbf{r})\phi_i(\mathbf{r}')$:

$$f_{ss}^{HF,i}(\mathbf{r},\mathbf{r}') = -\frac{\rho_i(\mathbf{r})\rho_i(\mathbf{r})}{\rho(\mathbf{r})\rho(\mathbf{r}')}\cdot\left\{\frac{\sum_j n_j\phi_j^*(\mathbf{r}')\phi_j(\mathbf{r})}{\phi_i^*(\mathbf{r})\phi_i(\mathbf{r}')}\right\} \tag{49}$$

To achieve the limiting case of eq.(34), the quantity in braces in eq.(49) would have go go to unity as $|\mathbf{r}-\mathbf{r}'| \rightarrow \infty$, which again is not the case.

The GX thus employs a classical approximation to the charge at large distances: eq.(35). Guo and Whitehead (1991) have rederived the GX theory to remove this feature; however, in this work, the GX as derived by Manoli was implemented into molecular calculations.

I.2 References.

Bethe, H. A. and R. Jackiw, 1968, *Intermediate Quantum Mechanics* (Benjamin/Cummings, Reading, Mass.)

Ceperley, D. M. and B. Alder, 1980, Phys. Rev. Lett. **45**, 566

Dirac, P. A. M., 1930, Proc. Camb. Philos. Soc. **26**, 376

Fermi, E., 1928, Z. Physik **48**, 73

Gopinathan, M. S., 1979, J. Phys. B: At. Mol. Phys. **12**, 521

Guo, Y. and M. A. Whitehead, in preparation

Heaton, R. A., J. G. Harrison and C. C. Lin, 1982, Solid State Commun. **41**, 827

Hohenberg, P. and W. Kohn, 1964, Phys. Rev. **136**, B864

Kohn, W. and L. J. Sham, 1965, Phys. Rev. **140**, A1133

Kutzelnigg, W., G. Del Re and G. Berthier, 1968, Phys. Rev. **172**, 49

Levy, M., 1982, Phys. Rev. A **26**, 1200

Manoli, S. D. and M. A. Whitehead, 1988a, Phys. Rev. A **38**, 639

Manoli, S. D. and M. A. Whitehead, 1988b, Phys. Rev. A **38**, 3187

Parr, R. and W. Yang, 1989, *Density-Functional Theory of Atoms and Molecules* (Oxford University Press, Oxford)

Pederson, M. R., R. A. Heaton and C. C. Lin, 1983, J. Chem. Phys. **80**, 1972

Pederson, M. R., R. A. Heaton and C. C. Lin, 1984, J. Chem. Phys. **82**, 2688

Perdew, J. P. and A. Zunger, 1981, Phys. Rev. B **23**, 5048

Schwarz, K., 1972, Chem. Phys. **10**, 345

Slater, J. C., 1951, Phys. Rev. **81**, 385

Slater, J. C., 1960, *Quantum Theory of Atomic Structure, Vol. 1 and 2* (McGraw-Hill, New York)

Slater, J. C., 1972, Adv. Quant. Chem. **6**, 1

Slater, J. C., 1974, *The Self-consistent Field for Molecules and Solids: Quantum Theory of Molecules and Solids, Volume 4* (McGraw-Hill, New York)

Teller, E., 1962, Rev. Mod. Phys. **34**, 627

Thomas, L. H., 1926, Proc. Camb. Philos. Soc. **23**, 542

Vosko, S. H., L. Wilk and M. Nusair, 1980, Can. J. Phys. **58**, 1200

I.3 *Molecular Calculations: The Multiple Scattering Method*

I.3.1 Introduction and Background

Multiple scattering theory includes a family of methods to solve the time-independent Schrödinger equation, originating from the cellular methods of solid state physics (Wigner and Seitz, 1933), where a suitably normalized plane wave of the form

$$|k>= e^{i\mathbf{k}\cdot\mathbf{r}}, \tag{1}$$

is substituted into the Schrödinger equation (Harrison, 1979). Slater (1937) introduced the muffin-tin potential, where the potential in the vicinity of the nucleus is assumed spherical, and between atomic spheres the potential is assumed constant. Plane waves from the spherical regions are augmented (hence the *Augmented Plane Wave (APW)* method) by additional plane waves in the constant potential region, which match the spherical waves at the sphere boundaries.

Johnson (1966) extended this concept to molecular systems, with the addition of an outer sphere boundary inscribing the entire system. The potentials $V(\mathbf{r})$ are:

$$V(\mathbf{r}) = \begin{cases} V^i(\mathbf{r_i}), & \text{inside the } i \text{ atomic spheres;} \\ V^O(\mathbf{r}), & \text{outside the outer sphere radius } \mathbf{r}_O \\ \overline{V}, & \text{otherwise.} \end{cases} \tag{2}$$

As shown in figure 1, **I** refers to the atomic sphere region, **II** to the constant-potential, intersphere region, and **III** to the region outside the inscribing sphere. The potential in region **II** is formed from an average of the atomic potentials, and is either spherically or arithmetically averaged.

The Schrödinger equation for region **I** takes the form, in Rydberg atomic units,

$$\left\{-\frac{1}{2}\nabla^2 + V(\mathbf{r})\right\}\Psi_{\mathbf{I}}(\mathbf{r}) = E\Psi(\mathbf{r}) \tag{3}$$

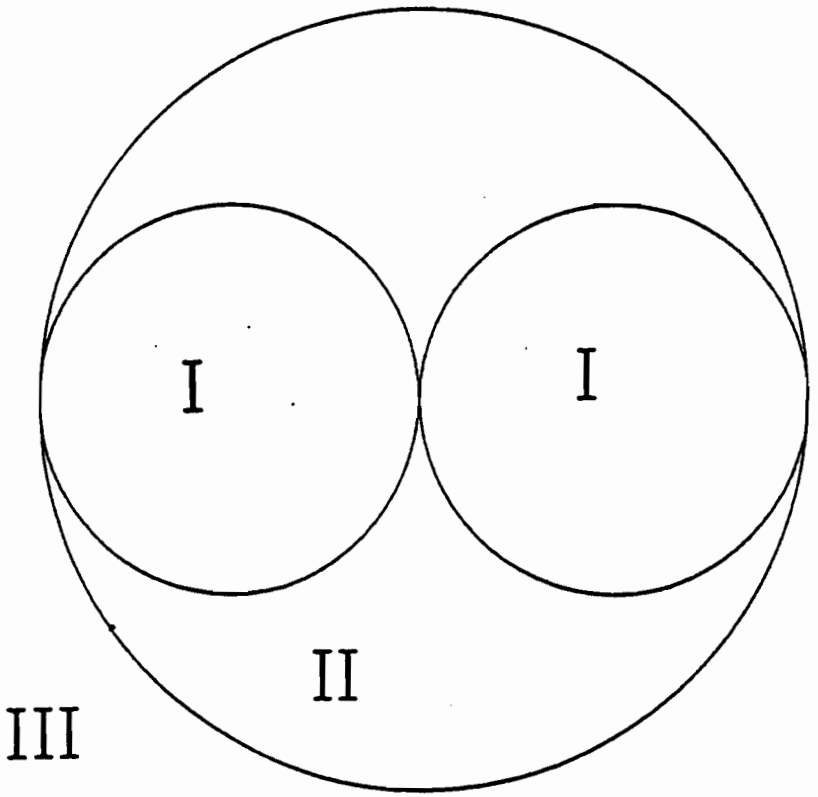

Figure 1. Muffin-tin potential regions in the MS-LDA method. Regions **I**, inside atomic spheres, with potential $V^i(\mathbf{r}_i)$; region **II**, outside the atomic spheres but within the outer sphere, with constant potential; region **III**, outside the molecular outer sphere, with potential $V(\mathbf{r})$.

(the Schrödinger equation for region **III** is similar); for region **II** it is

$$\left\{-\frac{1}{2}\nabla^2 + \kappa^2\right\}\Psi_{\mathbf{II}}(\mathbf{r}) = 0 \tag{4}$$

where

$$\kappa^2 = (E - \overline{V}) \tag{5}$$

The wavefunction $\Psi_{\mathbf{I}}(\mathbf{r})$ is expanded in the form

$$\Psi(\mathbf{r}) = \sum_{lm} C_{lm} R_l(r) Y_{lm}(\mathbf{r}) \tag{6}$$

where the coefficients C_{lm} are determined; $Y_{lm}(\mathbf{r})$ are spherical harmonics. The solution of the radial equation for $R_l(E;r)$ is identical (in form) to that for atoms:

$$\left\{-\frac{1}{2}\nabla_r^2 + \frac{l(l+1)}{r^2} + V(r) - E\right\}R_l(E;r) = 0 \tag{7}$$

There is one such equation for each scattering centre (conventionally an atomic nucleus); the coordinate r is referred to that centre.

Because there is no radial dependence in the potential for region **II**, the Schrödinger equation reduces to a standard wave equation whose solutions are spherical Bessel (or the related Hankel, modified Bessel or Neumann functions, depending on the value of E and the scattering phase). These are separated into the 'incident' and 'scattered' wave components, in terms of a partial-wave expansion similar to eq.(6):

$$\psi_{\mathbf{II}}^{inc}(\mathbf{r}) = \sum_{lm} B_{lm}^j \, i_l(\kappa r_j) \, Y_{lm}(\mathbf{r}), \qquad E < \overline{V} \tag{8}$$

$$\psi_{\mathbf{II}}^{inc}(\mathbf{r}) = \sum_{lm} B_{lm}^j \, j_l(\kappa r_j) \, Y_{lm}(\mathbf{r}), \qquad E > \overline{V} \tag{9}$$

$$\psi_{\mathbf{II}}^{sc}(\mathbf{r}) = \sum_{lm} A_{lm}^j \, k_l^{(1)}(\kappa r_j) \, Y_{lm}(\mathbf{r}), \qquad E < \overline{V} \tag{10}$$

$$\psi_{\mathbf{II}}^{sc}(\mathbf{r}) = \sum_{lm} A_{lm}^j \, n_l(\kappa r_j) \, Y_{lm}(\mathbf{r}), \qquad E > \overline{V} \tag{11}$$

where $j_l(\kappa r_j)$ is a spherical Bessel function, $n_l(\kappa r_j)$ a spherical Neumann function, $i_l(\kappa r_j)$ is a modified spherical Bessel function, and $k_l^{(1)}(\kappa r_j)$ a modified Hankel function of the first kind. (Johnson, 1973; Weinberger and Schwarz, 1975).

Standard boundary conditions hold for this system: the molecular wavefunction must be single-valued and continuous (i.e. matching first derivatives) at the sphere boundaries, and finite at large distance from the centre of the outer sphere. In addition, it is required that the incident wave at each scattering site equal the sum of all of the waves scattered from the other points and the outer sphere. These conditions allow certain of the partial-wave coefficients to be expressed in terms of others, and lead to the secular determinant:

$$\begin{vmatrix} [T^{-1}(E)]_{LL'}^{jj'} & -S_{LL'}^{jO}(E) \\ -S_{LL'}^{Oj'}(E) & -\delta_{LL'}\,[t_l^O(E)]^{-1} \end{vmatrix} \tag{12}$$

Expression (12) is written in a highly compacted notation; the terms are defined as follows:

$$S_{LL'}^{jO}(E) = 4\pi i^{l-l'} \sum_{L''} i^{-l''} I_{LL'}(L;L') \times j_{ll'}(\kappa R_{jO})\, Y_{L''}(\mathbf{R}_{jO}) \tag{13}$$

where

$$L = lm,$$

$I_{LL'}(L;L')$ is an integral over spherical harmonics, $j_{ll'}(\kappa R_{jO})$ is the spherical Bessel function, and $Y_{L''}(\mathbf{R}_{jO})$ is a spherical harmonic.

The term $t_l^O(E)$ is defined, using Wronskian notation, as

$$t_l^O(E) = -\frac{[k_l^{(1)}(\kappa b_O),\, R_l^O(E;b_O)]}{[i_l(\kappa b_O),\, R_l^O(E;b_O)]} \tag{14}$$

where, as before,$k_l^{(1)}(\kappa b_O)$ is the modified Hankel function of the first kind, and $i_l(\kappa b_O)$ is a modified spherical Bessel function. The expression $R_l^O(E;b_O)$ is the

radial function of equation (7). All of the components of $t_l^O(E)$ take arguments referring to the outer sphere.

The term $[T^{-1}(E)]_{LL'}^{jj'}$ is defined as

$$[T^{-1}(E)]_{LL'}^{jj'} = \delta_{jj'}\delta_{LL'}[t_l^j(E)]^{-1} - G_{LL'}^{jj'}(E) \tag{15}$$

in which the $\delta_{jj'}$ and $\delta_{LL'}$ are Dirac delta functions. The term $G_{LL'}^{jj'}(E)$ is a structure factor taking the same form as $S_{LL'}^{jO}(E)$ in equation (13); the term $t_l^j(E)$, similarly, follows the form of $t_l^O(E)$ as defined in equation (14). In both cases, the difference is that the functional arguments are referred to atomic rather than outer sphere boundaries.

Equation (12) represents the system to be solved in the Multiple Scattering method; Zeros of eq.(12) correspond to the one-electron eigenvalues.

Because the angular integrations (such as $I_{LL'}(L;L')$ in equation (13)) are products of Clebsch-Gordan coefficients, and the radial integrations are done numerically, the Multiple Scattering (MS) method is computationally efficient. Total times for computation scale approximately as N^2, where N is the number of partial-waves in the basis (Salahub, 1987); this in turn is proportional to the number of atoms in the molecule. Beyond assigning an appropriate l value to the partial-wave set on each atom, there is no basis set choice as in LCAO methods. The partial-wave coefficients A_L provide an unambiguous population analysis.

The crucial weakness in the MS is the muffin-tin potential, with its sever approximation of a constant-potential region. The discontinuity in the potential at the sphere boundary leads to a buildup of charge on the sphere surface (Grant and Whitehead, 1976).

Muffin-tin sphere sizes themselves are not well defined. The MS equations are valid for overlapping spheres (Rösch *et al.*, 1973), as long as the sphere does not enclose

another scattering site, and normalization is preserved, i.e. the total charge density is consistent with the total number of electrons. It was recognized early in the history of the method (Johnson, 1971) that overlapping the spheres improved results dramatically, by reducing the effective volume of the constant-potential region, but the choice of sphere radii and the resulting degree of overlap is arbitrary.

The most widely accepted technique for determing the atomic sphere radii was introduced by Norman (1976). This "Norman sphere" method partitions the charge among atoms by finding the point of minimum electrostatic potential (Srebrenik *et al.*, 1975); since the resulting sphere is neutral, this is equivalent to choosing a sphere which encloses the atomic number Z of charge. As these radii tend to give to large overlap percentages, a reduction factor is uniformly applied to all atomic spheres: a reduction to 88% of the "Norman radius" generally gives overlaps between adjacent atoms on the order of 25%.

Considerable theoretical effort has been extended to finding corrections to the muffin-tin approximation, and to removing it altogether. Williams and Morgan (1974) derived multiple scattering equations, from an integral equation (Green's function) starting point, which are more general than those outlined above; the formalism did not require muffin-tin spheres, and indeed the authors showed the muffin-tin potential was a special case of their own. Scheire and Phariseau (1974a,b,c, 1975a,b), and independently, Eyges (1974), developed multiple scattering equations for cellular regions of arbitrary shape. Unfortunately, none of these approaches has been implemented in a computer program.

In the following three sections, results are presented from Multiple-Scattering Local Density Approximation (MS-LDA) studies on three different classes of compounds. Section (**I**) treats the planar heterocycle series 2-imidazolidinenone, 2-imidazolidinethione and 2-imidazolidineselenone. Section (**II**) contains results of

calculations on the planar aromatic heterocycles 2,1,3-benzoxadiazole and its sulfur and selenium analogues. Section (**III**) gives results from the metal-chalcogen compound 2,1,3-benzoxadiazole$[Cr(CO)_5]_2$.

I.3.2 References.

Eyges, L., 1973, Annals of Physics **81**, 567

Grant, I. P. and M.A. Whitehead, 1976, Mol. Phys. **32**, 1181

Harrison, W. A., 1979, *Solid State Theory* (Dover, New York)

Johnson, K. H., 1966, J. Chem. Phys. **45**, 3085

Johnson, K. H., 1971, Int. J. Quant. Chem. **45**, 153

Johnson, K. H., 1973, in *Advances in Quantum Chemistry, Volume 7*, edited by P-O Löwdin (Academic Press, New York), p. 143

Norman, J. G., 1976, Mol. Phys. **31**, 1191

Rösch, N., W. Klemperer and K. H. Johnson, 1973, Chem. Phys. Lett. **23**, 149

Salahub, D. R., 1987, in *Ab Initio Methods in Quantum Chemistry II (Advances in Chemical Physics, Vol. LXIX)*, edited by K. P. Lawler (Wiley, New York), p. 447

Scheire, L. and P. Phariseau, 1974a, Chem. Phys. Lett. **26**, 149

Scheire, L. and P. Phariseau, 1974b, Physica **74**, 546

Scheire, L. and P. Phariseau, 1974c, Int. J. Quant. Chem. Symp. **8**, 110

Scheire, L. and P. Phariseau, 1975a, Int. J. Quant. Chem. **9**, 887

Scheire, L. and P. Phariseau, 1975b, Int. J. Quant. Chem. Symp. **9**, 106

Slater, J. C., 1937, Phys. Rev. **51**, 846

Srebrenik, S., R. Pauncz and H. Weinstein, 1976, Chem. Phys. Lett. **32**, 420

Weinberger, P. and K. Schwartz, 1975, in *Theoretical Chemistry, Physical Chemistry, Series Two, Volume 1*, edited by A. D. Buckingham and C. A. Coulson (Butterworths, London), p. 257

Wigner, E. and F. Seitz, 1933, Phys. Rev. **43**, 804

Williams, A. R. and J. van Morgan, 1974, J. Phys. C. **7**, 37

I.3.3 Electronic Structure and Quadrupole Couplings of the Heterocycles 2-imidazolidinenone, 2-imidazolidinethione and 2-imidazolidineselenone by the MS-LDA Method.

Abstract

Multiple-scattering local-density-approximation (MS-LDA) calculations, with both Xα and Vosko-Wilk-Nusair (VWN) exchange-correlation functionals, were performed on the ring compound 2-imidazolidinenone and its sulphur and selenium analogues. Calculated ionization potentials were insensitive to the functional choice, and agreed better with experiment than previous studies by other methods. Nitrogen nuclear quadrupole coupling constants were computed; these were sensitive to the functional choice, the VWN coupling constant being consistently lower than the Xα coupling constant. The principle moment, q_{zz}, was in good agreement with experiment: the Xα and VWN results bracketed experiment. However, the asymmetry parameters η were not well predicted. Trends along the series paralleled experimental results.

Introduction

Substituted azolidines of the form

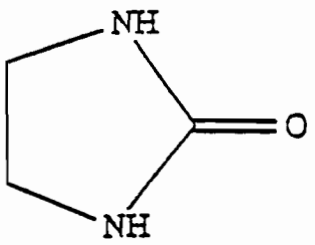

2-imidazolidinenone

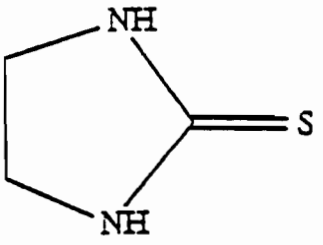

2-imidazolidinethione

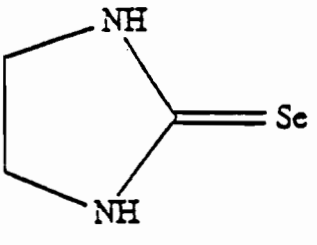

2-imidazolidineselenone

provide interesting variations in the π-electronic structure, particularly in the N–C–X conjugation (where X = O, S, or Se); the π-structure is interesting because these compounds serve as ligands in transition-metal complexes (Carlin and Holt, 1963; Devillanova et al., 1979, 1981). Valence and core ionization potentials have been correlated with calculated charge distributions (Andreocci et al., 1980b); nitrogen Nuclear Quadrupole coupling constants have been analyzed to elucidate the relative importance of the N^+=C–X^- resonance structure (Krause and Whitehead, 1973). Interpretations differ according to the calculation method used (EHT, CNDO/2, *ab initio*) (Andreocci et al., 1980a), and between ultra-violet photoelectron spectra (UPS) and nuclear quadrupole resonance (NQR) results .

The Multiple-Scattering Local-Density Approximation (MS-LDA) theory, with the Xα approximation to the exchange, has succesfully investigated the ionization potentials and electric field gradients (EFG) of a series of nitrogen-containing planar ring compounds (Case et al., 1980). Several papers (Bowmaker et al., 1985a,b,c) demonstrated the efficacy of the Xα method for calculating the principal component of the EFG, though it does not always reproduce good asymmetry parameters η, and works less well in charge-transfer studies (Bowmaker and Boyd, 1987).

The major weakness of the MS-LDA method is the use of the muffin-tin potential: regions of a molecule are assigned different forms of the potential; spherically symmetric within spheres (of arbitrary size) around each atom, constant outside of these spheres but within a sphere enclosing the molecule, and spherically symmetric outside the molecular enclosure. The intersphere, constant-potential region is the least physically correct. Planar compounds thus present a problem for the muffin-tin scheme, because up to 85% (in the present study) of the molecular sphere volume is occupied by the constant-potential region.

In this work, the MS-LDA is used with both the Xα and VWN exchange-correlation

potentials, and applied to the substituted azolidine compounds. The intention is threefold: to test the relative importance of the choice of exchange-correlation functional within a muffin-tin potential, to test the MS-LDA method when extended to systems containing two heteroatoms, and to give further chemical insight into the electronic structure of this homologous series.

Computational Details

The Multiple-Scattering Xα code of Case and Cook (1981) was modified (Berksoy and Whitehead, 1988) to include the exchange-correlation potential of Vosko, Wilk and Nusair (VWN) (1980). Experimental geometry was used for 2-imidazolidinethione (Wheatley, 1953). For the oxygen and selenium analogues, the geometries were taken from urea and selenourea (Kromhaut and Moulton, 1955; Rutherford and Calvo, 1969); this procedure is supported by the close resemblance in structure between thiourea and 2-imidazolidinethione: the C–S bond distance is 1.71 Å in each case; the N-C-S angles are 122° and 124°, respectively (Kuncher and Truter, 1958). Since the sulphur ring compound is planar (C_2v symmetry), a planar structure was assumed for the oxygen and selenium analogues.

Atomic sphere radii for the muffin-tin potential were chosen by the Norman (1976) criterion, with a reduction factor of 0.88. N and H radii determined this way were 1.62 and 1.16 Å, respectively, close to the values of 1.60 and 1.20 found to be optimal in Case's study (1980). The outer sphere was positioned at the point on the C_2 axis which minimized the outer sphere radius. An option in the program to place the outer sphere at an unweighted average of atomic coordinates resulted in a much larger radius, and therefore was not used.

Schwartz (1972) alpha values were used in the Xα calculations (alpha is 2/3 in the VWN). Calculations were performed at both the minimum partial wave basis, cor-

responding to the occupied levels, with l=3 on the outer sphere, and a larger partial wave basis with each l value increased by one over the minimum basis. Geometries and atomic sphere radii are in Figure 1; sphere radii and overlap percentages are in Table 1.

Valence ionization potentials (IP) were calculated by the transition state method, with half an electron removed from the highest fully-symmetric level (in this case, the $7a_1$ level). The highest IP (those whose experimental values have been reported) were also converged individually to their transition states. For core IP, the N $1s$, S $2p$ and Se $3p$ levels (usually treated as frozen cores) were symmetrized, and the half electron removed directly from the level of interest. All calculations, SCF or transition state, were converged to less than 10^{-5} in the potential.

Nitrogen nuclear quadrupole coupling constants were found using the one-electron properties code included in the MS-Xα program (Case and Cook, 1981). The program calculates electric field gradients; components q_{ii} of this tensor were converted to coupling constants $e^2 q_{ii} Q/h$ assuming a nitrogen quadrupole moment Q of 1.6×10^{-26} cm^2 (Von Niesson *et al.*, 1975). Atomic charges were determined by the charge-partitioning method (Case and Karplus, 1976), and include an allotment from both the inter and outer sphere regions of the muffin tin. Electric-field-gradient tensors were transformed from molecular to principal-axis frames with the aid of IMSL subroutines.

Results and Discussion

1. *Ionization Potentials*

Results for 2-imidazolidinethione IPs, comparing 4 different methods, (minimum and larger partial wave basis, Xα and VWN exchange-correlation functionals) are in figure 2. The O and Se results are similar: the distinguishing feature is the similarity between the Xα and VWN results. Some middle levels are shifted downward in both methods by increasing the basis (e.g. $6a_1$, $3b_1$, $1a_2$), but the effect is far smaller than that seen by manipulating, for example, muffin-tin sphere sizes (Case *et al.*, 1980).

The transition state method of Slater identifies the IP of a given orbital with the eigenvalue of that level when half an electron is removed; this has been shown to be the equivalent of correctly removing the self-interaction energy (Gopinathan, 1979), and gives good numeric results. Separate SCF calculations are required for each IP. Some researchers have noted (Preston *et al.*, 1976), however, that the values of the remaining, fully-occupied levels relaxed to close to their transition-state values; thus, only one SCF calculation need be done, with results independent (to ≤ 0.1 eV) of which orbital was designated for half-occupancy. This economy is often practiced, and is particularly useful for investigating large systems or clusters (Arratia-Perez and Malli, (1986).

This property of transition-state calculations did not hold for the compounds in this study. Figure 3 shows four first four IP of 2-imidazolidinethione as calculated with the VWN large basis in four separate transition state calculations: with the half-electron removed from the highest (by eigenvalue) occupied level ($3b_2$), and successively from the highest b_2, a_2, and a_1 levels (the next three highest occupied levels). The highest-occupied transition state calculation, $3b_2$, causes the $7a_1$

level to become the highest, ionization potential, in sharp contrast to both the individually-calculated levels and experimental assignments. The IP calculated by the $7a_1$ transition state (column 4) reproduce the qualitative aspects of experimental assignments (column 5): a lone pair(n) and π orbital close in energy, followed by a π, followed after a larger gap by a σ. In each of the $3b_2$, $2a_2$, $5b_1$ calculations, however, the remaining orbitals do not relax to transition-state values, and indeed differ by as much as 2.4 eV. Further, the ordering changes according to the choice of half-occupied orbital; only the $7a_1$ (σ) level giving results resembling both the full calculations and experiment.

This difference among choices of level for the transition state may be explained as follows: in the SCF calculation of 2-imidazolidinethione, the $3b_2(n)$ level has 0.75 of the electron density concentrated in the S lone pair, making it the most highly localized state; removal of half an electron from so specific a region will not be expected to relax the delocalized states. The $2a_2$ and $5b_1$ levels are indeed delocalized, and correspond to π bonding, but have significant portions of their populations in the constant-potential region (through the charge-partitioning scheme). The $7a_1$ level is both delocalized and concentrated in the atomic-sphere region; it yields the most useful IP if only one transition state calculation is done. Thus the highest *fully symmetric* occupied level, rather than simply the highest occupied level, is the best choice when only a single transition state calculation is done.

Table 2 shows the IP for the oxygen compound, as calculated by *ab initio*, CNDO/2 and the present method, and experiment. The column marked ($7a_1$) corresponds to the results for the $7a_1$ transition state; the column (each) gives the individually-converged results. In this case, the $7a_1$ calculation happens to get better agreement with previous methods in the assignment of the σ level; when converged individually, the oxygen lone pair n_O orbital ($3b_2$) becomes slightly lower (more negative)

in energy. The MS–VWN results agree with those of *ab initio* and CNDO/2 in assigning π orbitals to the two highest levels.

Results for the sulphur compound are in Table 3, which include in addition a CNDO/S calculation (Andreocci *et al.*, 1980b). As already noted, the $7a_1$ and individual MS–VWN results have the same ordering. There is disagreement, however, between the results of this work and the three earlier calculations as to the placement of the n_S level; while the others place it, along with π_{CS}, as one of the two highest, the MS–VWN assigns the two highest positions to the π levels (as in the oxygen compound), and puts the lone pair in third place.

Table 4 shows the selenium compound IP, along with the experimental and CNDO/2 results. Again the MS–VWN calculation gives different ordering than CNDO/2 for the π and lone-pair levels.

In each of the compounds, the σ level was given by previous calculations as σ_{CX}, the σ bond between the O, S or Se and the ring carbon. However, the MS–VWN results consistently give this $7a_1$ σ as the C–H bond; the C–X σ is at $5a_1$.

The core 1*s* IP's, in Table 5, prove sensitive to inclusion of correlation. The nitrogen 1*s* energy is significantly better by the VWN, both in absolute value, and more importantly, in the trend. Experimentally, the 1*s* IP is higher (less negative) in 2-imidazolinenone than in the other compounds, and the values in the S and Se compounds are similar. VWN calculations accurately reflect this pattern. The Xα values, in contrast, are not only several eV away from the experimental value, but worse do not follow the experimental trend.

In the S and Se 2*p* IP, the choice of potential is less important. VWN does move the S 2*p* slightly closer to the correct value, but has no effect on the Se 2*p*; both potentials give reasonable values for Se 2*p*, but poor values for S.

2. *Nuclear Quadrupole Coupling Constants and Charge Densities*

Components of the electric field gradient(EFG) tensor are calculated by the program in the molecular coordinate frame. The transformation to the EFG principal-axis frame is accomplished by finding the transformation matrix T which diagonalizes the EFG tensor; in the xz planar systems considered here, T will correspond to

$$T = \begin{pmatrix} \cos^2\theta - \sin^2\theta & 0 & 2\sin\theta\cos\theta \\ 0 & 1 & 0 \\ -2\sin\theta\cos\theta & 0 & -\sin^2\theta + \cos^2\theta \end{pmatrix}$$

(Lucken, 1969) where θ corresponds to the rotation angle about the y axis through the nitrogen atom. This same matrix projects out contributions to the principal-axis components from any particular state.

It is conventional in NQR to assign principal axes so that $q_{zz} > q_{yy} > q_{xx}$. With respect to the atomic positions shown in figure 1, q_{zz} is out of the plane, while q_{yy} is near the direction of the N–H bond; q_{xx} is at right angles to q_{yy}. Coupling constants corresponding to these principal components for each molecule and calculation scheme, along with the rotation angle with respect to the molecular coordinate system, are listed in Table 6.

The two compounds with reported EFG values (the -O and -S analogues) were studied by solid-state methods which do not allow determination of either the sign of q_{zz}, or the two smaller components. However, similar tri-coordinated nitrogen compounds have q_{zz} in the π direction (i.e. perpendicular to the ring) and q_{yy} along the N–H bond; these calculations conform to that pattern, with the caveat that the y principal axis does not quite coincide with the N–H bond direction.

The magnitude of q_{zz} is moderately well predicted by the large basis with either Xα or VWN exchange potentials. The asymmetry parameter

$$\eta = \frac{q_{yy} - q_{xx}}{q_{zz}}$$

is, however, poorly predicted; the relative values of the in-plane components q_{yy} and q_{xx} are badly predicted, but in the correct order (i.e. $q_{yy} > q_{xx}$); Case's MS-Xα calculations on planar nitrogen-containing heterocycles encountered similar difficulties, to the point where the relative sizes of q_{yy} and q_{xx} were *reversed* compared to experiment.

Large inaccuracies in the calculation of η reduce the predictive value of this method in Nuclear Quadrupole Resonance spectroscopy (where signal detection itself, especially of nitrogen resonances, is often difficult). For the nitrogen nucleus (spin = 1), q_{zz} and η are related to the measured transition frequencies $\nu_{\pm}$ by (Lucken, 1969)

$$\nu_{\pm} = \frac{3}{4} q_{zz}(1 \pm \frac{\eta}{3}).$$

The large partial-wave basis VWN calculation of 2-imidazolidinenone predicts ν_+ = 3.209, ν_- = 2.144 MHz, compared to the experimental values ν_+ = 3.253, ν_- = 2.731; the ν_+ value is good, but ν_- is too far off to be useful.

In comparing EFG values between small and large bases, two features arise: the principal component q_{zz} is reduced by about 20%, and the smallest component q_{xx} is substantially reduced, by factors of between 2 and 10. The reduction in q_{zz} is attributable to the inclusion of *d* partial waves on nitrogen; this allows some of the more highly directional *p* character to be diffused. The drastic change in q_{xx} (and thus in η) is brought about by the addition of a *p* partial wave on hydrogen; while the hydrogen *p* component along the N–H bond should not introduce much change in the q_{yy}, as the charge distribution remains dominated by the *s* population, but q_{xx}, the perpendicular direction, gains a *p* component that was not previously present, thus allowing the charge distribution to diffuse in that direction. The size of the muffin-tin sphere around H, also, exerts a large influence on the EFG values (Case *et al.*, 1980), but tuning sphere sizes to fit a given parameter is pointless.

The difference between Xα and VWN results is that the EFG's are always reduced, though not uniformly, by the VWN exchange-correlation. To investigate the reason for this, the states with largest contribution to the EFG were isolated, along with the corresponding percentages of nitrogen p population; these values are in Table 7 for the case of 2-imidazolinenone, and Table 8 for 2-imidazolidinethione.

The nitrogen p populations are often, by themselves, sufficient to predict the EFG (the basis of Townes and Dailey (1949) theory); in this work, only those states with a large percentage of nitrogen p make any significant contribution. It is reasonable, then, to look for the Xα – VWN difference in the N p partial waves.

Although the 8 (of 17 valence plus 8 core) states shown in Table 8 are the major contributors to the EFG, the effect of the others is far from negligible, and indeed the cumulative total from these 8 states is quite different. Nevertheless, shifts in these major components, between Xα and VWN calculations, are mirrored in the overall electronic totals.

Figure 4 shows the difference (Xα – VWN) in contribution to the $e^2q_{zz}Q/h$ coupling constant, overlayed with the the difference in % nitrogen p contribution, for the b_1 and a_1 states. The correlation between the two is remarkable, though it is not obvious from this evidence just why the VWN functional should cause these particular shifts in the p population.

Shifts in EFG reflect shifts in the electron density (the EFG is related directly to the Laplacian of the charge distribution (Array and Murgich, 1989)). Table 9 lists the gross atomic charges, as assigned by the charge-partitioning scheme. As with the IP, more change is caused by increasing the partial-wave basis than by including the VWN correlation. Nevertheless, the accumulation of small charge differences (e.g., from 8.68 to 8.37 for the charge on oxygen) significantly alters the molecular dipole moments, Table 10.

Dipole moment values showed much more sensitivity to the exchange-correlation functional in the large basis. The VWN results for minimum l are somewhat smaller than the Xα, but in the larger basis they are reduced more not only in absolute terms, but even more so relatively: the large l VWN dipole moments are half to two-thirds of the Xα.

The shift of electron density between the two methods can more clearly be seen in a density difference plot. Figures 5a-5e depict the density differences, Xα – VWN, for 2-imidazolidinethione in the large basis, for the total density and some of the individual levels. The upper half of each figure is the contour plot for the in-plane density differences (the molecular orientation is the same as in Figure 1), while the lower plot renders the same information in three dimensions.

Figure 5a shows the total density difference for all states contributing in the plane (b_1 and a_1). The in-plane slice does not necessarily reflect total charge distributions – the large spike on sulphur shows greater charge density in the Xα calculation, but in fact the total charge on sulphur is slightly higher in the VWN. In regions which can be identified as bonding – between the two carbons at the back of the ring, between carbon and nitrogen, nitrogen and hydrogen, and less so between carbon and sulphur, the density is higher in the Xα calculation.

The a_1 states do not, in general, make a significant contribution to this bonding region density difference. Figure 5b shows the $2a_1$ case, which is typical of the fully-symmetric levels. Though much structure is implied by the two-dimensional contour plot, the contour values themselves are small, as shown in the three-dimensional graph.

The $4b_1$ density difference appears in Figure 5c, where the higher bonding density for Xα is clearly seen between the backside carbon and nitrogen. The $3b_1$ level, Figure 5d, likewise shows more bonding electron density between these atoms for

the Xα. Finally, in the $2b_1$, Figure 5e, there is an excess density along the N–H and N–C bonds in the Xα.

These differences are reflected in the partial-wave populations for each state. Table 11 lists the main partial-wave contributions for the $4b_1$, $3b_1$ and $2b_1$ levels for the Xα and VWN electron populations. In each case, the partial waves involved in bonding are reduced by the VWN. The $4b_1$ N p and C p waves may be characterized as belonging to a p_σ bond between those atoms; the N p character is reduced in the VWN. A similar bond may be identified in the $3b_1$ level; here, both p populations are reduced. In $2b_1$, the largest partial-wave contributions turn out to be out of the plane, associated with the C–H bond, but here again the populations are lower in the VWN charge distribution.

The effect of including the VWN correlation functional, then, is to reduce the charge buildup in high-density regions. In principle, accounting for correlation should disperse charge to lower the energy; this expectation is fulfilled in this study despite the severity of the muffin-tin approximation.

3. *Resonance structures*

In a Townes and Dailey analysis of Nuclear Quadrupole Resonance data, Krause and Whitehead (1973) found the ionic structure of 2-imidazolidinethione to be highly favoured, i.e.,

$$\underset{\text{I. 42\%}}{\text{N–C=S}} \quad \leftrightarrow \quad \underset{\text{II. 58\%}}{\text{N}^+\text{=C–S}^-}$$

It was noted that the original crytallographic data (Wheatley, 1953) could be interpreted to yield an even higher fraction (78%) of the ionic form. Replacing the sulphur by oxygen substantially decreased the ionic character.

Ionic structures with decreasing positive charge on N along the series

$$O \rightarrow S \rightarrow Se,$$

were suggested by Andreocci *et al.* (1980a) from X-ray Photoelectron Spectra (XPS) and supported by evidence from the Ultraviolet Photoelectron Spectra of analogous compounds Andreocci *et al.* (1980b).

However, another XPS study (Takahashi and Yabe, 1968) found no evidence for an ionic form, and suggested that the N—C=S system was covalent. Calculations by CNDO/2 and STO-3G methods (Bossa *et al.*, 1981) placed a small *negative* charge on nitrogen.

In the present study, the total net charge on the nitrogen atoms varied from negative (more than the atomic number) to slightly positive, according to whether the small or large partial-wave basis was used (table 10). Of the four schemes, the VWN large basis is expected to be the most reliable. This large VWN basis assigns significant excess charge to the terminal heteroatom (-0.37 for O, -0.40 for S, and -0.48 for Se), a slight charge deficiency on the nitrogen (about +0.1 for each compound), and a considerable net positive charge on the intervening carbon (+0.57 in the O compound, +0.42 for the other two). This distribution is much closer to a resonance structure of the form

$$N\text{–}C^{+}\text{=}S^{-}$$

III.

The CNDO/2 calculation was in fact in reasonable agreement with this form: (though its authors chose to interpret the nitrogen in terms of a positive π charge, thus favoring structure II) the carbon atom did have significant net positive charge (+0.28 in the sulphur compound, +0.46 in the oxygen case).

More interesting, still another XPS study (Sato *et al.*, 1969) provided evidence (a

narrow SKβ line) of a highly ionic $C^+=S^-$ bond character, in agreement with the proposed structure III.

Trends in the total nitrogen charge follow those from experimental binding energies: less positive when oxygen is the exocyclic atom (thus lowering the binding energy), more positive, and similar to one another, for the sulphur and selenium cases. Again the CNDO/2 calculations for the O and S compounds agreed, albeit shifting more charge (the nitrogen fractional charge was 0.075 electron less positive in the oxygen compound) than did the present calculation (0.04 electron when a large basis was used).

When 2-imidazolidinethione and its selenium analogue are ligands in transition metal complexes, they are thought to coordinate through the sulphur or selenium atom; it was proposed by qualitative arguments that the coordination is through the ligand π system (Devillanova, 1981). Thus, in addition to the total charge on the exocyclic atom, it is pertinent to examine the total π charge. Table 12 lists the total electron population involved in π states for each of the atoms N, C and X (where X=O, S or Se), for the VWN large basis calculation on each compound. Of six valence electrons, oxygen, for example, puts 1.71 of that population into π levels; sulphur and selenium contribute about 1.81 and 1.84 electron more. The pattern in this series, of changes between the oxygen and sulphur analogues, with little change in going from sulphur to selenium, is maintained here: the π populations shift on going from O to S, but the S and Se profiles are virtually identical.

Because these are delocalized π states, nothing can be said directly about the "double-bond" character between carbon and oxygen as opposed to that between carbon and sulphur. Further, the closeness between the π populations on S and Se preclude definitive statements on the relative binding strengths of these two ligands, although the slight increase in Se π population does correlate with 2-

imidazolidineselenone being higher in the nepheluaxetic series than its sulphur analogue (Carlin and Holt, 1963). However, the reduction both in excess charge and in π population on the oxygen compound suggests that complexes formed with 2-imidazolinenone will be less stable than those using the sulphur or selenium.

Conclusions

The inclusion of the Vosko-Wilk-Nusair exchange-correlation potential in MS-LDA calculations in this series of planar ring compounds had no effect on the valence ionization potentials; it significantly improved the $1s$ core IP, and gave lower but not necessarily improved values of nuclear quadrupole coupling constants. Its inclusion is therefore recommended where core-level phenomena are concerned, as for example ref. (Tse *et al.*, 1989). The correlation functional moves charge out of high density regions.

The widely accepted practice, in transition-state calculations, of converging to only one half-occupied level (typically the highest occupied) can lead to erroneus results, and must be used with caution. Converging to the highest fully-symmetric occupied level is more reliable.

The MS-LDA method yields good values for valence IP (particularly when compared with other methods) in these compounds, despite the severity of the muffin-tin approximation.

An increased partial-wave basis is required to approach the experimental values of the principal component of the electric field gradient. Asymmetry parameters were not well predicted by any of the methods.

The lower total and π charges on the oxygen atom, compared to sulphur and selenium, suggest that 2-imidazolinenone is a less stabilizing ligand than the sulphur and selenium forms.

Table 1. Muffin-tin sphere sizes and overlaps for 2-imidazolidinenone (X = O), 2-imidazolidinethione (X = S) and 2-imidazolidineselenone (X = Se).

X	R_H	R_N	R_C	R_X	R_{out}	% C-X overlap	% intersphere
O	1.16	1.62	1.63	1.70	5.29	37	83
S	1.16	1.62	1.61	2.44	6.61	25	85
Se	1.16	1.61	1.55	2.67	6.96	37	81

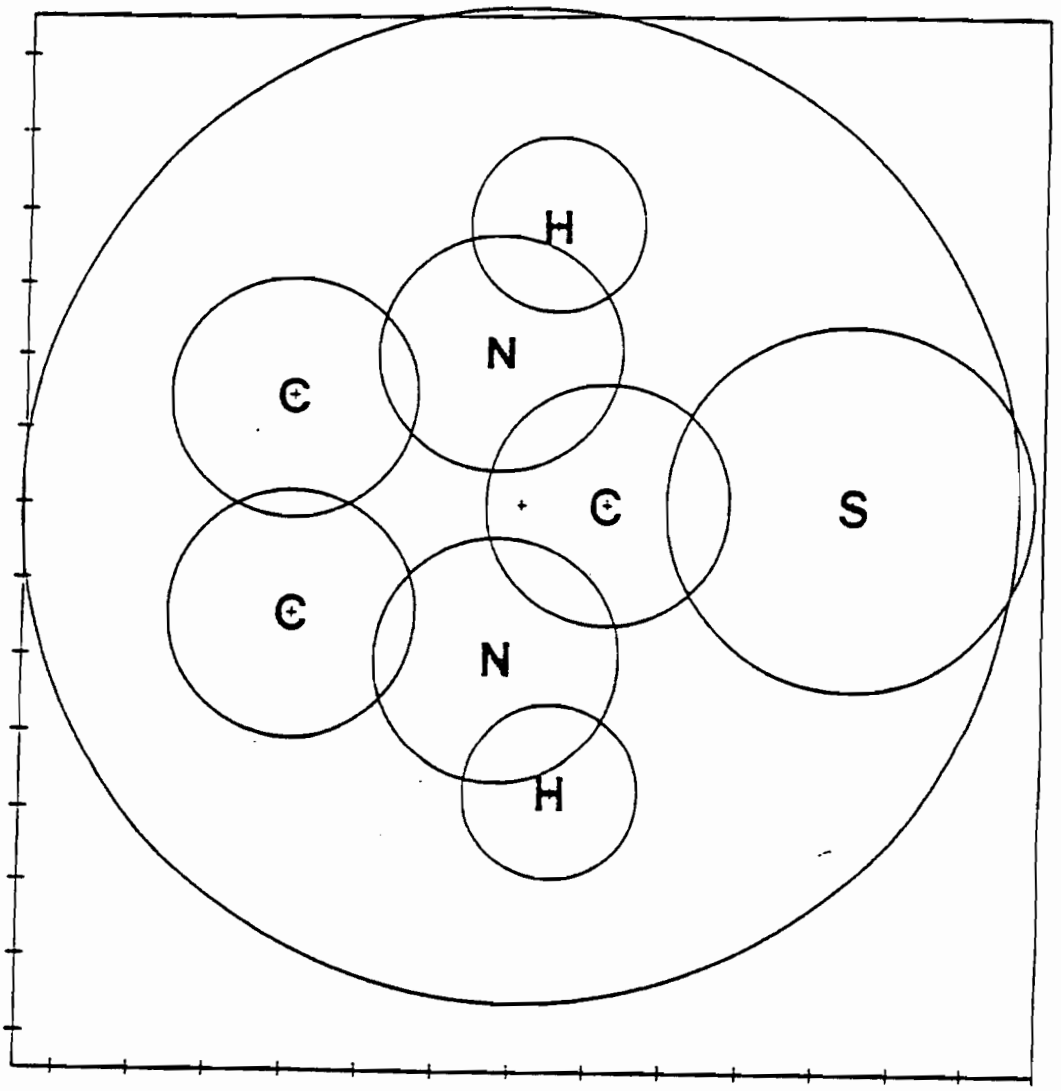

Figure 1. Atomic positions and muffin-tin sphere sizes for 2-imidazolidinethione. The axes are scaled in intervals of 1 atomic unit.

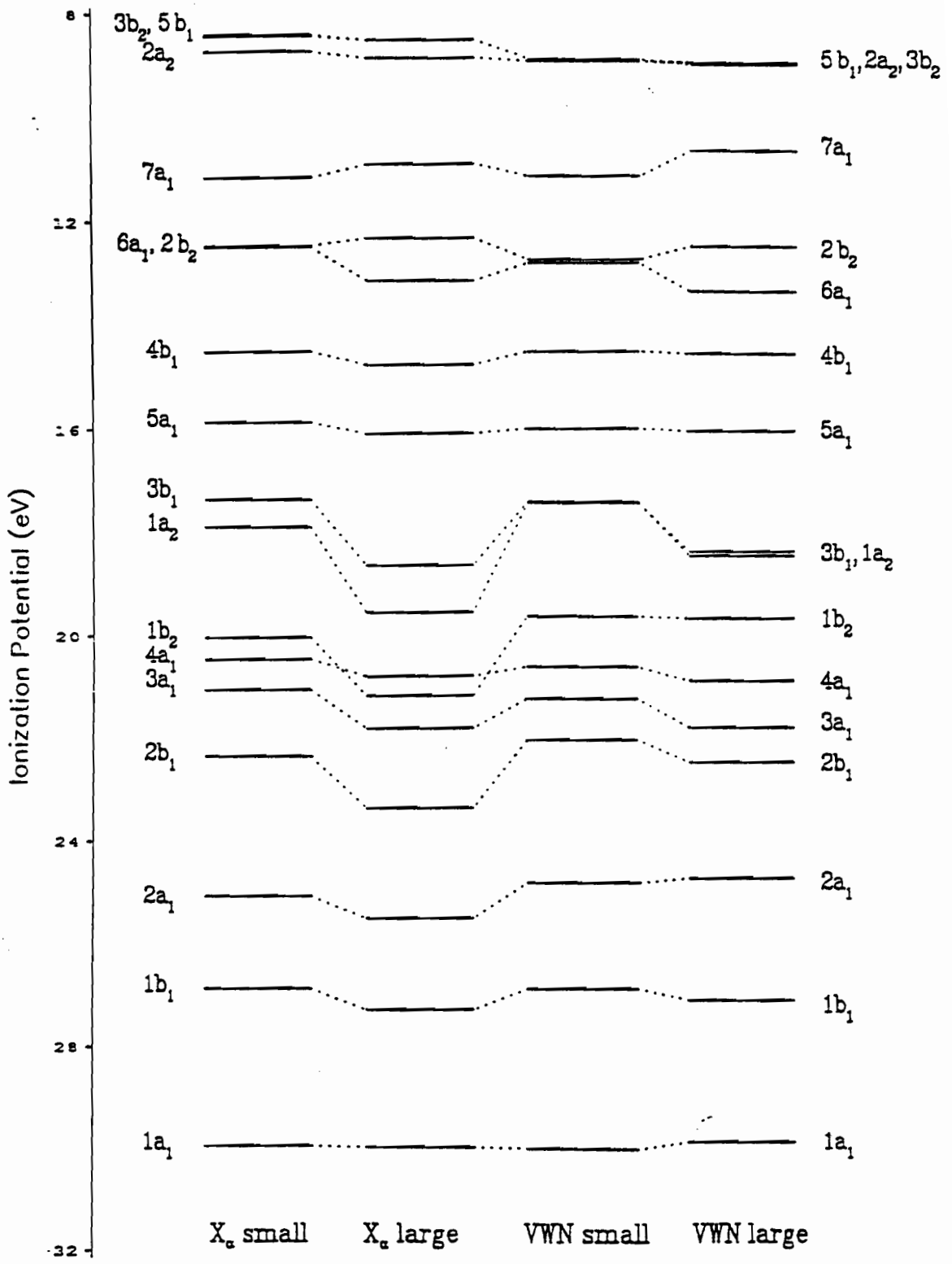

Figure 2. Valence ionization potentials, eV, of 2-imidazolidinethione calculated by the transition state method, and four different procedures: Xα with minimum (small) and extended (large) partial wave basis, and VWN with minimum (small) and extended (large) partial wave basis.

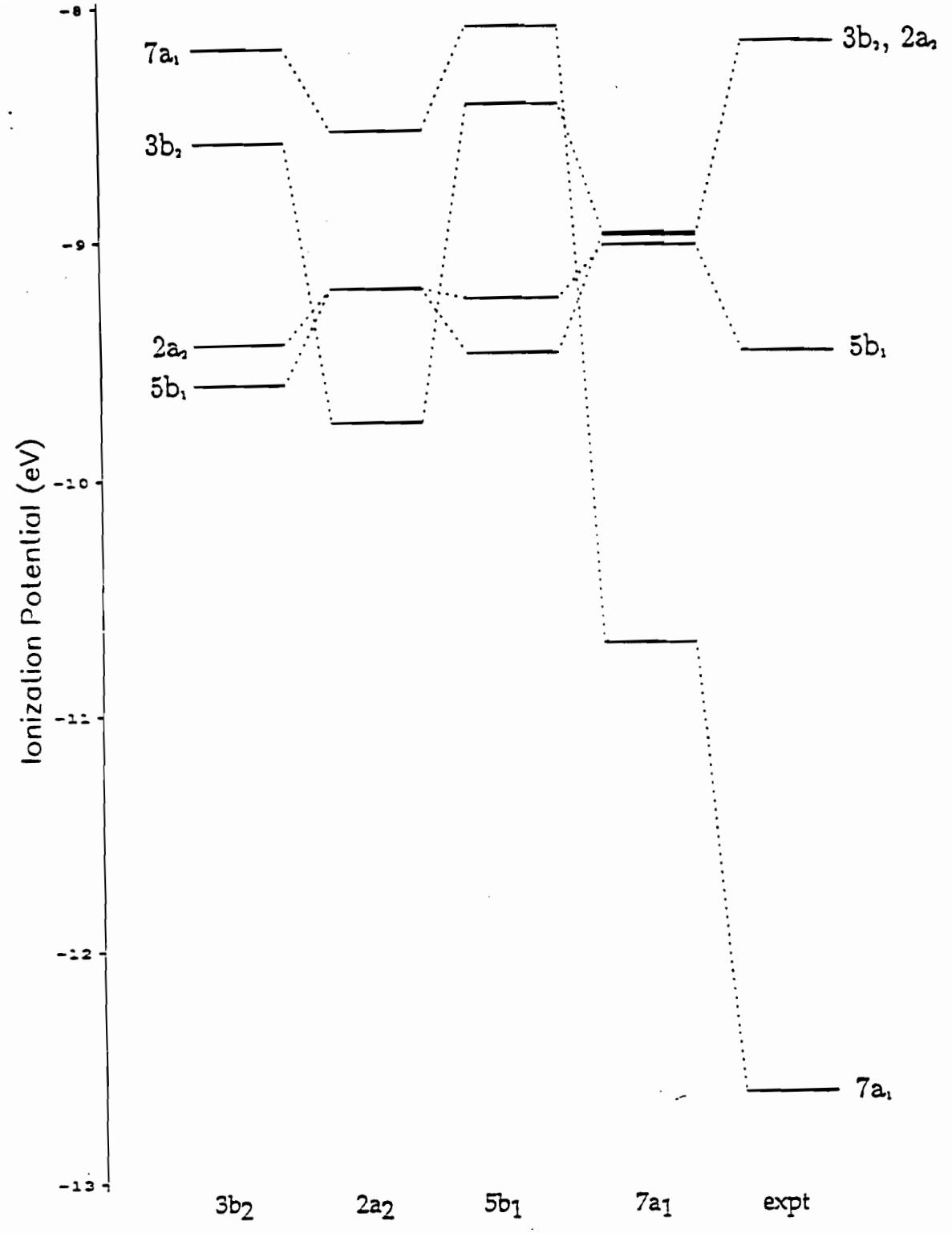

Figure 3. Ionization potentials, eV, of the four highest occupied levels of 2-imidazolidinethione, using the VWN potential and extended partial wave basis. States shown on the horizontal axis refer to which state was half-occupied for the transition state calculation.

Table 2. Transition-state IP of 2-imidazolidinethione, using VWN with large partial wave basis. Comparison of separate calculation for each level to single calculation on $7a_1$ level (-eV).

	$3b_2$	*each*	$7a_1$	*expt*[a]
$3b_2(\pi)$	8.58	8.97	8.58	8.15
$2a_2(\pi)$	9.43	8.98	9.20	8.15
$5b_1(n)$	9.60	9.02	9.24	9.46
$7a_1$	8.18	10.69	10.69	12.6

Table 3. 2-imidazolinenone ionization potentials, several methods compared (-eV).

abinitio[a]	CNDO/2[b]	MS – VWN ($7a_1$)[c]	MS – VWN (*each*)	expt[a]
$6.82(\pi_{NCO})$	$12.05(\pi_N)$	9.02	$9.42(\pi_N)$	9.55
$7.76(\pi_N)$	$12.17(\pi_{CO})$	9.62	$10.18(\pi_{NCO})$	9.8
$7.81(n_O)$	$12.93(n_O)$	$9.86(n_O)$	$10.90(\sigma)$	10.16
$12.13(\sigma_{CO})$	$16.32(\sigma_{CO})$	$10.90(\sigma)$	$11.10(n_O)$	13.6

(a). Andreocci, 1980*a*

(b). Andreocci, 1980*b*

(c). Where no assignment of level is listed, it is the same as the following column.

Table 4. 2-imidazolidinethione ionization potentials, several methods compared (-eV).

abinitio[a]	CNDO/2[b]	CNDO/S[c]	MS – VWN ($7a_1$)	MS – VWN (*each*)	expt[a]
4.06(n_S)	9.78(π_{NCS})	9.14(n_S)	8.97	8.58(π_{NCS})	8.15
4.09(π_{CS})	9.71(n_S)	9.25(π_{CO})	8.98	9.20(π_N)	8.15
8.72(π_N)	12.95(π_N)	11.98(π_N)	9.02	9.24(n_S)	9.46
9.59(σ_{CS})	13.73(σ_{CS})	13.37(σ_{CS})	10.69	10.69(σ)	12.6

(a). Andreocci, 1980*a* (b). Andreocci, 1980*b* (c). Guimono, 1974

Table 5. 2-imidazolineselenone ionization potentials, several methods (eV).

CNDO/2[a]	MS – VWN ($7a_1$)[b]	MS – VWN (*each*)[c]	expt[a]
9.40(n_{Se})	8.54(π_{NCSe})	9.14(π_N)	7.45
9.52(π_{NCSe})	8.57(π_N)	9.47(n_{Se})	7.74
13.16(π_N)	9.26(n_{Se})	9.57(π_{NCSe})	9.47
13.78(σ_{CSe})	11.15(σ)	11.15(σ)	12.1

(a). Andreocci, 1980*a* (b). Where no assignment of level is listed, it is the same as the following column.
(c). In this work, π_N is $2a_2$; $\pi_{NCX}, 3b_2$; $n_X, 5b_1$; $\sigma, 7a_1$ (X is O, S or Se).

Table 6. Core ionization potentials, eV, for the nitrogen 1*s* level in 2-imidazolidinethione and its S and Se analogues, and the S 2*p* and Se 3*p* levels, by several calculation methods and experiment.

	Xα		VWN		CNDO/2[a]	*ab initio*[a]	EHT[a]	expt[a]
	min l	large l	min l	large l				
N 1*s*, O	397.5	398.9	393.6	393.9	393.9	393.3	394.3	393.9
N 1*s*, S	398.0	399.3	394.1	394.8	395.9	395.6	396.6	395.9
N 1*s*, Se	398.2	399.7	394.3	395.2	396.2	·	·	396.2
S 2*p*	169.9	170.6	168.7	169.0	159.1	161.0	159.6	159.1
Se 3*p*	159.1	159.7	158.9	159.3	·	·	·	161.2

(a). Andreocci *et al.* (1980)

Table 7. Xα, VWN and experimental nitrogen nuclear quadrupole coupling constants $e^2 q_{ii} Q/h$ $(i = z, y, x)$ for each of the ethyleneurea analogues (MHz).

	Xα		VWN		experiment[a]
	min 1	large 1	min 1	large 1	
2 – imidazolinenone					
zz	-5.309	-4.105	-4.904	-3.569	3.989
yy	3.129	3.140	2.940	2.850	*
xx	2.180	0.965	1.965	0.720	*
η	0.179	0.530	0.199	0.597	0.262
θ	8	20	8	20	
2 – imidazolidinethione					
zz	-5.043	-3.792	-4.638	-3.366	3.624
yy	3.471	3.517	3.267	3.229	*
xx	1.572	0.275	1.372	0.137	*
η	0.376	0.855	0.409	0.919	0.322
θ	10	16	10	15	
2 – imidazolidineselenone					
zz	-5.053	-4.177	-4.653	-3.648	
yy	3.388	3.763	3.176	3.427	
xx	1.664	0.403	1.477	0.221	
η	0.341	0.807	0.365	0.879	
θ	10	16	10	14	

(a). Krause and Whitehead, 1973

Table 8. Electronic contributions to the coupling constants $e^2 q_{ii} Q/h$ $(i = z, y, x)$ by state for 2-imidazolinenone, large l (MHz). The total N p-orbital contribution (normalized to 1) is indicated by % N p.

state	% N p		zz		yy		xx	
	Xα	VWN	Xα	VWN	Xα	VWN	Xα	VWN
$2a_2$	82	78	4.60	4.36	-9.19	-8.72	4.59	4.36
$2b_2$	20	20	1.18	1.04	-1.98	-1.71	0.79	0.67
$3b_2$	40	40	2.20	2.15	-4.29	-4.17	2.08	2.03
$3b_1$	48	48	0.79	0.73	3.07	2.99	-3.87	-3.72
$4b_1$	40	38	-4.23	-4.07	2.57	2.37	1.66	1.70
$4a_1$	46	46	-1.04	-0.96	2.69	2.65	-1.65	-1.70
$5a_1$	7	6	-0.70	-0.54	0.51	0.43	0.19	0.12
$6a_1$	38	38	-1.90	-2.15	2.39	2.42	-0.48	-0.27
total:			0.90	0.56	-4.23	-3.74	3.31	3.19
overall total:			-0.32	-0.57	0.10	0.63	0.22	-0.06
nuclear:			1.29		-4.20		2.92	
net:			0.97	0.72	-4.10	-3.57	3.14	2.85

Table 10. Atomic charges. C_1 is the carbon bonded to the exocyclic atom; C_2 refers to the carbons at the back side of the ring. Atoms in parentheses next to H identify those to which the hydrogen is bonded.

	Xα		VWN	
	min 1	large 1	min 1	large 1
O	8.70	8.42	8.68	8.37
C_1	5.34	5.45	5.33	5.43
N	7.19	6.95	7.17	6.91
H(N)	0.82	0.92	0.82	0.92
C_2	5.80	5.69	5.80	5.69
H(C)	1.04	1.11	1.05	1.13
S	16.62	16.37	16.64	16.40
C_1	5.53	5.60	5.52	5.58
N	7.10	6.91	7.08	6.87
H(N)	0.80	0.92	0.80	0.91
C_2	5.80	5.75	5.81	5.76
H(C)	1.04	1.14	1.05	1.16
Se	34.69	34.47	34.72	34.48
C_1	5.59	5.62	5.57	5.58
N	7.09	6.92	7.07	6.86
H(N)	0.80	0.91	0.80	0.90
C_2	5.79	5.73	5.79	5.75
H(N)	1.03	1.13	1.04	1.16

Table 9. Electronic contributions to the coupling constants $\epsilon^2 q_{ii} Q/h$ $(i = z, y, x)$ by state for 2-imidazolidinethione, large l (MHz). The total N p-orbital contribution (normalized to 1) is indicated by % N p.

state	% N p		zz		yy		xx	
	Xα	VWN	Xα	VWN	Xα	VWN	Xα	VWN
$2a_2$	80	77	4.84	4.60	-9.64	-9.17	4.80	4.57
$2b_2$	38	35	2.09	1.89	-3.77	-3.40	1.68	1.52
$3b_2$	17	18	0.93	0.95	-1.79	-1.84	0.86	0.89
$3b_1$	46	44	1.04	0.75	2.91	2.74	-3.95	-3.49
$4b_1$	41	38	-4.70	-4.50	2.67	2.49	2.03	2.02
$4a_1$	38	42	-0.07	-0.19	2.21	2.45	-2.13	-2.28
$5a_1$	22	18	-2.25	-1.94	1.34	1.12	0.91	0.82
$6a_1$	22	26	-1.50	-1.89	1.61	1.75	-0.11	0.14
total:			0.36	-0.35	-4.45	-3.83	4.10	4.18
overall total:			-1.13	-1.30	0.49	0.91	0.64	0.39
nuclear:			1.41	1.41	-4.28	-4.28	2.87	2.84
net:			0.28	0.14	-3.79	-3.37	3.52	3.23

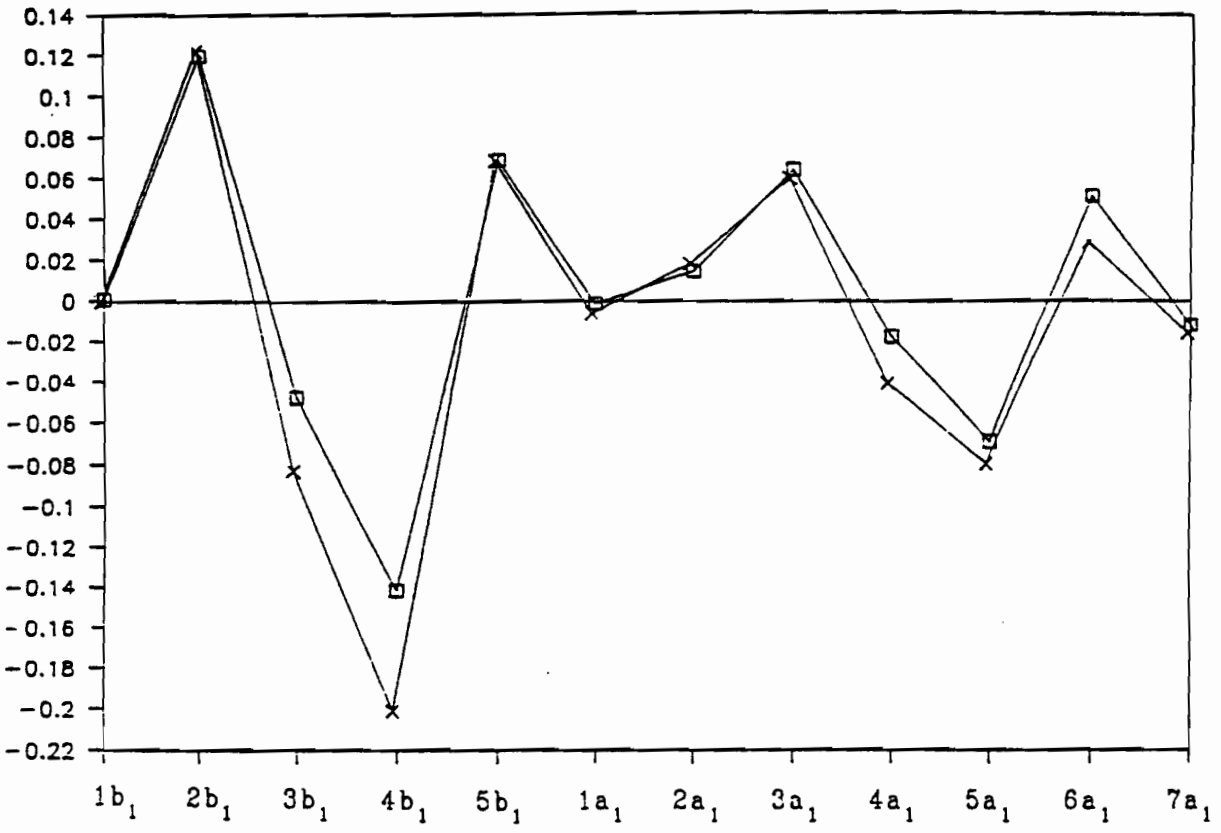

Figure 4. Difference in the contribution to the nuclear quadrupole coupling constant $e^2q_{zz}Q/h$, indicated by $\sqcap$, together with the difference in % p population on nitrogen, indicated by $\times$, between the Xα and VWN calculations. Values on the vertical axix are both MHz and % p, those on the horizontal axis are particular irreducible representations.

Table 11. Dipole moments, debye, for 2-imidazolidinenone and its S and Se analogues, by four methods: Xα and VWN potentials, minimum and extended (large) partial wave bases.

	Xα		VWN	
	min l	large l	min l	large l
O	5.25	2.36	4.42	1.31
S	8.17	1.59	7.79	1.10
Se	8.25	4.34	8.09	2.61

Table 12. Major partial-wave populations for the $4b_1$, $3b_1$ and $2b_1$ states of 2-imidazolidinethione, Xα and VWN calculations with large basis.

state	description	Xα	VWN
$4b_1$	N p	0.406	0.380
	C p	0.250	0.250
$3b_1$	N p	0.464	0.438
	C p	0.346	0.292
$2b_1$	C s	0.375	0.346
	H $s+p$	0.360	0.320

Table 13. Total π populations, after charge partitioning, for the N–C=X fragment, from the VWN large basis calculation.

	O	S	Se
C	0.72	0.76	0.76
N	1.44	1.37	1.37
X	1.71	1.81	1.84

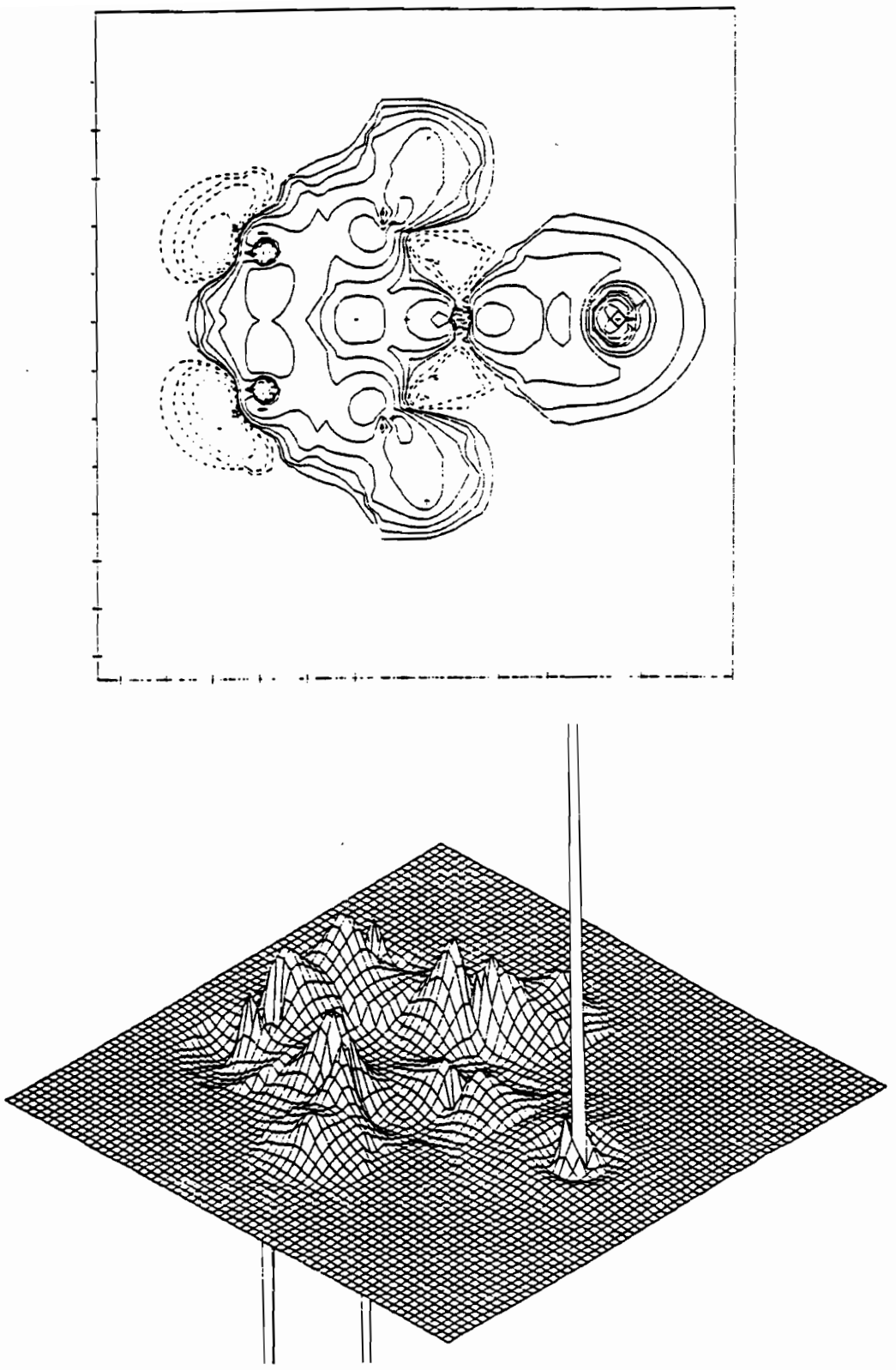

Figure 5a. Total electron density difference, between Xα and VWN calculations, for 2-imidazolidinethione, in the plane of the molecule. Nuclear positions are marked '+', and the orientation is as in Figure 1, with the sulfur atom on the right. The contour plot and the 3-dimensional plot below it represent the same information. Plots 5a - 5e are all drawn at the same scale.

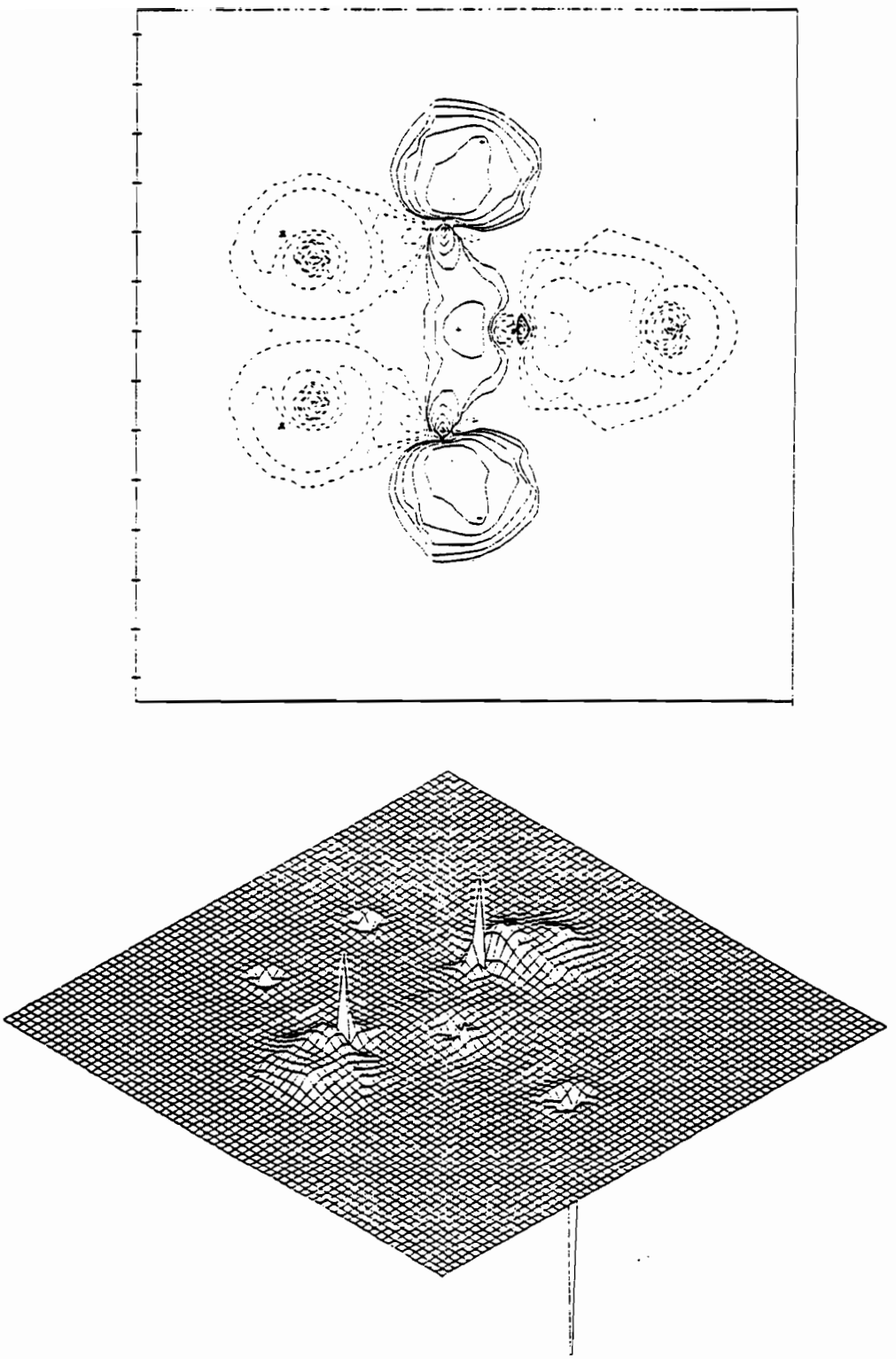

Figure 5b. $2a_1$ electron density difference, between Xα and VWN calculations, for 2-imidazolidinethione, in the plane of the molecule.

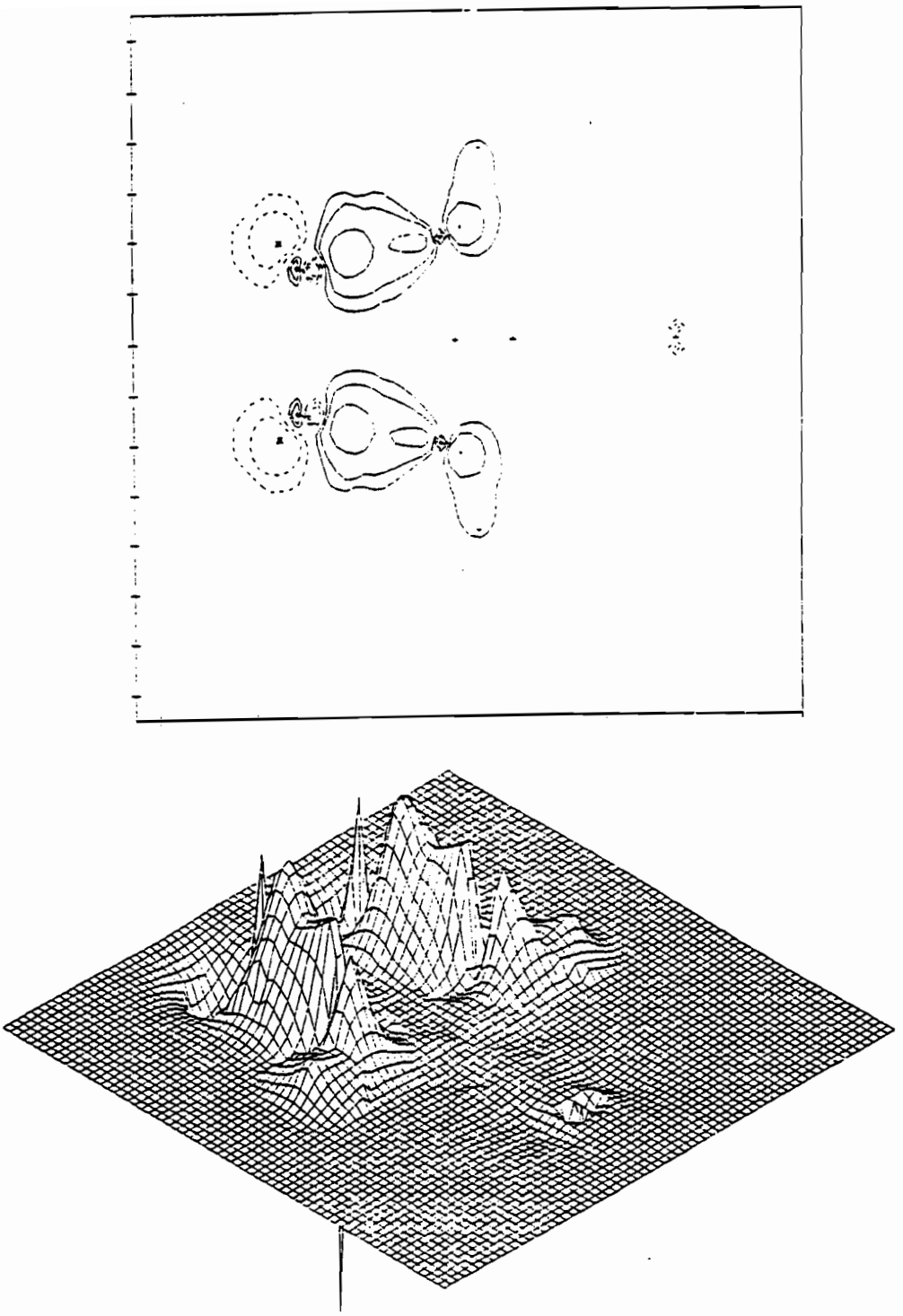

Figure 5c. $4b_1$ electron density difference, between Xα and VWN calculations, for 2-imidazolidinethione, in the plane of the molecule.

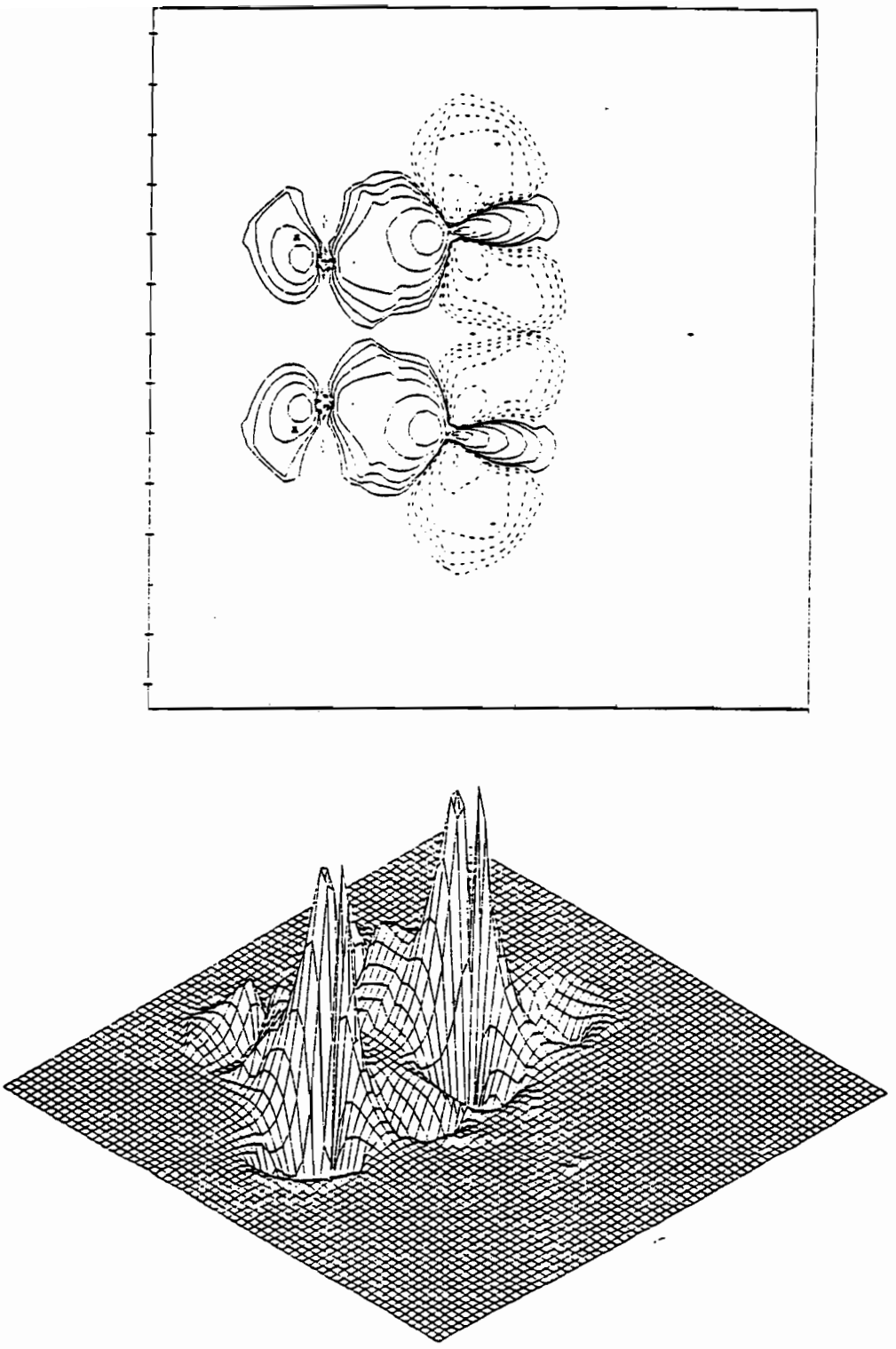

Figure 5d. $3b_1$ electron density difference, between Xα and VWN calculations, for 2-imidazolidinethione, in the plane of the molecule.

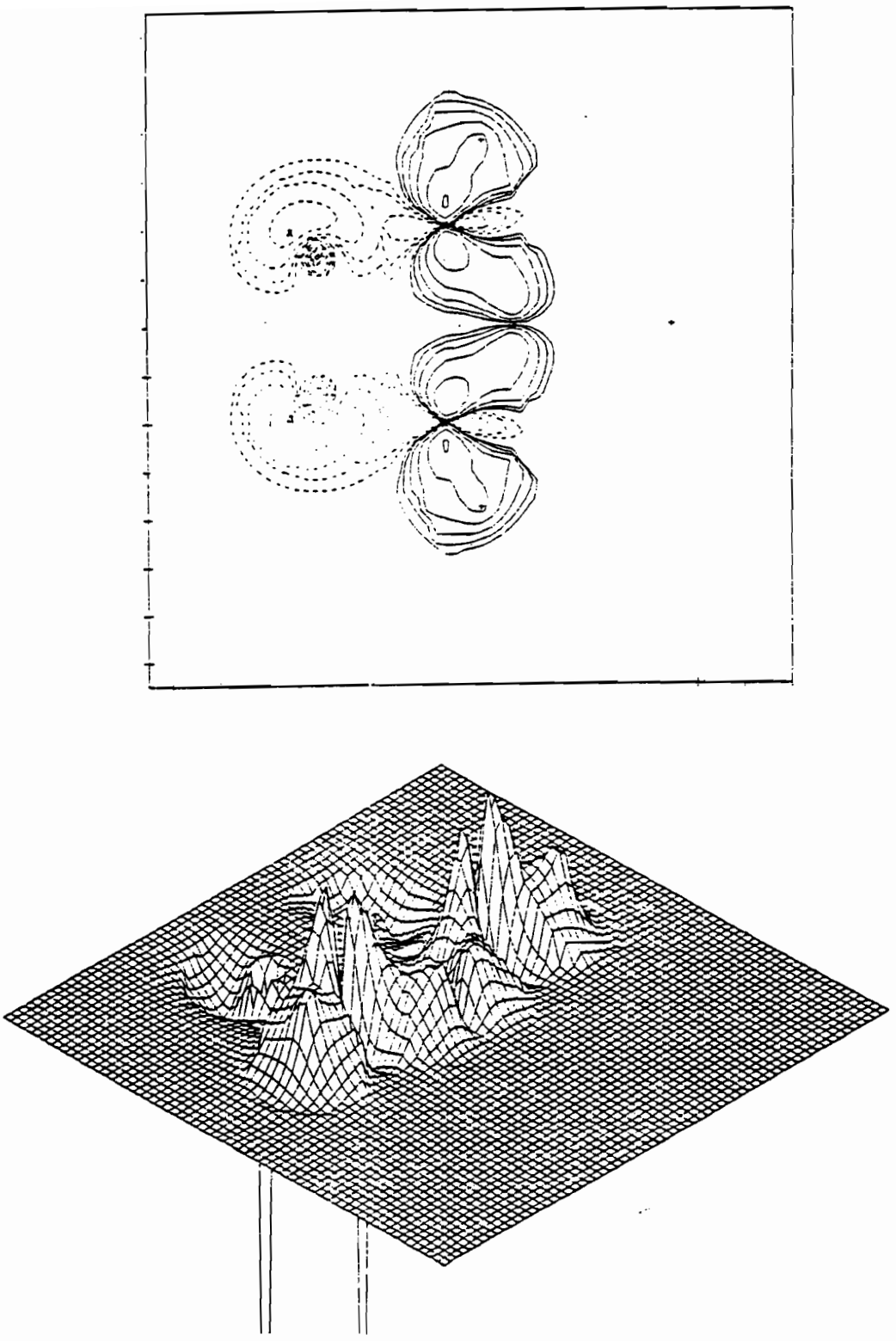

Figure 5e. $2b_1$ electron density difference, between Xα and VWN calculations, for 2-imidazolidinethione, in the plane of the molecule.

References.

Andreocci, M. V., M. Bossa, F. A. Devillanova, C. Furlani, G. Mattogno, G. Verani and R. Zanoni, 1980a, J. Mol. Struct. **69**, 151

Andreocci, M. V., M. Bossa, F. A. Devillanova, C. Furlani, G. Mattogno, G. Verani and R. Zanoni, 1980b, J. Mol. Struct. **71**, 227

Arratia-Perez, R. and G. L. Malli, 1986, J. Chem. Phys. **85**, 6610

Array, Y. and J. Murgich, 1989, J. Chem. Phys. **91**, 293

Berksoy, E. M. and M. A. Whitehead, 1988, J. Chem. Soc., Faraday Trans. 2 **84**, 1707

Bossa, M., C. Furlani, G. Mattagno and R. Zanoni, 1981, Gazz. Chim. It. **111**, 1

Bowmaker, G. A. and P. D. W. Boyd, 1987, J. Chem. Soc., Faraday Trans. 2 **83**, 2211

Bowmaker, G. A., P. D. W. Boyd and R. J. Sorrenson, 1985a, J. Chem. Soc., Faraday Trans. 2 **80**, 1125

Bowmaker, G. A., P. D. W. Boyd and R. J. Sorrenson, 1985b, J. Chem. Soc., Faraday Trans. 2 **81**, 1023

Bowmaker, G. A., P. D. W. Boyd and R. J. Sorrenson, 1985c, J. Chem. Soc., Faraday Trans. 2 **81**, 1627

Carlin, R. L. and S.L.Holt,Jr., 1963, Inorg. Chem. **2**, 849

Case, D. A. and M. Karplus, 1976, Chem. Phys. Lett. **39**, 33

Case, D. A., M. Cook and M. Karplus, 1980, J. Chem. Phys. **73**, 3294

Case, D. A., M. Cook, 1981, Quantum Chemistry Program Exchange Bulletin **1**, 98

Devillanova, F. A., C. Furlani, G. Mattogno, G. Verani and R. Zanoni, 1979, J. Inorg. Nucl. Chem. **41**, 1111

Devillanova, F. A., C. Furlani, G. Mattogno, G. Verani and R. Zanoni, 1981, Gazz. Chim. It. **110**, 19

Gopinathan, M. S., 1979, J. Phys. B: At. Mol. Phys. **12**, 521

Guimono, C. and G. Pfister-Guillouzo, 1974, Tetrahedron **30**, 3831

Krause, L. and M. A. Whitehead, 1973, Mol. Phys. **25**, 99

Kromhaut, R. A. and W. G. Moulton, 1955, J. Chem. Phys. **23**, 1673

Kuncher, N. C. and M. R. Truter, 1958, J. Chem. Soc., 2551

Lucken, E. A. C., 1969, *Nuclear Quadrupole Coupling Constants* (Academic Press. London, 1969)

Norman, J. G., 1976, Mol. Phys. **31**, 1191

Preston, H. J. T., J. J. Kaufman, J. Keller, J. B. Danese and J. W. D. Connolly, 1976, Chem. Phys. Lett. **37**, 55

Rutherford, R. S. and C. Calvo, 1969, Z. Krist. **128**, 229

Sato, T., Y. Takahashi and K. Yabe, 1969, Bull. Chem. Soc. Jap. **42**, 3

Schwarz,k, 1972, Chem. Phys. **10**, 345

Takahashi, Y. and K. Yabe, 1968, Bull. Chem. Soc. Jap. **40**, 298

Townes, C. H. and B. P. Dailey, 1949, J. Chem. Phys. **17**, 325

Tse, J. S., Z. F. Liu, J. D. Bozek, and G. M. Bancroft, 1989, Phys. Rev. A **39**, 1791

Von Niesson, W., G. H. F. Diercksen and L. S. Cederbaum, 1975, Chem. Phys. **10**, 345

Vosko, S. H., L. Wilk and M. Nusair, 1980, Can. J. Phys. **58**, 1200

Wheatley, P. J., 1953, Acta Cryst. **6**, 369

Krause, L. and M. A. Whitehead, 1973, Mol. Phys. **25**, 99

Kromhaut, R. A. and W. G. Moulton, 1955, J. Chem. Phys. **23**, 1673

Kuncher, N. C. and M. R. Truter, 1958, J. Chem. Soc., 2551

Lucken, E. A. C., 1969, *Nuclear Quadrupole Coupling Constants* (Academic Press. London, 1969)

Norman, J. G., 1976, Mol. Phys. **31**, 1191

Preston, H. J. T., J. J. Kaufman, J. Keller, J. B. Danese and J. W. D. Connolly, 1976, Chem. Phys. Lett. **37**, 55

Rutherford, R. S. and C. Calvo, 1969, Z. Krist. **128**, 229

Sato, T., Y. Takahashi and K. Yabe, 1969, Bull. Chem. Soc. Jap. **42**, 3

Schwarz,k, 1972, Chem. Phys. **10**, 345

Takahashi, Y. and K. Yabe, 1968, Bull. Chem. Soc. Jap. **40**, 298

Townes, C. H. and B. P. Dailey, 1949, J. Chem. Phys. **17**, 325

Tse, J. S., Z. F. Liu, J. D. Bozek, and G. M. Bancroft, 1989, Phys. Rev. A **39**, 1791

Von Niesson, W., G. H. F. Dierckson and L. S. Cederbaum, 1975, Chem. Phys. **10**, 345

Vosko, S. H., L. Wilk and M. Nusair, 1980, Can. J. Phys. **58**, 1200

Wheatley, P. J., 1953, Acta Cryst. **6**, 369

1.3.4 Supplementary Material

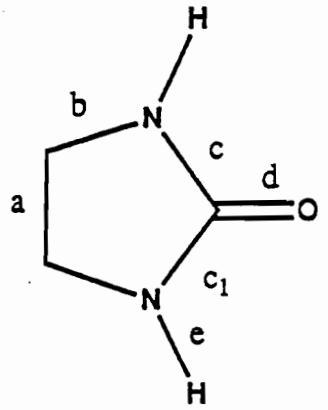

a = 1.54
b = 1.46
c = 1.33
d = 1.26
e = 1.00

$\angle$ a b = 102°
$\angle$ b c = 112°
$\angle$ c d = 126°
$\angle$ c c_1 = 110°
$\angle$ c_1 e = 124°

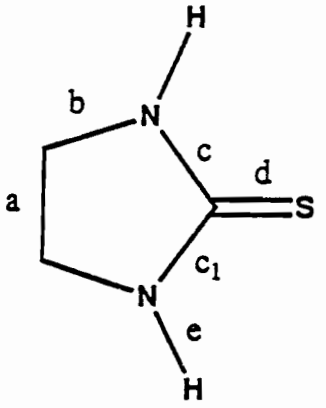

a = 1.54
b = 1.46
c = 1.32
d = 1.71
e = 1.00

$\angle$ a b = 102°
$\angle$ b c = 112°
$\angle$ c d = 126°
$\angle$ c c_1 = 110°
$\angle$ c_1 e = 124°

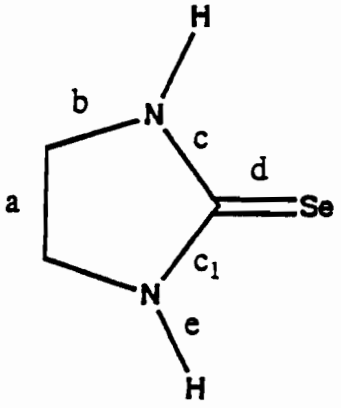

a = 1.54
b = 1.46
c = 1.32
d = 1.86
e = 1.00

$\angle$ a b = 102°
$\angle$ b c = 112°
$\angle$ c d = 126°
$\angle$ c c_1 = 110°
$\angle$ c_1 e = 124°

Figure A1. Bond distances and angles used in the calculations for 2-imidazolidinenone, 2-imidazolidinethione and 2-imidazolidineselenone.

Table A1. One-electron eigenvalues, au, for 2-imidazolinenone valence levels, calculated by the MS-LDA method with Xα and VWN exchange-correlation functionals at minimum ("low") and extended ("large") partial wave bases.

state	xa low	xa high	vwn low	vwn high
$7a_1$	-0.520885	-0.435400	-0.521303	-0.425524
$2a_2$	-0.426671	-0.422366	-0.442350	-0.430772
$3b_2$	-0.446755	-0.454418	-0.480911	-0.478329
$5b_1$	-0.449290	-0.462134	-0.486526	-0.488515
$2b_2$	-0.711174	-0.690952	-0.731536	-0.702211
$6a_1$	-0.719154	-0.751221	-0.740398	-0.756131
$4b_1$	-0.807612	-0.783441	-0.808700	-0.771667
$1a_2$	-0.970452	-0.929878	-0.939943	-0.867727
$5a_1$	-0.933633	-0.924287	-0.947434	-0.928184
$1b_2$	-1.135651	-1.067207	-1.110615	-1.013979
$3b_1$	-1.055013	-1.132340	-1.059349	-1.120026
$2b_1$	-1.327540	-1.275082	-1.308712	-1.233771
$4a_1$	-1.296532	-1.322427	-1.303574	-1.320469
$3a_1$	-1.341455	-1.363895	-1.358858	-1.344767
$2a_1$	-1.538224	-1.475540	-1.527032	-1.461535
$1b_1$	-1.744429	-1.759902	-1.748326	-1.753361
$1a_1$	-1.973882	-1.964366	-1.980129	-1.959659

Table A2. One-electron eigenvalues, au, for 2-imidazolidinethione valence levels, calculated by the MS-LDA method with Xα and VWN exchange-correlation functionals, at minimum ("low") and extended ("high") partial wave bases.

state	Xa min l	Xa high l	VWN min l	VWN high l
$7a_1$	-0.520890	-0.435402	-0.521302	-0.425518
$2a_2$	-0.426682	-0.422365	-0.442345	-0.430759
$3b_2$	-0.446755	-0.454418	-0.480871	-0.478328
$5b_1$	-0.449288	-0.462135	-0.486480	-0.488517
$2b_2$	-0.711181	-0.690952	-0.731521	-0.702203
$6a_1$	-0.719155	-0.751221	-0.740366	-0.756124
$4b_1$	-0.807620	-0.783441	-0.808696	-0.771655
$1a_2$	-0.970454	-0.929881	-0.939945	-0.867720
$5a_1$	-0.933636	-0.924288	-0.947411	-0.928179
$1b_2$	-1.135653	-1.067210	-1.110616	-1.013973
$3b_1$	-1.055021	-1.132339	-1.059339	-1.120014
$2b_1$	-1.327543	-1.275084	-1.308710	-1.233763
$4a_1$	-1.296540	-1.322426	-1.303565	-1.320458
$3a_1$	-1.341454	-1.363897	-1.358817	-1.344763
$2a_1$	-1.538227	-1.475542	-1.527022	-1.461530
$1b_1$	-1.744437	-1.759900	-1.748318	-1.753347
$1a_1$	-1.973889	-1.964365	-1.980117	-1.959646

Table A3. One-electron eigenvalues, au, for 2-imidazolidineselenone calculated by the MS-LDA method, with Xα and VWN exchange-correlation functionals at minimum ("low") and extended ("large") partial wave bases.

state	Xα low	Xα high	vwn low	vwn high
$7a_1$	-0.537100	-0.476655	-0.539937	-0.438006
$2a_2$	-0.428290	-0.444049	-0.445786	-0.449792
$3b_2$	-0.421711	-0.421194	-0.464194	-0.464853
$5b_1$	-0.421230	-0.421289	-0.466342	-0.468532
$2b_2$	-0.701164	-0.694519	-0.722826	-0.705968
$6a_1$	-0.698700	-0.717323	-0.724876	-0.735527
$4b_1$	-0.821364	-0.822345	-0.824956	-0.793653
$1a_2$	-1.006954	-1.014420	-0.979206	-0.899317
$5a_1$	-0.949527	-0.941286	-0.966804	-0.938138
$1b_2$	-1.169138	-1.144931	-1.146420	-1.041868
$3b_1$	-1.064725	-1.175145	-1.070866	-1.162950
$2b_1$	-1.354978	-1.342521	-1.338061	-1.263279
$4a_1$	-1.271744	-1.276429	-1.301909	-1.308088
$3a_1$	-1.319792	-1.382431	-1.328066	-1.362900
$2a_1$	-1.554975	-1.511463	-1.542209	-1.452652
$1b_1$	-1.755026	-1.797380	-1.760307	-1.791326
$1a_1$	-1.979776	-1.996018	-1.987353	-1.993149

I.3.5 Electronic Structure, Ultraviolet Transition Energies and Quadrupole Couplings of the Planar Heterocycles 2,1,3-benzoxadiazole, 2,1,3-benzothiadiazole and 2,1,3-benzoselenadiazole by the MS-LDA Method

Abstract

Multiple-scattering local-density-approximation (MS-LDA) calculations, using both the Xα and VWN exchange-correlation functionals, were performed on the planar heterocycles 2,1,3-benzoxadiazole and its sulphur and selenium analogues. Ionization energies, first excited (ultraviolet) transition energies, dipole moments and nuclear quadrupole coupling constants were computed. The experimental photoelectron spectrum of the selenium compound was assigned. The influence of correlation and basis set size on these properties was examined. Partial wave population analysis was performed to help resolve ambiguities in the resonance structures.

Introduction

The electronic structure of the π system, of 2,1,3-benzoxadiazole and its sulfur and selenium analogues is interesting because many possible canonical forms can be generated:

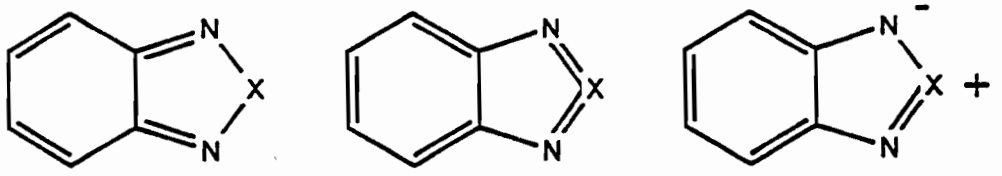

I II III

(Weinstock and Shinkai, 1984). Additional ionic forms have been proposed:

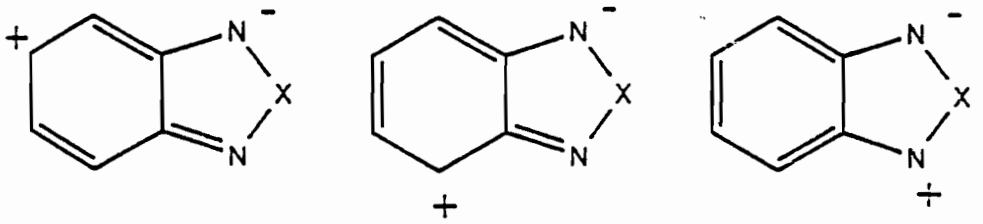

IV V VI

(Krause and Whitehead, 1973). Structure I shows the common representation of the series; by analogy to quinone, it is called the *ortho*–quinoide form.

Much experimental work has investigated the relative importance of the structures above. If the *o*–quinoide form predominates, there will be double-bond fixation and diene-like reactivity; otherwise, benzenoid characteristics should be observed. Evidence of both has been found, and none of the structures pictured is consistent with all of the data.

Nuclear magnetic resonance spectra were interpreted (Cheeseman and Turner, 1974) as caused by through-bond interactions, showing the importance of I and III. Dipole moment measurements (Hill and Sutton, 1949) suggested a more benzene-like structure for the Se compound compared to the O and S analogues, while x-ray results, in contrast (Luzzati, 1951), suggested that the O compound had the most benzene character.

The importance for ground and excited-state spectra of both the overall π electron distribution, and the lone pairs on the nitrogens or the terminal heteroatom, were addressed by several semiempirical studies (Kamiya, 1970; Grunwell and Danison, 1972; Clark *et al.*, 1973; Bylina and Korobkov, 1974; Abu-Eittah *et al.*, 1986) and *ab initio* (Palmer and Kennedy, 1978) calculations. Other interesting properties of the substituted versions of 2,1,3-benzothiadiazole have been reported: they act as

radioprotective agents in organisms to reduce the damaging effects of exposure to ionizing radiation (Vladimirov *et al.*, 1983). The mechanism is not understood, but activity was correlated to electronic structure. The compounds also serve as ligands in transition-metal complexes (Kaim and Kohlmann, 1985, 1989), coordinated through the N atom.

Because the Multiple Scattering Local Density Approximation method has been succesful in treating electronic structure and properties in planar heterocycles (Case *et al.*, 1980; Wrinn and Whitehead, 1990), calculations by this method were performed to investigate some of the electronic structure ambiguities presented by the 2,1,3-benzoxadiazole series. Also, features of the method itself were tested by varying both the size of the partial wave basis, and the choice of exchange-correlation potential.

Computational Details

Experimental equilibrium geometries were used for all three compounds, figure 1. There are conflicting sets of geometry data for 2,1,3-benzoxadiazole and 2,1,3-benzothiadiazo. Luzzati (1951) used x-ray crystallography, while Brown *et al.* (1970) interpreted microwave spectra, which involved making simplifying assumptions about the 6-membered ring angles; the x-ray values were used in this study.

The Norman (1976) criterion, with a reduction factor of 0.88, was used to determine the atomic sphere radii. The outer sphere origin was placed on the C_2 symmetry axis at the point which minimized the total outer-sphere volume; the outer sphere radius was chosen to be slightly less (0.2 au) than the radius tangent to the outermost atomic sphere. Values for the sphere radii, along with percentage overlap of N–O (or N–S, N–Se), and the percentage of intersphere volume, are shown in Table 1. The muffin-tin sphere radii are shown in three dimensions in figure 2, where both the

extent of overlap among the atomic spheres, and the size of the constant-potential intersphere region is evident.

Calculations were performed with both a minimum basis of partial waves, with l values only as large as the occupied atomic levels and $l = 3$ on the outer sphere, and a larger basis where each l value is increased by 1. Both the Xα (with Schwartz (1972) α values) exchange-only functional and the Vosko-Wilk-Nusair (1980) exchange-correlation functional were used.

Ionization potentials (IP) were calculated for the valence levels using transition-state method , where half an electron is removed from the level of interest. Excited-state absorptions were also calculated by the transition- state method, where one-half an electron is removed from the lower level, and one-half electron placed in the higher level of the absorbance transition. In all cases, the SCF iterations were converged until below 10^{-5} in the potential.

Nuclear quadrupole coupling constants for the nitrogen atom were found from the one-electron properties program of Case and Cook (1981). The program yields electric field gradient tensor components q_{ij} in molecule coordinates; these were converted to principle-axis components q_{ii} using standard LINPACK (Dongerra *et al.*, 1979) routines, and the q_{ii} converted to coupling constants $e^2 q_{ii} Q/h$ assuming a nitrogen quadrupole moment Q of 1.6×10^{-26} cm^2 (von Niesson *et al.*, 1975).

Results and Discussion

1. *One-electron eigenvalues and charge distributions.*

In an earlier study, Palmer and Kennedy (1978) compared calculated one-electron energies across a series such as

$$\text{isobenzofuran} \rightarrow \text{anthranil} \rightarrow \text{furazan}(2,1,3-\text{benzoxadiazole})$$

for the oxygen heteroatom and a similar series for the S case. They examined the one-electron energy trend as a function of the number of nitrogen adjacent to the heteroatom: no nitrogen, one, or two. The results showed that the one-electron levels decreased uniformly for nearly all levels as more N atoms were introduced.

In this study, in contrast, the number of N atoms remained fixed at two, and the terminal heteroatom was changed from O to S to Se. The three compounds are isoelectronic in the valence levels, and have nearly identical energy ordering of the eigenvalues. Differences among the three are to be expected, however, from the large electronegativity differences among the three atoms O (electronegativity of 3.5 on the Pauling (1960) scale), S (2.5) and Se (2.4). Properties directly influenced by electronegativity differences would show similarities between the S and Se compounds, which together differ from the O heterocycle.

The one-electron eigenvalues for the occupied and first two excited states, calculated by low and high partial wave bases, and Xα and VWN exchange– correlation functionals, are shown in Table 2 for 2,1,3-benzoxadiazole; for the S analogue in Table 3, and for the Se compound in Table 4.

A superficial inspection of the orbital energies shown in Tables 2, 3 and 4 reveals no obvious trend, corresponding to electronegativites or otherwise. The 2,1,3-benzothiadiazole $2a_2$ (HOMO) level, for example, is closer to the $2a_2$ of the oxygen

compound than it is to that of the selenium (0.399, 0.394 and 0.378 au, for the S, O and Se cases, respectively, for the VWN large basis calculation). To distinguish trends, it is necessary to look more closely at individual cases.

The $1b_1$ (π) level corresponds to the traditional concept of a π bond between the heteroatom O, S or Se and the two adjacent nitrogen. The partial wave populations of N and the heteroatom p for the VWN high case are shown in Table 5. No other individual atom contributes a significant population to this state, which provides the basis for structure **II**, the benzenoid form with double bonds between the heteroatom and both nitrogen.

Because the $1b_1$ level is a direct interaction between the heteroatom and the adjacent nitrogen, its one-electron energy trends unambiguously follows electronegativity trends over the three compounds: the eigenvalues are -1.097 au for 2,1,3-benzoxadiazole, and -0.847 and -0.803 au for the S and Se analogues, respectively. The greater electronegativity of the oxygen atom is mirrored in the lower one-electron energy; the similarities between sulfur and selenium atom electronegativities, slightly less for Se, is also reflected in their $1b_1$ values. The pattern here follows the observation by Hout *et al.* (1984), that an electronegative element will serve to lower the orbital energy .

Gross population trends for the $1b_1$ levels also follow closely on electronegativities. Table 6 shows the total heteroatom populations in each compound, as calculated by the large basis with VWN correlation. The values given are the percentage of the total, for a given level, contributed by all the partial waves centred on that nucleus and within the atomic sphere; it does not include any contribution from charge partitioning the intersphere or outer sphere regions. The total populations for this level are in the Table 0.523, 0.239 and 0.205 for the O, S and Se compounds, respectively – the trend observed in the eigenvalues.

For other levels, the correspondance between population and electronegativity is not shown so directly. The symmetry orbitals calculated in this study are delocalized, and take their nodal properties from the irreducible representation to which they belong (Cotton, 1971); unlike the $1b_1$ case cited above, they do not, in general, correspond to chemical bonds.

Some relationships are still recognizable, however, between the total charges shown in Table 6 and the one-electron levels given in Tables 2, 3 and 4. In the remaining π levels, in particular, the charges and eigenvalues follow one another closely: in the $2b_1$ level, there is increasing heteroatom charge in going from oxygen (0.082) to sulfur (0.200) to selenium (0.340). The corresponding one-electron eigenvalues are -0.651, -0.604, and -0.589, following the trend observed for $1b_1$ of decreasing eigenvalue for increasing heteroatom charge. For the $3b_1$ level, the sulfur atom takes more charge than do the oxygen and selenium (0.175 versus 0.057 and 0.003, respectively), and the eigenvalues follow the pattern in that the 2,1,3-benzothiadiazole eigenvalue is raised with respect to the other two (-0.467 versus -0.475 and -0.476). However, the heteroatom charges in this case are much smaller than in $1b_1$ and $2b_1$, so the correlation between charge and eigenvalue is less strong. The $1a_2$ level, also π, shows a similar correlation, though likewise reduced by the reduced total charge on the O, S or Se. In the remaining π level, $2a_2$, the heteroatom contribution is so insignificant (0.003, 0.006 and 0.003 for O, S and Se) that it cannot influence the one-electron level; this π (LUMO) level has most of its population on the benzene ring.

A few of the remaining states ($6a_1$, $8a_1$ and $7b_2$) follow this pattern, of increasing heteratom charge giving a decreased eigenvalue, but they do not do so in an interpretively useful way. The delocalized symmetry molecular orbitals are useful in interpreting delocalized π levels, and when the heteroatom participates in the π

state, its charge distribution and electronegativity are important.

The effect of correlation on these levels may be seen by comparing the Xα and VWN values at the same basis size. Table 2 shows the VWN eigenvalues to be uniformly lower (more negative) than the corresponding Xα values, in the range of 0.010 to 0.015 au. This is consistent with both the pattern discussed above and with earlier findings: correlation drives charge out of high density regions (Wrinn and Whitehead, 1990), and a more dispersed charge gives lower one-electron eigenvalues.

The effect of the partial wave basis size is more pronounced: the larger basis yields higher eigenvalues, shifted by as much as 0.070 au (for example, the $2b_1$ for both Xα and VWN in 2,1,3-benzoxadiazole). The shifts downward induced by correlation, and the shift upward by larger partial wave basis, are consistent in all three compounds, as shown in Tables 3 and 4.

2. *Ionization Potentials*

Two conventions are practiced with regard to calculating transion-state ionization potentials (IP) with density functional methods: more rigorously, the half electron is removed from the level being calculated, and the resulting one-electron energy is identified with the ionization potential of that level. Removing half an electron has been shown to be equivalent to removal of spurious self-interaction energy (Gopinathan, 1979), and gives results closer to experimental IPs than do Hartree-Fock one-electron energies. The other convention is to remove the half-electron from the highest-occupied level, and assume that all other states have relaxed to their transition-state values, i.e., only one transition-state calculation is done.

The latter method was examined critically by Wrinn and Whitehead (1990), who found that the approximation may not always be valid, and that further, if the approximation were made to use only one transition-state calculation, the best

choice was to remove the half electron from the highest *fully-symmetric* state, rather than the highest occupied.

Figure 3 shows calculated IPs for 2,1,3-benzoxadiazole, using the VWN large basis, with the half electron removed successively from the highest a_1, b_2, b_1 and a_2 levels. The highest 17 valence levels are shown; the figure shows very little difference among the four calculations. The only significant shift is in the $7b_2$ level (the highest b_2); when it is the state with half an electron, it moves downward enough to cross below the neighboring $10a_1$.

The effect of choice of level for the transition-state calculation is shown in further detail in figure 4, where the highest 6 valence states of 2,1,3-benzoxadiazole are shown, along with experimental values. Even at the expanded scale of this figure, no important difference is seen between the $2a_2$, $3b_1$ and $10a_1$ columns. The calculated IPs are shifted higher than the experimental ones, and except for the crossing of the $2b_1$ level, follow the same order.

Table 7 shows the results for 2,1,3-benzoxadiazole transition-state ionization potentials, as calculated with the large partial wave basis and VWN correlation functional. Two columns of values are given for this calculation: the IPs as calculated for each state individually (marked "each" in the Table), and those resulting from a single transition-state calculation of the highest a_1 level (marked "$10a_1$"). Earlier *ab initio* results, and experiment, are also shown.

The two sets of IPs, the individual ones and those approximated from the $10a_1$ calculation, are remarkably close for almost every level. Except for an interchange of the $1b_1$ and $6a_1$, the ordering of levels in each is identical. This behavior is in sharp contrast to the 2-imidazolidinone series of planar heterocycles (Wrinn and Whitehead, 1990), and means that the single a_1 transition-state calculation is a good approximation for this series.

Accordingly, IPs for the other two compounds in the present study were done with the half electron removed from the $10a_1$ level. Table 8 shows the results, along with *ab initio* and experimental values, for 2,1,3-benzothiadiazole. Table 9 gives the IPs from the present study, and experimental values, for 2,1,3-benzoselenadiazole. For both Tables 8 and 9, the values given are for VWN large basis, $10a_1$ transition state.

The calculated ionization potentials are not simply shifted by a constant amount from the one-electron eigenvalues. For example, the 2,1,3-benzoxadiazole $2a_2$ IP is -8.0 eV, while the one-electron energy is -10.7 eV, a shift of 2.7 eV. In contrast, the $2b_1$ values are -17.7 eV and -11.6 eV for the eigenvalue and transition-state IP, respectively, for a shift of 5.1 eV. Nor is the shift by a constant percentage; the two values cited are shifted by 25% and 35%, respectively, of the one-electron energy.

Many researchers using the Multiple-Scattering method, especially for calculations on large systems, have practiced the economy of identifying the one-electron energies with the ionization potentials; the assumption was made that each state would be shifted in energy by a nearly constant amount (e.g. Salahub, 1978; Eyermann and Chung-Phillips, 1984). The present study shows that this assumption is not always valid.

The ordering of IPs is nearly identical for the O, S and Se compounds over the entire valence range, as can be seen in Tables 7, 8 and 9. The only exception to this agreement is the reversal of the $1a_2$ and $2b_1$ energy orders on going from 2,1,3-benzoxadiazole to the sulfur analogue; the $1a_2$ is higher than the $2b_2$ by 0.4 eV in the O compound, whereas that order is reversed for both the S and Se compounds. This reversal is mirrored by the atomic populations of the terminal heteroatom for these states, shown in Table 6. The $1a_2$ population from oxygen atom is 0.122; it drops to 0.026 and 0.011 for S and Se, respectively. The $2b_1$ population, on the other hand, is 0.082 for O, but 0.197 and 0.340 for the S and Se. This pattern is

the same as observed for the π one-electron energies: increased charge contribution from the heteroatom corresponds to an raising of the energy of that level.

The experimental IPs were measured by photoelectron spectroscopy (PES) for 2,1,3-benzoxadiazole and 2,1,3-benzothiadiazole by Clark *et al.* (1973), who used the semi-empirical PPP (Pariser and Parr, 1953) method to aid in assigning peaks and interpreting band shapes. The PES experiments on these compounds, together with the Se compound, were repeated by Palmer and Kennedy (1978); they used a Gaussian *ab initio* calculation with a minimal basis set to make the peak assignments.

While there was general agreement between the two studies, they disagreed on the third band of both 2,1,3-benzoxadiazole: Clark assigned it to a nitrogen lone pair, while Palmer's study assigned it to the $1a_2$ (π) level. Table 7 shows the MS-LDA third IP as $1a_2$, with very good numeric agreement with experiment (11.2 eV for the transition-state value, versus 11.5 for experiment), thus confirming the *ab initio* assignment of Palmer and Kennedy.

The present results differ with Palmer's, however, in the ordering of the fourth ionization potential of 2,1,3-benzoxadiazole. The *ab initio* result was $7b_2$, a nitrogen lone pair (N^-). The present study found the fourth level to be $2b_1$, a π level. The ordering of the two nitrogen lone pairs was also different in this study: the fifth level is $10a_1$ (N^+), the sixth ($7b_2$ (N^-)). This disagreement held also for the sulfur compound; as shown in Table 8, the *ab initio* result placed $7b_2$ as the 3rd-highest level, while the present results put $7b_2$ in the 6th position, with π levels occupying the four highest ionization potentials. As mentioned earlier, the IP orderings were identical for the S and Se compounds, so 2,1,3-benzoselenadiazole also has the four highest levels as π, and the $10a_1$ (N^+ nitrogen lone pair) higher than the $7b_2$ (Table 9).

The relative positioning of the nitrogen lone pairs with respect to the π levels is im-

portant in determining the role of σ interaction with a metal, when this compound serves a ligand (Wrinn and Whitehead, 1991). The relative ordering of the symmetric and antisymmetric nitrogen lone pairs, N^+ and N^-, is important in gauging the relative strength of nitrogen interaction through the intervening C-C bond; a higher energy for N^+ would indicate a stronger through-bond coupling (Clark *et al.*, 1973.

The multiple-scattering local-density-approximation method has proven to be reliable in predicting ionization potentials (Johnson, 1977; Case, 1982). The ordering of nitrogen lone pairs and π levels is consistent in this study over all three compounds, despite very different Norman sphere overlaps between the nitrogen and the heteroatom (Table 1). These results suggest that the previous assignments of these levels need to be reconsidered; in light of the renewed interest in these compounds (Kaim *et al.*, 1989), a more rigorous calculation should be done to resolve the discrepancies.

3. *Excited States*

Excited state transitions were measured in the gas phase for 2,1,3-benzothiadiazole (BTD) by Hallas and Wright (1969), who assigned the experimental peaks as $^1A_1 \rightarrow {}^1A_1$,a strong peak at 306 nm, and $^1A_1 \rightarrow {}^1B_2$ a much weaker peak at 328 nm. This transition is therefore $\pi \rightarrow \pi^*$, polarized on the in-plane axis.

The authors argued that the 328 nm transition was localized on the 6-membered ring, since little change was observed in the coarse vibrational structure upon replacement of sulfur by oxygen or selenium.

Gordon and Yang (1971) repeated these measurements on single crystals, obtaining the same results. They did further measurements on deuterium-substituted versions of BTD, and concluded that the 328 nm transition could not be simply that of

perturbed benzene: the isotopic shift per deuterium atom was less then half of that of benzene itself. This led these workers to stress the dominance of the "o-quinoid" structure (**1**) over the resonance structure (**2**)

A further set of measurements were done by Abu-Eittah *et al.* (1985), who augmented their study with SCF-CI calculations, and discussed the interpretation in terms of $\pi \rightarrow \pi^*$ and $n \rightarrow \pi^*$ transitions. Transitions were identified as $A_1 \rightarrow B_2$, a B_1 transition polarized along the short axis of the molecule (perpendicular to the symmetry axis), and $A_1 \rightarrow A_1$,

In this work, the excited state transition energies were determined in two ways: by taking the difference between one-electron eigenvalues, and by Slater's transition state method. Using differences in eigenvalue energies is not strictly valid; the orbital eigenvalues are shifted from being the unrelaxed (Koopman's Theorem) one-electron energies by the incorrect inclusion of self-interaction, as discussed earlier. However, taking a difference between two levels can result in cancellation of errors; the eigenvalues are often simply shifted upwards (to less negative energies) compared to the transtion state energies, retaining the same ordering and relative spacing.

The transition state method for excited states removes half an electron from the ground state level, and places half an electron in the excited level; the excitation energy is then the difference between the two transition state eigenvalues (Johnson, 1977).

The valence levels in the ground state of each of the C_{2v}, closed-shell compounds in this series are $(a_2)^4(b_1)^8(b_2)^{14}(a_1)^{20}$, A_1. The ground state should be a singlet $^1A_1$, but because spin-polarized calculations were not considered in this study, they will not be referred to in the discussion. Values for the ground state one-electron eigenvalues are given in tables 4.5, 4.6 and 4.7, along with eigenvalues for the two lowest unoccupied molecular orbitals (LUMO). Because the LUMO belongs to the b_1

irreducible representation, a HOMO-LUMO transition results in a B_2 state (Cotton, 1971), that is a $A_1 \rightarrow B_2$ transition.

4. *Nitrogen Nuclear Quadrupole Coupling Constants*

Two of the compounds in this series, the S and Se analogues, were studied by solid-state Nuclear Quadrupole Resonance (NQR) spectroscopy (Krause and Whitehead, 1973), which measured room-temperature quadrupolar resonances of the N atom. Analysis of results in that case proceeded from assumptions about the hybridization (chosen to be sp_2 on the N) and position of the in-plane principle electric-field gradient axis (chosen parallel to the N lone pair). The N lone pair angle was chosen within a Townes and Dailey model (1949) to satisfy both the known reactivities and dipole moment, for the case of O, or the NQR and electron spin resonance (ESR) results, in the case of Se. It was concluded for 2,1,3-benzothiadiazole that electron density was delocalized; structures **IV** - **VI** must contribute some (unspecified) amount to account for reactivity, and structure **II** is necessary to reduce the lone pair occupancy on N to satisfy the NQR and dipole moment results. For the Se compound, structures were assigned specifically as **IV**, 20%, **VI**, 20%, and **II**, 10%.

Results for the MS-LDA calculations of N NQR coupling constants, asymmetry parameters, in-plane principle axis angles and the experimental results, are given in Table 4.4. With regard to the choice of method (low and high partial wave bases, Xα and VWN exchange- correlation potentials), the pattern follows that found in the imidazolidine series: more reliable results are given by the larger-basis calculation, the Xα and VWN values for the principle moment q_{zz} bracket those of experiment, and the asymmetry parameter η is not well predicted. The q_{zz} is correctly predicted to be perpendicular to the plane of the molecule, and the calculated values (for the VWN large basis) compare well to experiment: 3.62 versus 3.42 MHz for the S compound, 3.71 versus 3.41 for the Se. Equally important to

the numeric agreement is the trend: the two q_{zz} values are very similar for both calculated and experiment. The calculated results for the O compound predict a much higher q_{zz} value, 5.12 MHz, than in the S and Se analogues; the experimental value is expected to follow this trend.

Unlike the imidazolidine series studied earlier (Wrinn and Whitehead, 1990), in the present compounds the N atom is directly bonded to only two other atoms; the in-plane principle axis q_{yy} is thus identified with a N lone pair rather than a bond direction. The "lone pair" angle θ is shown in Table 12; it is the rotation angle required to diagonalize the electric field gradient tensor in the molecular coordinate frame (Lucken, 1969), and indicates the direction of the q_{yy} principle component. The θ values for the O compound are smaller than for the other two: 71° in the VWN large basis, compared to 79° and 77° for the S and Se compounds, respectively. In all cases θ is pointed slightly further away from the terminal heteroatom X than would be the case for a simple $\angle$ X N C bisector. The angle θ (and thus q_{yy}) points significantly more toward the heteroatom in the O case, and is nearly the same in the S and Se compounds; this trend is in conformity with the higher O, and close S and Se, electronegativity values.

5. *HOMO-LUMO partial wave populations.*

The behaviour of these compounds as reactants, or as ligands in transition-metal compounds will be sensitive to the π electronic structure; π levels comprise both the highest occupied molecular orbital (HOMO), $2a_2$, and the lowest unoccupied (LUMO), $4b_1$. The atomic partial wave contributions to these states is shown in Table 13 (for the HOMO) and Table 14. The scattered-wave method allows unambiguous assignment of the population of atomic partial waves for a particular molecular orbital, and thus removes the need for any assumptions, about hybridization.

In Tables 13 and 14, the labels C_1, C_2 and C_3 refer to the three symmetry-unique carbon atoms, starting from the end of the molecule (C_3 is the closest to the N atom). Because these are π levels, only the p and d partial wave contributions are shown. In the HOMO, $2a_2$, there is no p contribution from the terminal heteroatom; this level is dominated in all three molecules by π interactions between the benzene portion and the nitrogen atom.

In the low partial-wave basis, the HOMO is dominated by the p population on C_2; when d waves are included, C_2 gains almost no d population, but C_1 and C_3 gain d contributions on the order of 2–3% in each molecule, whether the Xα or VWN hamiltonian. The larger basis also decreases overall population on N: from 19.9 to 16.8 % in 2,1,3-benzoxadiazole, by similar amount in the S compound, and from 16.3 to 11.3% in the Se case. The larger basis increases the population on on C_3: from 5.1 to 8.9% in 2,1,3-benzoxadiazole (VWN), from 2.5 to 6.5% in the S compound, and from 2.3 to 6.1 in the Se analogue. The overall effect of the larger basis set is a smoothing of the orbital density, reducing the population on the two most popoulated atoms (C_2 and N), while increasing it on the others.

There is esentially no difference in these partial wave populations between the Xα or VWN results; they are either identical, as in the Se compound, or differ by a few tenths of a percent.

Chemically, there is agreement again with the heteroatom electronegativity series: C_1 in the O compound contributes 14% p character, while C_1 in the S and Se compounds contributes 21 and 20%, respectively. The N atom has a higher overall population, 16.8%, in the O compound than in the other two, 11.5 and 11.3%, respectively. The O compound is different from the other two analogues, which are similar to one another.

The LUMO partial wave populations, Table 14, are characterized by a large p

population on the N atom, and significant p contributions from the other atoms in the ring. Only the N is sensitive to the change from low to high partial wave basis: the p contribution drops from 47.9 to 40.2% in 2,1,3-benzoxadiazole, from 51.9 to 42.7% in the S analogue, and from 44.9 to 38.0% in the Se compound. The C atom p populations are unchanged by the change of basis, and the terminal heteroatom p contribution is slightly reduced. The larger basis does, however, change the net population on each atom through a d-wave contribution; the C_3 atom, adjacent to the N, is particularly sensitive, gaining 4% in each molecule.

As in the HOMO, LUMO populations are unaffected by correlation: the largest difference between the Xα and VWN populations is 0.8% in the S and Se atoms; the other atoms shift by only 0.1%.

The C_2 and C_3 populations follow the pattern of the O compound being different from the S and Se: C_2 contributes 13.8% to the LUMO in 2,1,3-benzoxadiazole, but only 3.0 and 4.2%, respectively, in the S and Se analogues. The C_3 total population is 10.7% in the oxygen compound, but 23.9 and 31.3% in the S and Se compounds. The populations of C_1 and N, in contrast, were similar in each of the compounds, while the heteroatom π population was similar between O and S, 15.3 and 17.2%, but different for Se, 7.5%. The important overall quality of the LUMO is the availability, for reactions, of an empty π orbital concentrated on the nitrogen atom but with significant delocalization over the entire ring.

5. *Dipole Moments*

Molecular dipole moments, calculated by minimum and large partial wave bases, and Xα and VWN functionals, are in Table 15, along with experimental values. The basis set size was extremely important to reproducing the correct trend in the values, with O > S > Se. The minimum basis set calculation, unlike experiment, showed little difference between the S and Se compound values; the value

for the O compound was erroneous: 1.24 D for 2,1,3-benzoxadiazole compared to 2.59 D for the sulphur analogue, when experimentally the O compound has a dipole moment more than twice the magnitude of the 2,1,3-benzothiadiazole. The large partial wave basis agrees with the trend of the experiment: a large dipole moment on 2,1,3-benzoxadiazole, a smaller one on 2,1,3-benzothiadiazole, and a still smaller dipole moment on the Se analogue. The absolute numeric agreement is not good: the calculated value underestimates the 2,1,3-benzoxadiazole dipole moment by 0.5 D, overestimates the S compound value by 1.0 D, and underestimates the Se compound by 1.2 D, enough to reverse the direction of the dipole with respect to experiment. Including correlation through the VWN functional resulted in small but not systematic changes in the larger basis calculation: the O compound was unchanged, the S compound was shifted by 0.6 D away from experiment, the Se compound shifted by 0.3 D towards experiment.

Hill and Sutton (1949) interpreted their experimental dipole moments in terms of Pauling electronegativities (Pauling, 1960), which give estimated values of 2.96, 1.76 and 1.64 for the O, S and Se, respectively. While the electronegativity trend, O > S > Se, parallels that observed, their estimated dipole moment of 2,1,3-benzoxadiazole was much less than the experimental, and that of the Se compound was much more. This was attributed to resonance structure **IV**: the negative charge on N would reduce charge buildup on the heteroatom, thus lowering the overall dipole moment), counteracted by structure **II**: more charge is concentrated by the double bonds at the heteroatom end of the structure, thus increasing the dipole moment over that expected by naive electronegativity arguments.

The dipole moment calulated for 2,1,3-benzoxadiazole is higher the electronegativity estimate, and close to the experimental value; this result suggests that ionic resonance structures of type **IV** are not important, and that the double-bond fixation

of type **II** is present.

Conclusions

The π bonding structure was found to correlate well with the electronegativity of the heteroatom. Differential relaxation in Slater transition calculations of IP was found to be minimal, in contrast to that found in a previous study of heterocycles. The experimental IP of the Se compound in this series have been assigned for the first time. One-electron properties, especially quadrupole coupling constants and dipole moments, were much more sensitive to basis set size than to inclusion of a correlation functional. The LUMO, though concentrated on the N atom, was found to be delocalized over the ring, suggesting why these molecules have the flexibility to react with either benzenoid or dienoid character.

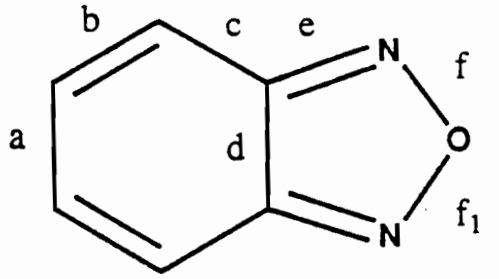

a = 1.43
b = 1.43
c = 1.43
d = 1.43
e = 1.35
f = 1.20

∠ a b = 120°
∠ b c = 120°
∠ c d = 120°
∠ d e = 101°
∠ e f = 113°
∠ f f_1 = 112°

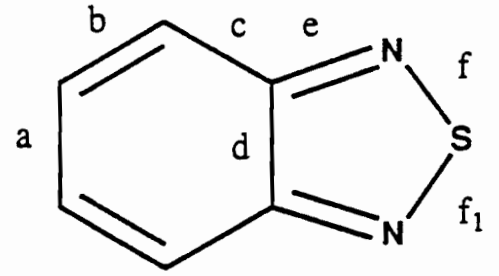

a = 1.42
b = 1.29
c = 1.46
d = 1.41
e = 1.34
f = 1.60

∠ a b = 121°
∠ b c = 120°
∠ c d = 119°
∠ d e = 114°
∠ e f = 105°
∠ f f_1 = 102°

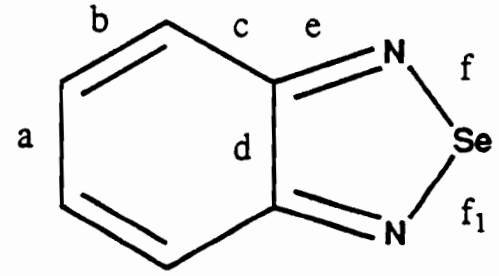

a = 1.42
b = 1.30
c = 1.42
d = 1.46
e = 1.30
f = 1.83

∠ a b = 123°
∠ b c = 118°
∠ c d = 119°
∠ d e = 118°
∠ e f = 104°
∠ f f_1 = 95°

Figure 1. Bond distances and angles used in the calculations for 2,1,3-benzoxadiazole, 2,1,3-benzothiadiazole and 2,1,3-benzoselenadiazole (from Luzzati, 1951)

Table 1. Muffin-tin sphere sizes, N – heteroatom overlaps and percentage of intersphere volume for 2,1,3-benzoxadiazole and its S and Se analogues.

X	R_C	R_C	R_C	R_N	R_X	R_{out}	% N–X overlap	% intersphere
O	1.72	1.72	1.64	1.55	1.46	6.65	33	84
S	1.68	1.68	1.64	1.68	2.11	7.43	25	87
Se	1.67	1.67	1.62	1.71	2.39	7.79	19	87

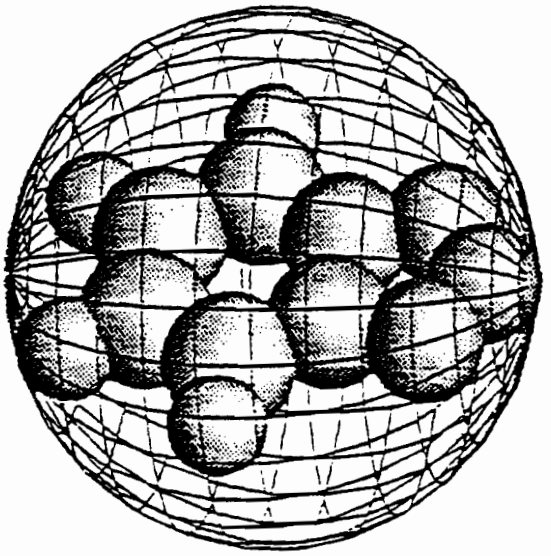

Figure 2. Atomic positions and muffin-tin sphere sizes for 2,1,3-benzothiadiazole. Solid spheres are for atoms, the wire-frame is the outer sphere; orientation is as in Figure 1.

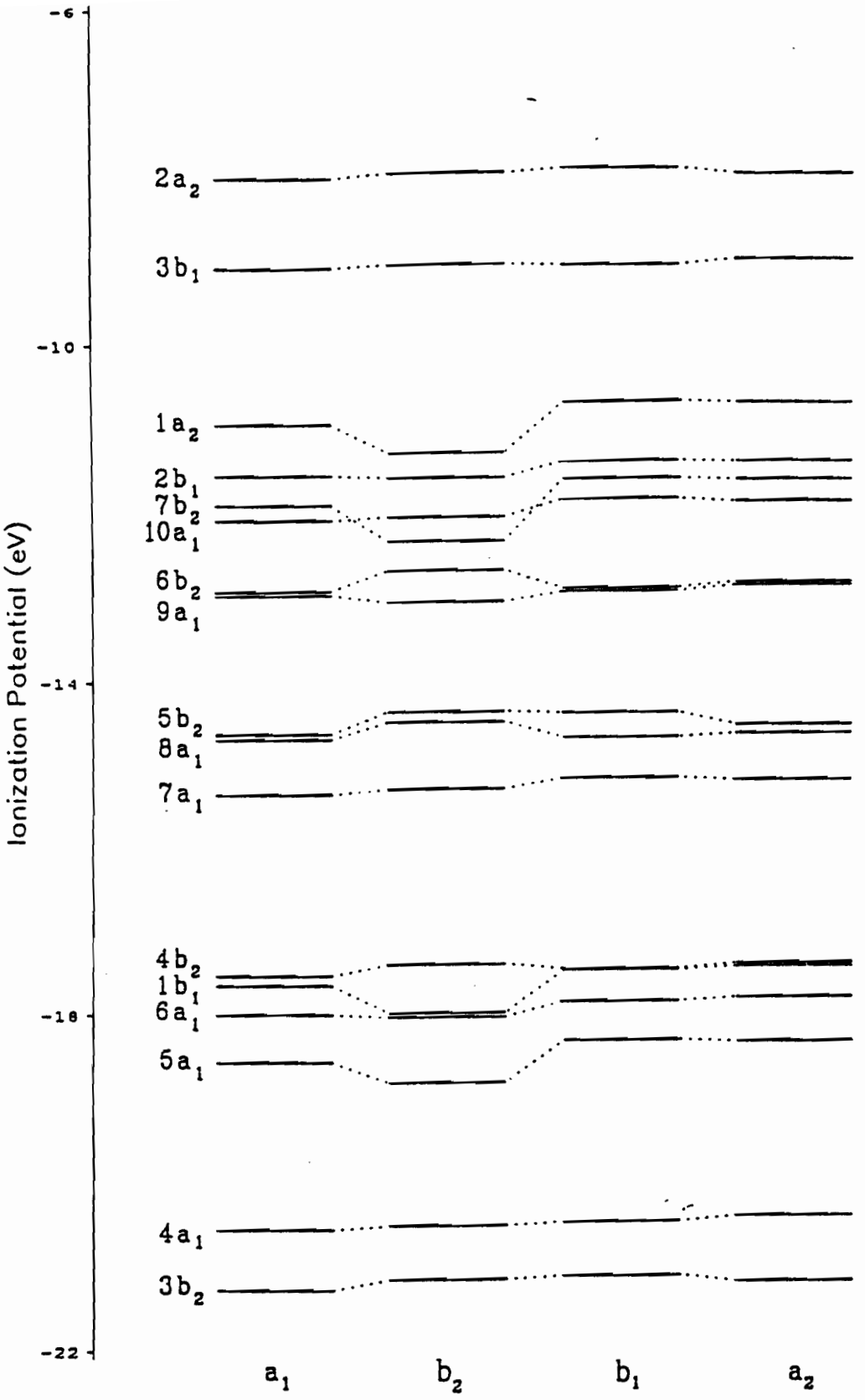

Figure 3. Valence Ionization Potentials, eV, for 2,1,3-benzoxadiazole, calculated by the transition-state method, with VWN exchange-correlation and large partial wave basis. States shown along the horizontal axis indicate the irreducible representation to which half occupancy was assigned.

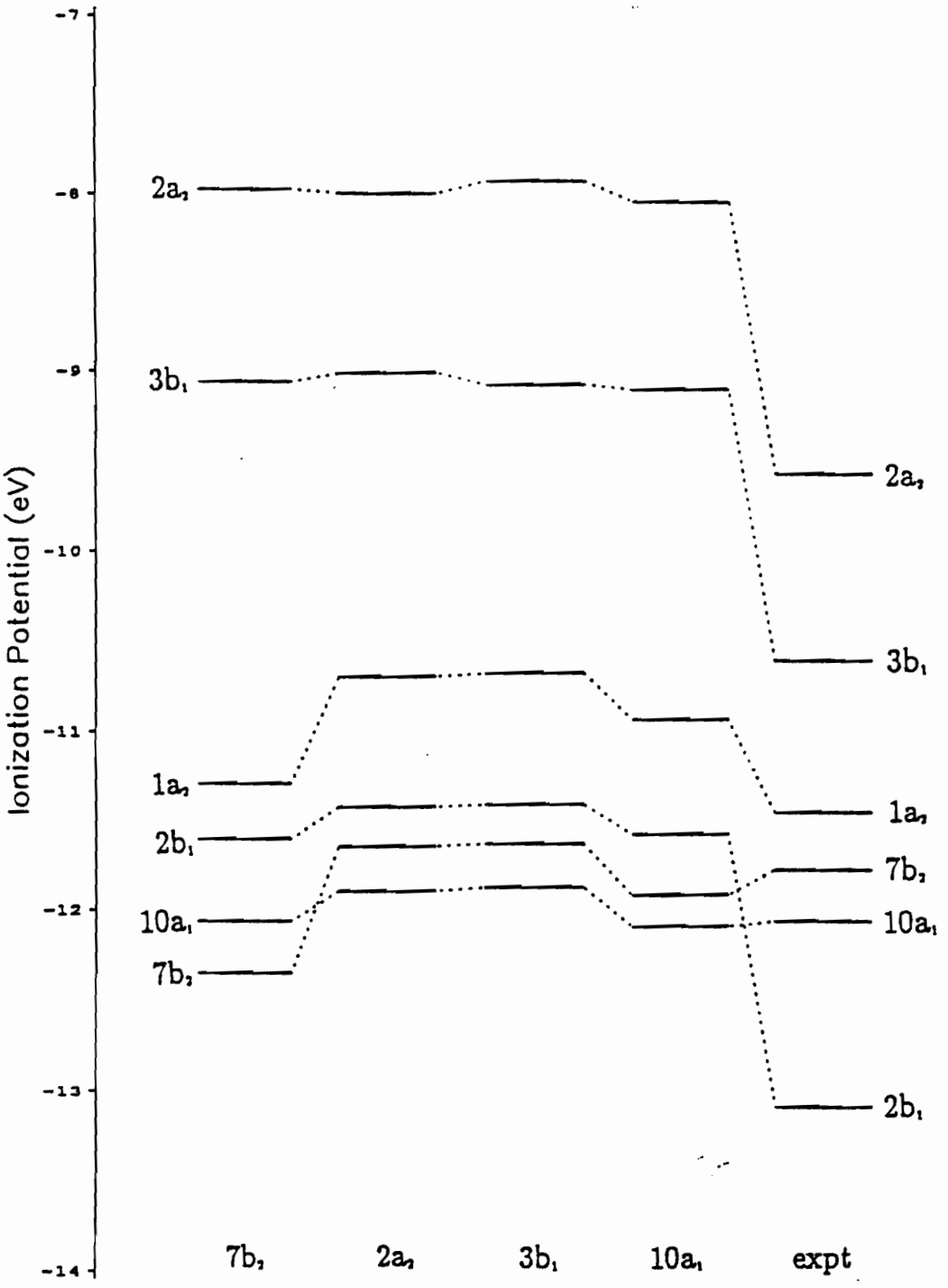

Figure 4. Valence Ionization Potentials, eV, for 2,1,3-benzoxadiazole, for the 6 highest occupied levels, calculated by the transition-state method, with VWN exchange-correlation and large partial wave basis, and experiment. States shown along the horizontal axis indicate the specific level to which half occupancy was assigned.

Table 2. 2,1,3-benzoxadiazole one-electron eigenvalues, au, including the two lowest unoccupied levels, calculated by the MS-LDA method with Xα and VWN exchange-correlation functionals at low and high partial-wave bases. Where the ordering between methods differs, VWN high results take precedence.

state	Xα low	Xα high	VWN low	VWN high
$11a_1$	-0.15154	-0.13277	-0.18804	-0.17062
$4b_1$	-0.24574	-0.20574	-0.26536	-0.22219
$2a_2$*	-0.42804	-0.37389	-0.45135	-0.39403
$3b_1$	-0.51390	-0.45431	-0.53761	-0.47459
$1a_2$	-0.63670	-0.58209	-0.65804	-0.59960
$2b_1$	-0.69989	-0.63015	-0.72386	-0.65072
$6b_2$	-0.77950	-0.65531	-0.78750	-0.66799
$10a_1$	-0.67787	-0.67010	-0.68979	-0.67413
$7b_2$	-0.70940	-0.74660	-0.72622	-0.74308
$9a_1$	-0.78911	-0.74263	-0.80092	-0.74555
$5b_2$	-0.90546	-0.86592	-0.91096	-0.86034
$8a_1$	-0.94444	-0.87024	-0.95582	-0.87212
$7a_1$	-0.97840	-0.90906	-0.99182	-0.91350
$4b_2$	-1.13637	-1.07532	-1.14623	-1.07496
$1b_1$	-1.13360	-1.07975	-1.15558	-1.09731
$6a_1$	-1.15637	-1.11055	-1.17073	-1.11477
$5a_1$	-1.20889	-1.14371	-1.22283	-1.15355
$4a_1$	-1.36970	-1.29631	-1.38020	-1.29829
$3b_2$	-1.41133	-1.34810	-1.42128	-1.34874
$3a_1$	-1.59093	-1.49876	-1.60230	-1.50175
$2b_2$	-1.56416	-1.52089	-1.57696	-1.52585
$2a_1$	-1.82461	-1.76013	-1.83657	-1.76474
$1b_2$	-2.07568	-2.11936	-2.08912	-2.12387
$1a_1$	-2.78697	-2.79432	-2.79978	-2.79837

* Highest occupied molecular orbital (HOMO)

Table 3. 2,1,3-benzothiadiazole one-electron eigenvalues, including the two lowest unoccupied levels, calculated by the MS-LDA method with Xα and VWN exchange-correlation functionals at low and high partial-wave bases. Where the ordering between methods differs, VWN high results take precedence.

state	Xα low	Xα high	VWN low	VWN high
$11a_1$	-0.16553	-0.14546	-0.20495	-0.18335
$4b_1$	-0.25251	-0.23524	-0.27849	-0.25459
$2a_2$*	-0.42621	-0.37849	-0.45203	-0.39949
$3b_1$	-0.49180	-0.44390	-0.52168	-0.46725
$2b_1$	-0.63899	-0.57964	-0.67026	-0.60420
$1a_2$	-0.64053	-0.62373	-0.66568	-0.64170
$10a_1$	-0.66166	-0.65864	-0.67732	-0.66234
$7b_2$	-0.72943	-0.71427	-0.81010	-0.72797
$9a_1$	-0.78982	-0.75911	-0.81263	-0.77315
$6b_2$	-0.79908	-0.83571	-0.75191	-0.79618
$1b_1$	-0.86561	-0.82339	-0.89654	-0.84709
$8a_1$	-0.83721	-0.83571	-0.86259	-0.85210
$5b_2$	-0.91212	-0.86954	-0.92337	-0.86816
$7a_1$	-0.99460	-0.93533	-1.00786	-0.93759
$6a_1$	-1.03842	-0.97275	-1.05945	-0.98221
$4b_2$	-1.06523	-1.04572	-1.08158	-1.04881
$5a_1$	-1.20827	-1.14061	-1.22324	-1.14467
$4a_1$	-1.32324	-1.29048	-1.34172	-1.29655
$3b_2$	-1.30879	-1.32198	-1.33119	-1.33303
$2b_2$	-1.55632	-1.50678	-1.56772	-1.50554
$3a_1$	-1.57043	-1.55037	-1.59125	-1.55688
$2a_1$	-1.71302	-1.65142	-1.72865	-1.65777
$1b_2$	-1.83926	-1.87468	-1.85494	-1.87871
$1a_1$	-2.09768	-2.07307	-2.11904	-2.08296

* Highest occupied molecular orbital (HOMO)

Table 4. 2,1,3-benzoselenadiazole one-electron eigenvalues, including the two lowest unoccupied levels, calculated by the MS-LDA method with Xα and VWN exchange-correlation functionals at low and high partial-wave bases. Where the ordering between methods differs, VWN high results take precedence.

state	Xα low	Xα high	VWN low	VWN high
$11a_1$	-0.17734	-0.14553	-0.21808	-0.18505
$4b_1$	-0.26703	-0.22222	-0.29541	-0.24838
$2a_2$*	-0.43191	-0.35408	-0.45969	-0.37844
$3b_1$	-0.50418	-0.44392	-0.54054	-0.47557
$2b_1$	-0.62426	-0.55290	-0.65944	-0.58916
$1a_2$	-0.67432	-0.62060	-0.70164	-0.64607
$10a_1$	-0.64875	-0.63146	-0.67491	-0.65001
$7b_2$	-0.71197	-0.67848	-0.73864	-0.70379
$9a_1$	-0.77424	-0.71999	-0.79451	-0.73424
$6b_2$	-0.81340	-0.78028	-0.82577	-0.77981
$1b_1$	-0.83661	-0.77109	-0.86844	-0.80338
$5b_2$	-0.94955	-0.86515	-0.96177	-0.86776
$8a_1$	-0.89909	-0.86175	-0.92585	-0.88487
$7a_1$	-1.01953	-0.92264	-1.03526	-0.93391
$6a_1$	-1.07658	-0.97068	-1.09900	-0.98503
$4b_2$	-1.06599	-1.03370	-1.08724	-1.04641
$5a_1$	-1.23313	-1.12413	-1.24974	-1.13359
$3b_2$	-1.27025	-1.19907	-1.29242	-1.22112
$4a_1$	-1.33488	-1.25893	-1.35597	-1.27188
$2b_2$	-1.59149	-1.49327	-1.60377	-1.49507
$3a_1$	-1.51706	-1.49233	-1.54957	-1.52556
$2a_1$	-1.73659	-1.61783	-1.75188	-1.62612
$1b_2$	-1.92366	-1.93497	-1.93959	-1.94539
$1a_1$	-2.06103	-2.04057	-2.08051	-2.05527

* Highest occupied molecular orbital (HOMO)

Table 5. Partial wave composition (percent) for the p waves of nitrogen and the terminal heteroatom X (= O, S or Se) in the $1b_1$ level of 2,1,3-benzoxadiazole and its S and Se analogues, as calculated with the VWN high basis.

	N	X
2,1,3-benzoxadiazole	0.112	0.516
2,1,3-benzothiadiazole	0.156	0.230
2,1,3-benzoselenadiazole	0.163	0.199

Table 6. Total atomic populations in each valence level for the terminal heteroatom in 2,1,3-benzoxadiazole (O), 2,1,3-benzothiadiazole (S) and 2,1,3-benzoselenadiazole (Se), before charge partitioning, as calculated with the VWN large basis.

state	O	S	Se
$2a_2$	0.0031	0.0058	0.0032
$1a_2$	0.1220	0.0263	0.0115
$3b_1$	0.0567	0.1749	0.0031
$2b_1$	0.0825	0.1971	0.3405
$1b_1$	0.5232	0.2390	0.2053
$7b_2$	0.0013	0.0653	0.1250
$6b_2$	0.0308	0.0044	0.0160
$5b_2$	0.0013	0.0012	0.0006
$4b_2$	0.0065	0.0354	0.0745
$3b_2$	0.0200	0.2498	0.2247
$2b_2$	0.0864	0.0136	0.0021
$1b_2$	0.4267	0.1087	0.0214
$10a_1$	0.0300	0.0307	0.1578
$9a_1$	0.0277	0.1746	0.1022
$8a_1$	0.0101	0.4046	0.2518
$7a_1$	0.0643	0.0142	0.0828
$6a_1$	0.3741	0.0680	0.0618
$5a_1$	0.1607	0.0131	0.0036
$4a_1$	0.0741	0.0628	0.0435
$3a_1$	0.0271	0.1853	0.5425
$2a_1$	0.0893	0.1578	0.0429
$1a_1$	0.5734	0.2635	0.0813

Table 7. 2,1,3-benzoxadiazole ionization potentials: *ab initio*, VWN with large partial wave basis, and experiment (eV).

ab initio[a]	assignment	MS-VWN $10a_1$	MS-VWN each	assignment	expt[a]
9.78	$2a_2$	8.04	7.99	$2a_2$	9.58
11.90	$3b_1$	9.11	9.08	$3b_1$	10.62
13.39	$1a_2$	10.94	11.19	$1a_2$	11.46
13.95	$7b_2$	11.57	11.56	$2b_1$	11.78
14.09	$10a_1$	12.10	12.10	$10a_1$	12.07
15.12	$9a_1$	11.92	12.35	$7b_2$	13.10
15.43	$2b_1$	12.99	13.26	$9a_1$	
15.78	$6b_2$	12.94	13.65	$6b_2$	13.91
16.58	$8a_1$	14.63	15.23	$5b_2$	14.38
17.76	$5b_2$	14.70	15.24	$8a_1$	15.47
19.20	$1b_1$	15.35	15.46	$7a_1$	16.38
19.33	$7a_1$	17.53	17.86	$4b_2$	
19.83	$4b_2$	17.65	18.69	$1b_1$	
20.91	$6a_1$	18.00	18.19	$6a_1$	
23.45	$3b_2$	18.57	19.13	$5a_1$	17.50
23.47	$5a_1$	20.56	20.73	$4a_1$	
25.76	$4a_1$	21.28	21.49	$3b_2$	18.8
22.36	$3a_1$	23.31	23.64	$3a_1$	18.84
22.58	$2b_2$	23.77	24.23	$2b_2$	19.79
23.86	$2a_1$	27.00	27.51	$2a_1$	22.94
28.07	$1b_2$	31.91	33.14	$1b_2$	26.01
28.12	$1a_1$	41.03	42.68	$1a_1$	

a. Palmer and Kennedy, 1978

Table 8. 2,1,3-benzothiadiazole ionization potentials: *ab initio*, VWN with large partial wave basis, and experiment (eV).

ab initio[a]	assignment	MS-VWN $10a_1$	assignment	expt[a]
9.14	$2a_2$	8.80	$2a_2$	9.00
10.43	$3b_1$	9.63	$3b_1$	9.55
12.10	$7b_2$	11.43	$2b_1$	10.71
12.51	$1a_2$	11.78	$1a_2$	11.32
12.84	$10a_1$	12.41	$10a_1$	
14.09	$2b_1$	12.90	$7b_2$	12.83
14.65	$9a_1$	13.62	$9a_1$	
15.10	$6b_2$	14.29	$6b_2$	
15.29	$8a_1$	14.46	$1b_1$	13.55
17.10	$5b_2$	14.55	$8a_1$	14.75
17.30	$1b_1$	15.20	$5b_2$	
18.55	$7a_1$	16.11	$7a_1$	15.75
18.77	$4b_2$	16.63	$6a_1$	
19.17	$6a_1$	17.52	$4b_2$	
		18.95	$5a_1$	
		20.76	$4a_1$	
		20.77	$3b_2$	
		23.79	$2b_2$	
		24.19	$3a_1$	
		25.69	$2a_1$	
		28.16	$1b_2$	
		30.88	$1a_1$	

a. Palmer and Kennedy, 1978

Table 9. 2,1,3-benzoselenadiazole ionization potentials: MS-VWN with large partial wave basis, and experiment (eV).

MS-VWN	assignment	expt[a]
7.56	$2a_2$	8.81
8.88	$3b_1$	9.30
10.43	$2b_1$	10.55
11.30	$1a_2$	11.30
11.47	$10a_1$	12.85
12.12	$7b_2$	13.4
12.58	$9a_1$	
13.26	$6b_2$	
13.39	$1b_1$	14.67
14.46	$5b_2$	15.65
14.66	$8a_1$	16.5
15.29	$7a_1$	
16.11	$6a_1$	
16.96	$4b_2$	
18.07	$5a_1$	18.44
19.28	$3b_2$	
20.02	$4a_1$	
23.11	$2b_2$	
23.40	$3a_1$	
24.82	$2a_1$	
29.40	$1b_2$	
30.80	$1a_1$	

a. Palmer and Kennedy, 1978

Table 10. $^1A_1 \rightarrow {}^1B_2$ excited-state transition energies, eV, for (a) 2,1,3-benzoxadiazole (b) 2,1,3-benzothiadiazole and (c) 2,1,3-benzoselenadiazole calculated in this study by both ground-state eigenvalue differences, $\Delta\epsilon_i$, and the transition state method, SCF-CI and experiment.

(a) 2,1,3-benzoxadiazole

method	$\Delta\epsilon_i$	transition state	SCF-CI[a]	expt[b]
Xα low	2.480	2.732	4.12	3.875
Xα high	2.289	2.524		
VWN low	2.530	2.767		
VWN high	2.338	2.553		

(b) 2,1,3-benzothiadiazole

method	$\Delta\epsilon_i$	transition state	SCF-CI[a]	expt[b]
Xα low	2.363	2.748	4.26	3.780
Xα high	1.949	2.358		
VWN low	2.361	2.741		
VWN high	1.971	2.349		

(c) 2,1,3-benzoselenadiazole

method	$\Delta\epsilon_i$	transition state	expt[b]
Xα low	2.244	2.543	3.483
Xα high	1.794	2.157	
VWN low	2.235	2.522	
VWN high	1.779	2.105	

a. Abu-Fittah *et al.* (1985) b. Hallas and Wright (1969)

Table 11. $^1A_1 \rightarrow {}^1A_1$ excited-state transition energies, eV, for (a) 2,1,3-benzoxadiazole (b) 2,1,3-benzothiadiazole and (c) 2,1,3-benzoselenadiazole calculated in this study by both ground-state eigenvalue differences, $\Delta\epsilon_i$, and the transition state method, SCF-CI and experiment.

(a) 2,1,3-benzoxadiazole

method	$\Delta\epsilon_i$	transition state	SCF-CI[a]	expt[b]
(a) $^1A_1 \leftarrow {}^1A_1$				
Xα low	3.649	3.923	4.15	4.397
Xα high	3.383	3.612		
VWN low	3.704	3.965		
VWN high	3.434	3.644		

(b) 2,1,3-benzothiadiazole

method	$\Delta\epsilon_i$	transition state	SCF-CI[a]	expt[b]
Xα low	3.256	3.440	4.79	4.052
Xα high	2.839	3.000		
VWN low	3.309	3.489		
VWN high	2.893	3.046		

(c) 2,1,3-benzoselenadiazole

method	$\Delta\epsilon_i$	transition state	expt[b]
Xα low	3.227	3.394	3.838
Xα high	3.016	3.167	
VWN low	3.335	3.489	
VWN high	3.091	3.235	

a. Abu-Eittah *et al.* (1985) b. Hallas and Wright (1969)

Table 12. Xα, VWN and experimental nitrogen nuclear quadrupole coupling constants $e^2q_{ii}Q/h$ $(i = z, y, x)$ for 2,1,3-benzoxadiazole and its S and Se analogues (MHz).

property	Xα		VWN		experiment[a]
	min l	large l	min l	large l	
2,1,3-benzoxadiazole					
zz	5.605	5.110	5.417	5.108	
yy	-4.667	-4.700	-4.631	-4.700	
xx	-0.938	-0.410	-0.786	-0.407	
η	0.665	0.839	0.710	0.840	
θ	72	71	72	71	
2,1,3-benzothiadiazole					
zz	3.817	3.802	3.730	3.620	3.424
yy	-2.874	-3.141	-2.904	-3.149	*
xx	-0.943	-0.661	-0.826	-0.470	*
η	0.506	0.652	0.557	0.749	0.140
θ	77	79	77	79	
2,1,3-benzoselenadiazole					
zz	2.862	3.575	2.874	3.706	3.414
yy	-2.206	-2.415	-2.231	-2.431	*
xx	-0.657	-1.159	-0.643	-1.275	*
η	0.541	0.351	0.553	0.312	0.112
θ	81	78	80	77	

a. Krause and Whitehead, 1973

Table 13. Partial wave composition (percent) for the highest occupied molecular orbital (HOMO), $2a_2$, for selected atoms, of 2,1,3-benzoxadiazole and its S and Se analogues.

	C_1		C_2		C_3		N		X
method	*p*	*d*	*p*	*d*	*p*	*d*	*p*	*d*	*d*
2,1,3-benzoxadiazole									
Xα low	15.7	·	59.6	·	5.4	·	19.3	·	·
VWN low	15.7	·	59.3	·	5.1	·	19.9	·	·
Xα high	14.0	2.3	55.1	0.1	6.4	2.8	14.2	0.2	1.0
VWN high	14.0	2.4	54.7	0.1	6.0	2.9	14.8	2.0	1.2
2,1,3-benzothiadiazole									
Xα low	24.3	·	58.6	·	2.7	·	14.4	·	·
VWN low	24.3	·	58.3	·	2.5	·	14.8	·	·
Xα high	20.1	3.5	54.5	0.6	4.8	1.8	8.4	2.9	1.1
VWN high	21.1	3.6	54.2	0.6	4.6	1.9	8.6	2.9	1.2
2,1,3-benzoselenadiazole									
Xα low	22.9	·	57.5	·	2.4	·	16.1	·	1.1
VWN low	22.9	·	57.3	·	2.3	·	16.3	·	1.1
Xα high	20.4	3.6	53.6	0.6	3.9	2.2	11.0	0.3	0.8
VWN high	20.2	3.6	53.5	0.6	3.9	2.2	11.0	0.3	0.8

Table 14. Partial wave composition (percent) for the lowest unoccupied molecular orbital (LUMO) $4b_1$, for selected atoms, of 2,1,3-benzoxadiazole and its S and Se analogues.

	C_1		C_2		C_3		N		X	
method	*p*	*d*	*p*	*d*	*p*	*d*	*p*	*d*	*p*	*d*
Xα low	14.3	·	13.1	·	7.6	·	48.2	·	16.8	·
VWN low	14.5	·	13.8	·	7.0	·	47.9	·	16.9	·
Xα high	14.6	1.4	12.2	1.1	7.1	4.0	40.7	1.7	14.0	1.2
VWN high	14.7	1.5	12.7	1.1	6.5	4.2	40.2	1.8	14.1	1.2
2,1,3-benzothiadiazole										
Xα low	10.4	·	2.4	·	20.1	·	51.5	·	15.6	·
VWN low	10.7	·	2.6	·	20.1	·	51.9	·	14.7	·
Xα high	10.6	0.4	1.3	1.5	20.1	3.8	42.6	1.0	14.4	3.3
VWN high	10.7	0.4	1.5	1.5	20.0	3.9	42.7	1.0	13.6	3.6
2,1,3-benzoselenadiazole										
Xα low	14.4	·	3.6	·	26.2	·	44.8	·	8.3	2.7
VWN low	14.6	·	3.7	·	26.6	·	44.9	·	7.4	2.9
Xα high	15.1	0.6	2.1	2.1	26.9	3.9	38.2	1.6	6.5	1.7
VWN high	15.2	0.7	2.1	2.1	27.3	4.0	38.0	1.6	5.7	1.8

Table 15. Dipole moments, debye, for 2,1,3-benzoxadiazole (indicated by O), 2,1,3-benzothiadiazole (S) and 2,1,3-benzoselenadiazole (Se), calculated using MS-LDA wavefunctions at large (indicated by large l) and minimum (min l) partial-wave basis, Xα and VWN exchange-correlation functionals, and experimental results.

	Xα		VWN		expt[a]
molecule	min l	large l	min l	large l	
O	−1.43	−3.54	−1.24	−3.55	−4.03
S	−2.44	−2.13	−2.59	−2.75	−1.73
Se	−2.04	+0.55	−2.28	+0.26	−0.94

a. Hill and Sutton (1949)

References.

Abu-Eittah, R., A. Nigm, M. Hamed and A. El-Azhary, 1986, Can. J. Spectrosc. **31**, 149

Brown, N. M. D., D.G. Lester and J. K. Tyler, 1969, Spectrochim. Acta **26A**, 2133

Bylina, A. S. and V. S. Korobkov, 1974, Sintez, Analiz I Struktura Organ. Soedin. **6**, 84

Case, D. A., M. Cook and M. Karplus, 1980, J. Chem. Phys. **73**, 3294

Cheeseman, G. W. H. and C. J. Turner, 1974, Org. Mag. Res. **6**, 430

Clark, P. A., R. Gleiter and E. Heilbronner, 1973, Tetrahedron **29**, 3085

Cohen, E. R. and B. N. Taylor, 1986, *The 1986 Adjustment of the Fundamental Physical Constants* (CODATA Bulletin 63, Pergamon, Elmsford, NY) as quoted by E. R. Cohen and B. N. Taylor, Physics Today, August 1988. *

Cotton, F. A., 1971, *Chemical Applications of Group Theory* (Wiley-

* The values used for physical constants were

$$h = 6.626\,075\,5 \times 10^{-34}\,J\,sec$$

$$c = 299\,792\,458\ m\,sec^{-1}$$

and for conversion from hartree atomic units for energy, E_h,

$$E_h = 4.359\,748\,2 \times 10^{-18}\,J$$

$$= 27.211\,396\,1\ eV$$

Interscience, New York)

Gordon, R. D. and R. F. Yang, 1971, J. Mol. Spectrosc. **39**, 295

Grunwell, J. R. and W. C. Danison, Jr., 1973, Int. J. Sulfur Chem. **8**, 379

Hallas, J. M. and R. A. Wright, 1969, Spectrochim. Acta **25A**, 1211

Hill, R. W. and L. E. Sutton, 1949, J. Chim. Phys. **46**, 244

Kaim, W. and S. Kohlmann, 1985, Inorg. Chim. Acta **101**, L21

Kaim, W., S. Kohlmann, A. J. Lees and M. Zulu, 1989, Z. anorg. allg. Chem. **575**, 97

Kamiya, M., 1970, Bull. Chem. Soc. Jpn. **43**, 3344

Krause, L. and M. A. Whitehead, 1973, Mol. Phys. **25**, 99

Lucken, E. A. C., 1969, *Nuclear Quadrupole Coupling Constants* (Academic Press, London)

Luzzati, V., 1951 Acta Cryst. **4**, 193

Palmer, M. H. and M. F. Kennedy, 1978, J. Mol. Struct. **43**, 33

Pariser, R. and R. G. Parr, 1953 J. Chem. Phys. **21**, 466

Pauling, L., 1960, *The Nature of the Chemical Bond and the Structures of Molecules and Crystals: An Introduction to Modern Structural Chemistry* (Cornell University Press, Ithaca, NY)

Salahub, D. R., 1978, J. Chem. Soc., Chem. Commun., 385.

Townes, C. H. and B. Dailey, 1949, J. Chem. Phys. **17**, 325

Vladimirov, V. G., V. K. Mukhomorov, Yu. E. Strel'nikov, N. S. Tsepova and A. V. Kokushkina, 1983, Radiobiologiya **23**, 616

Weinstock, L. M. and I. Shinkai, 1984, in *Comprehensive Heterocyclic Chemistry, Vol. 6*, edited by A. R. Katritzky and C. W. Rees (Pergamon Press, Oxford), p. 513

Wrinn, M. C. and M. A. Whitehead, 1990, J. Chem. Soc., Faraday Trans. **86**, 889

I.3.6 Electronic Structure of 2,1,3-benzoxadiazole[$Cr(CO)_5$]$_2$ by the MS-LDA Method

Abstract

Multiple-Scattering Local-Density-Approximation (MS-LDA) calculations were performed on the binuclear complex of $Cr(CO)_5$ and the planar heterocycle 2,1,3-benzoxadiazole. Nuclear quadrupole coupling constants, atomic charges, and orbital populations were computed, and compared to those in the isolated heterocycle. Significant charge depletion was calculated for the heterocyclic oxygen on going into the metal complex, and the ring adopted a more benzenoid character. An attempt to speed SCF convergence by using converged fragments for the starting potential was not successful, suggesting large differences between electronic structure of the isolated and ligand heterocycle.

Introduction

The binuclear transition complex 2,1,3-benzoxadiazole[$Cr(CO)_5$]$_2$, where each Cr atom is coordinated to a nitrogen on the heterocyclic ring, is a member of a novel class of recently synthesized group of chalcogenide metal carbonyls (Kaim *et al.*, 1989). These compounds exhibit metal-to-ligand charge transfer, and form stable anion radicals, due to interaction between the metal and the π system of the ring (Kaim and Kohlmann, 1985). The heterocycle ligand in this compound has a highly delocalized π system (Wrinn and Whitehead, 1991 and references therein); metal interactions with such ligands is of interest for understanding problems as diverse as metalloenzyme mechanisms and conducting polymers (Zulu and Lees, 1988).

The Multiple-Scattering Local-Density-Approximation (MS-LDA) method has been used successfully to investigate planar heterocycles involving both one and two (Case

et al., 1980; Wrinn and Whitehead, 1990) heteroatoms, and has also been used to study the electronic structure of the 2,1,3-benzoxadiazole ligand of the present compound (Wrinn and Whitehead, 1991).

A preliminary investigation is made of the ground state electronic structure of a one of this family of compounds. Particular attention was paid to the response of the heterocycle to the transition from an isolated molecule to a ligand, and to the ground state interaction between the nitrogen and chromium.

Computational Details

Experimental coordinates of the compound were not available; for the heterocyclic part, the coordinates of the isolated molecule were used. Bond distances and angles for the $Cr(CO)_5$ fragments were inferred from similar compounds. Several cases are reported of Cr-carbonyl complexes coordinated to a nitrogen in an aromatic ring (Bätzel and Boese, 1981; Ries *et al.*, 1984; Feldhoff *et al.*, 1986) the N–Cr distance is in the range of 2.11 to 2.17 Å. In these analogous compounds the CO group opposite the N atom was bound more tightly, and had Cr–C and C–O bond lengths shorter then those perpendicular to the N–Cr axis. As well, the four planar CO ligands were not in the plane of the Cr, but moved slightly toward the heterocylic ligand. The planar CO were placed in a position staggered with respect to the benzofurazan. A schematic diagram of the molecular geometry chosen, along with bond distance and angles, are shown in Figure 1.

Muffin-tin radii were initially chosen by the Norman criterion, with a reduction factor of 0.88. However, it was not possible to converge the calculation at this choice of sphere radii; the long distance between the N and Cr atoms meant that the Norman radii for each would not overlap. Accordingly, the Cr muffin-tin radius, 2.16 Å, by the reduced Norman method, was increased to 2.60 Å. This distance allowed

for a small amount of overlap with the N sphere ($\approx$ 2%), without introducing an unreasonable amount of overlap between Cr and the other ligands. The outer sphere was centred on the axis of symmetry at a position to minimize the outer-sphere volume; as in previous MS-LDA calculations of planar heterocycles, the intersphere, constant-potential region comprised a large percentage (84%) of the total intersphere volume. The sphere radii and overlaps are shown in Table 1; a 3-dimensional plot of the muffin-tin and outer spheres is shown in Figure 2.

The VWN exchange-correlation functional (Vosko *et al.*, 1986) was used The partial wave basis used $l = 0$ on hydrogen, $l = 1$ on carbon, nitrogen and oxygen, $l = 2$ on chromium, and $l = 3$ on the outer sphere; it thus corresponds to a minimum basis. Frozen cores were used on all heavy atoms, resulting in a total of 94 valence levels. Point group symmetry (C_{2v}) was employed.

It was extremely difficult to converge the self-consistent field (SCF) calculations. The close spacing of one-electron eigenvalues made it necessary to use a very small mixing factor (0.001) in the early iterations, and to check frequently that no levels had been skipped.

An earlier MS-LDA study (Berksoy and Whitehead, 1988) of large metal–aromatic complexes had encountered similar convergence difficulties. In an attempt to mitigate this problem, the MS-LDA program was modified to accept potential input from molecular fragments; in this case, 2,1,3-benzoxadiazole and $Cr(CO)_6$. Each precursor molecule was converged at the same muffin-tin radii and partial wave basis as would be used in the larger complex. The resulting potentials (truncated to remove one CO ligand in the $Cr(CO)_6$ case) were then used as the starting point for the large SCF calculation. For comparison, the SCF calculation was also run in the conventional manner, where the starting potential is a simple superposition of converged atomic potentials.

Unfortunately, the "converged-fragment" method did not improve convergence behaviour. Not only was the process as unstable as the conventional approach, but when it finally did converge, it did so to an excited state. Convergence was achieved with the conventional method, to the level of 10^{-4} in the potential, after 250 iterations. A graph of the convergence behaviour is given in Figure 3, where the both the total energy and the convergence factor (the largest change in the potential between successive iterations) are plotted against the number of iterations. The convergence was plotted logarithmically in order to fit it to the same scale as the energy; the important feature of Figure 3 is that the total energy is seen to stabilize long before the system is fully converged. The slope in the convergence increases (the convergence becomes more rapid) at a point just below half the number of iterations; this corresponds to the change in the SCF mixing factor from 0.001 to a larger value, and caused a momentary increase in the energy value. The spike in the convergence curve near the end of the SCF corresponds to another increase in the mixing factor.

Ionization potentials (IP) were calculated using the Slater transition state method, where the system is converged with half an electron removed from the level of interest. An adiabatic technique (Guo *et al.*, 1989) was used to obtain the transition state from the converged ground state: 0.1 electron was removed from the ionized level, and the SCF was run to convergence. This process was repeated in 0.1 electron increments until the half electron removal was achieved. This approach gave a smooth path between the converged ground state and the converged transition state, with none ot the difficulties encountered in obtaining the ground state initially.

The transition state was calculated only once, with the half electron removed from the highest a_1 level; the remaining levels were assumed to relax to their approximate transition state IP values. This approximation is often employed in MS-LDA

studies, and has been shown to be valid for the heterocyclic compound used in this complex (Wrinn and Whitehead, in preparation).

Nuclear quadrupole coupling constants were calculated using the the one-electron properties program of Case and Cook (1981).

Results and Discussion

One-electron energies, Densities of States and Charge Transfer.

The one-electron eigenvalues for all valence levels, along with the ionization potentials (IP), are shown in Table 2. As observed in the calculation of the heterocycle alone, there was not a complete agreement in the orderings of the eigenvalues and IPs; the $15b_1$ level was several steps higher in the IP calculation, and some closer interchanges occurred in the middle range. Overall ordering was in reasonable agreement. The IP values were shifted downward much more uniformly (almost all are shifted by .11 au) than was the case in the heterocyle study, indicating that differential relaxation was not an important factor for this compound. The one-electron eigenvalues, though not strictly identified with physical energies in LDA theory, are thus suitable in this case for examining physical trends.

The large number of molecular orbitals (MO) (91 valence levels, when the lowest unoccupied manifold is included) makes interpretation difficult by examining tabulated values, or constructing traditional MO level diagrams. Density of states plots provide an alternate and more convenient presentation of results.

The density of states at energy E, $D(E)$, is defined as the number of states (orbitals, levels) between E and dE:

$$D(E) = \frac{dN(E)}{dE}$$

where $N(E)$ is the number of states with energy less than E (Raimes, 1972; Hoffman

1988). When the number of calculated levels approaches a continuum, a plot of the density of states is more appropriate than a level diagram.

Numeric calculation of densities of states (DOS)is a complicated procedure, usually performed in k space (Ladik, 1988). However, for purposes of visualization, qualitative DOS plots may be constructed by placing a distribution function around each level. This method has been employed with both Gaussian:

$$D(E) = e^{-(\frac{E-E_i}{\sigma})^2}$$

(Salahub, 1978) and Lorentzian distributions:

$$D(E) = \sum_i \frac{\sigma/\pi}{(E-E_i)^2 + \sigma^2}$$

(Baerends, 1978). In both cases the σ value is assigned no physical meaning, but is scaled to enhance visual interpretation.

The molecule in this work presents a case intermediate between the discrete energy levels of a small molecule and the quasi-continuum of a very large system; DOS plots thus provide a useful aid in visualizing orbital structure. The Lorentzian distribution was used in generating the plots.

Figure 4 shows the total density of states for both the occupied energy levels and the first band of unoccupied MO; the Fermi (highest occupied) level is shown as a dashed vertical line. The gap between the "HOMO–LUMO" bands is immediately apparent.

A closer view of density of states around the Fermi level is shown in Figure 5. A partial DOS is also shown; the dashed curve in the Figure depicts the π states. The unoccupied peak is seen to be dominated by contributions from π levels. This is important for metal-to-ligand charge transfer, since that mechanism is understood to be a donation of metal d electrons to an empty ligand π level. An unoccupied π

system is present, albeit at a higher energy; the distance between the HOMO and LUMO peaks is about 8 eV.

Hückel molecular orbital (MO) calculations have been performed on a similar series of compound, with W substituting for Cr (Kaim *et al.*, 1987). A correlation was drawn between the MO coefficient on nitrogen in the π^* orbital and the expected degree of metal-to-ligand charge transfer; a higher coefficient implied more charge transfer.

This simple picture is not followed in the present calculations. Of the 6 unoccupied orbitals in the first unoccupied π manifold, only one has a significant contribution from the nitrogen atom. In that case, the $17a_2$ (third-highest unoccupied a_2), is 6% nitrogen p; the chromium d contributes slightly over 1%. In this same state, however, the 3 carbons of the benzene component of the ligand form 82%; the $26b_2$ level also has a very strong benzene-like contribution. In the remaining 4 unoccupied π levels, the partial wave contributions from the heterocyle are well-delocalized. Thus, while there is a π system available to the Cr for charge transfer, it spreads over the entire ring and is not attributable to a local interaction with the N atom.

Charge Densities, Orbital Interactions and Nuclear Quadrupole Coupling Constants.

The atomic partial charges for the metal complex, and for the heterocycle alone, are shown in Table 3. The first pair of columns in Table 3 show the charge assigned each atom during the SCF procedure, which does not account for the charge accumulated in the constant-potential intersphere region. Because of the large intersphere volume, the total intersphere charge at convergence was 14.7 electrons; these were assigned to the atoms through a charge-partitioning scheme which scales to both

the atoms SCF charge and to the amount of atomic sphere surface in contact with the intersphere region (Case and Karplus, 1976)

Both SCF and partitioned charges were in agreement in the overall trend; so no artifact is being introduced by the charge-partitioning scheme. Both cases show substantial reduction in the heterocyle O charge: by 0.7 electrons for the charge-partioned values. Most of this charge has migrated to benzene fragment of the ring: the three symmetry-unique carbon atoms gain 0.150, 0.081 and 0.112 electrons, for a total of 0.686. The 0.807 excess charge on metal Cr comes at the expense of the carbonyl carbons, which are seen in the Table to be charge deficient. The nitrogen total atomic charge is the least affected of any atom, with only a 0.027 difference between the ring and metal complex.

The overall migration of charge to the benzene portion of the compound was shown in the change of molecular dipole moment. The heterocyle itself was calculated to have a dipole moment of 1.24 D toward the O; the metal complex dipole was computed to be 3.62 D in the *opposite* direction, toward the benzene ring.

In the isolated heterocycle, total charge on O has been modelled as a competition between σ acceptance and π donation (Palmer and Kennedy, 1978). The metal-ligand interaction is also considered to be a σ–π balance, with the ligand acting as a σ donor (Kaim *et al.*, 1987). To examine change in σ density between the metal complex and the ring alone, plots were prepared of both the total in-plane density, and the difference density between the metal complex and the isolated ring. The orientation of atoms in these figures (and the molecular orbital plots, below), along with the muffin-tin sphere radii, are shown in Figure 6, where the Cr and N spheres are seen to overlap, in contrast to the Norman sphere picture of Figure 2. The total density is shown in contour format in Figure 7a, and in 3-dimensional form in Figure 7b. The density difference plots are shown in the same formats in Figures

8a and 8b.

The total σ density in Figures 7a and 7b shows strong interaction along the N–Cr–C–O axis, and significant involvement as well of the ring oxygen. This bonding is in direct contrast to the results found by Berksoy and Whitehead (1988, 1991), for both aluminium-containing and diphenyl–Pb compounds; there the metal atom was found to have virtually no σ interaction with its surroundings.

When the isolated heterocyle density is subtracted from the total, Figures 8a and 8b, the strong σ interaction between N and Cr is still clearly seen; even though the N lone pair density has been removed, there are still positive contours (visible as a hill in Figure 8b). Other perturbations in the heterocycle density seen in Figures 8a and 8b are an increase in the H atom density in the benzene fragment, and an increase in the ring oxygen lone pair density. The N–O σ interaction has been decreased.

The highest occupied σ states do not involve metal-to-ligand interactions. Figure 9 shows the orbital contour diagram for the highest-occupied orbital, $23b_2$ in the plane of the heterocycle ligand. The orbital is shown to be entirely composed of Cr d interacting with the carbonyls C and O p orbitals. The next-highest σ level, $25a_1$, is similar.

It is necessary to descend more than 0.5 au in energy, to the largest DOS peak in Figure 4, before finding significant metal-ligand bonding with the ring. Figure 10 presents the orbital contours for $14a_1$, which show this orbital is highly delocalized. Not only are there interactions between between Cr and N, but between Cr and the closest C on the benzene ring. In the population analysis of this state, no individual atom contributes more than 6% to the total orbital density.

Contours for the $13b_2$ level, Figure 11, do show direct Cr–N σ bonding; Cr contributes both p and d overlaps with the N p, which also overlaps with the O p in

the ring. As with the $14a_1$ level, however, this molecular orbital is delocalized.

The $12b_2$ contours, Figure 12, show very similar interactions among the Cr, N and O, and similar delocalization. An interesting feature of this level is the interaction between a Cr *d* and the H in the benzene portion of the ring, suggesting that a Cr–H interaction may help to stabilize the complex.

To visualize π interactions, contour diagrams were made from the orbital values in a slice 1 au above the plane of the 2,1,3-benzoxadiazole ligand. As with the σ levels, the highest π MO, $14a_2$, shows no interaction between Cr and the ring, and is confined to the Cr–carbonyl fragments.

The next-highest π level, $13a_2$, is shown in Figure 13. This MO corresponds to a traditional model of metal-to-ligand π interaction, since the orbital overlaps between Cr and the ring are with the N atom only. The benzene π system is self-contained, supporting the charge analysis given above of a benzenoid resonance structure for the heterocycle. The ring O atom is not involved in this level.

The $16b_1$ level, Figure 14, is primarily a stong π interaction between Cr and the carbonyl C, but does include a small overlap with two of the C atoms in the ring. The N contribution to the state is of *s* character, but is not in phase with the small Cr–ring interaction.

The $15b_1$ contours, like those of $16b_1$, show a strong interaction between Cr and the carbonyl C, but include direct bonding between Cr and N. Interactions for the ring C atoms are confined to the benzen portion.

In the next π MO, $14b_1$ in Figure 16, there is also direct Cr–N bonding; those two atoms' wavefunctions overlap only with one another. The benzene section is once again shown to be independent of heteroatom section of the ligand.

The nitrogen nuclear quadrupole coupling constants, derived from electric field gra-

dient (EFG) tensor values, are shown in Table 4 for both the Cr complex and the isolated heterocycle. The orientation of the principle axis components remains consistent between the free and complexed forms; Q_{zz} is perpendicular to the plane of the ring. The θ value given in the Table is the rotation angle to diagonalize the electric field gradient tensor in the molecular coordinate system according to the transformation (for the heterocycle in the yz plane):

$$T = \begin{pmatrix} 1 & 0 & 0 \\ 0 & \cos^2\theta - \sin^2\theta & 2\sin\theta\cos\theta \\ 0 & -2\sin\theta\cos\theta & -\sin^2\theta + \cos^2\theta \end{pmatrix}$$

(Lucken, 1969). The Q_{yy} component for N in the Cr complex is rotated 68° with respect to the horizontal axis, pointing precisely along the direction of the N–Cr bond. In the free heterocycle, Q_{yy} does not point exactly along the expected N lone pair axis. Values for the N Q_{zz} and Q_{yy} are considerably higher in the Cr complex: more than twice for the Q_{zz} oriented toward the π system, and more than 4 times for the Q_{yy} aligned to the N–Cr bond. Since the nuclear electric field gradient is dominated by p-orbital contributions, the higher Q_{yy} provides further evidence of N–Cr $p - -\sigma$ bonding. The assymetry parameter η, defined as

$$\eta = \frac{q_{yy} - q_{xx}}{q_{zz}}$$

remain qualitatively the same for both compounds.

Conclusions

The compound 2,1,3-benzoxadiazole$[Cr(CO)_5]_2$ was investigated for the first time using a local density functional method. Results suggest that in the heterocyclic substituent, there is a significant shift of charge away from the oxygen compared to the charge distribution in the isolated heterocycle. Strong evidence was obtained, both from charge distribution and molecular orbital contours, to show that the heterocycle adopts a benzenoid structure in this complex, in contrast to the partial dienyl quality observed in the free state.

Because of the use of muffin-tin potentials, and the lack of a known equilibrium geometry, these results must be regarded as preliminary. Indeed, the extreme difficulties encountered in SCF convergence suggest that the geometry used in this study is far from equilibrium; even the assumption, made by the earlier investigators, that the Cr coordinates through the nitrogen rather than the oxygen, may well be wrong, and bears reexamination. A more detailed study is in progress, using a more rigorous implementation of the local density method, with full geometry optimization.

Table 1. Selected muffin-tin sphere sizes (bohr) and overlap percentages. The C_a and O_a are the atoms "axial" to N; C_p and O_p are those planar to the Cr. Radius values are by Norman Norman criterion, except for Cr (see text).

	radius	overlap	% overlap
O_a	1.64	C_a–O_a	50
C_a	1.62	C_a–Cr	22
O_p	1.63	C_p–O_p	51
C_p	1.62	C_a–Cr	17
Cr	2.60	Cr–N	2
N	1.54	N–O	33
C	1.64	C–N	24
O	1.46		

Table 2. Benzofurazan[$(Cr(CO)_5]_2$ eigenvalues and ionization potentials (au), as calculated with the VWN exchange- correlation functional and minimum partial-wave basis.

state	eigenvalue	state	ionization potential
$16b_1$	-0.5627783	$16b_1$	-0.6722792
$14a_2$	-0.5836063	$14a_2$	-0.6995301
$23b_2$	-0.5929806	$23b_2$	-0.7094671
$25a_1$	-0.5940780	$25a_1$	-0.7104952
$22b_2$	-0.6185718	$15b_1$	-0.7274678
$24a_1$	-0.6186968	$22b_2$	-0.7342847
$15b_1$	-0.6201341	$24a_1$	-0.7343918
$13a_2$	-0.6658041	$13a_2$	-0.7652722
$14b_1$	-0.7693534	$14b_1$	-0.8694653
$12a_2$	-0.9943216	$12a_2$	-1.0991614
$13b_1$	-1.0154374	$13b_1$	-1.1175753
$23a_1$	-1.0236493	$23a_1$	-1.1237896
$21b_2$	-1.0529599	$21b_2$	-1.1517978
$12b_1$	-1.0547394	$12b_1$	-1.1642120
$11a_2$	-1.0552171	$20b_2$	-1.1643724
$22a_1$	-1.0552867	$11a_2$	-1.1646242
$20b_2$	-1.0554388	$22a_1$	-1.1649475
$10a_2$	-1.0681606	$10a_2$	-1.1768178
$11b_1$	-1.0688558	$11b_1$	-1.1774860
$19b_2$	-1.0761876	$19b_2$	-1.1854988
$21a_1$	-1.0778462	$21a_1$	-1.1867532
$18b_2$	-1.0856907	$18b_2$	-1.1945548
$9a_2$	-1.0867656	$9a_2$	-1.1954044
$10b_1$	-1.0869013	$10b_1$	-1.1955276
$20a_1$	-1.0869900	$20a_1$	-1.1957047
$19a_1$	-1.1481493	$19a_1$	-1.2531153
$9b_1$	-1.1486779	$9b_1$	-1.2630056

continued...

Table 2. Benzofurazan[$(Cr(CO)_5]_2$ eigenvalues and ionization potentials (au), continued (page 2 of 3)

state	eigenvalue	state	ionization potential
$8a_2$	-1.1500010	$8a_2$	-1.2642663
$17b_2$	-1.1541186	$17b_2$	-1.2684567
$18a_1$	-1.1567263	$18a_1$	-1.2698048
$16b_2$	-1.1729614	$16b_2$	-1.2832667
$17a_1$	-1.2220151	$8b_1$	-1.3531815
$16a_1$	-1.2399164	$7a_2$	-1.3532836
$8b_1$	-1.2407304	$7b_1$	-1.3555306
$7a_2$	-1.2408261	$6a_2$	-1.3555706
$15b_2$	-1.2420860	$17a_1$	-1.3325192
$7b_1$	-1.2433085	$16a_1$	-1.3459473
$6a_2$	-1.2433524	$15b_2$	-1.3515837
$14b_2$	-1.2522480	$14b_2$	-1.3633494
$15a_1$	-1.2549860	$15a_1$	-1.3670188
$13b_2$	-1.2649834	$13b_2$	-1.3754105
$14a_1$	-1.2668219	$14a_1$	-1.3808360
$12b_2$	-1.2805475	$12b_2$	-1.3923972
$5a_2$	-1.2964866	$5a_2$	-1.4176077
$6b_1$	-1.2965037	$6b_1$	-1.4176223
$13a_1$	-1.3604331	$13a_1$	-1.4690645
$11b_2$	-1.3889763	$11b_2$	-1.5062214
$12a_1$	-1.3940400	$12a_1$	-1.5071132
$10b_2$	-1.4478262	$10b_2$	-1.5482963
$9b_2$	-1.4843962	$9b_2$	-1.5947104
$11a_1$	-1.4853091	$11a_1$	-1.5956166
$4a_2$	-1.4896250	$4a_2$	-1.5996536
$5b_1$	-1.4900458	$5b_1$	-1.6000576
$8b_2$	-1.4921735	$8b_2$	-1.6022701
$10a_1$	-1.4923915	$10a_1$	-1.6024240

continued...

Table 2. Benzofurazan[$(Cr(CO)_5]_2$ eigenvalues and ionization potentials (au), continued (page 3 of 3)

state	eigenvalue	state	ionization potential
$9a_1$	-1.5588718	$9a_1$	-1.6606987
$8a_1$	-1.6645865	$8a_1$	-1.7662469
$3a_2$	-1.6826649	$3a_2$	-1.7964259
$4b_1$	-1.6826823	$4b_1$	-1.7964429
$7b_2$	-1.6831621	$7b_2$	-1.7968999
$7a_1$	-1.6832098	$7a_1$	-1.7969242
$6b_2$	-1.7549263	$6b_2$	-1.8562016
$6a_1$	-1.8534427	$6a_1$	-1.9567269
$3b_1$	-1.8575460	$3b_1$	-1.9646923
$5a_1$	-1.9792406	$5a_1$	-2.0837939
$5b_2$	-2.0269633	$5b_2$	-2.1327379
$4a_1$	-2.3241228	$4a_1$	-2.4301145
$4b_2$	-2.8573930	$4b_2$	-2.9805423
$3a_1$	-2.8574408	$3a_1$	-2.9806175
$3b_2$	-2.8802011	$3b_2$	-2.9917026
$2b_2$	-2.9346100	$2b_2$	-3.0589975
$2a_1$	-2.9346204	$2a_1$	-3.0590081
$2a_2$	-2.9347491	$2a_2$	-3.0591651
$2b_1$	-2.9347638	$2b_1$	-3.0591788
$1b_2$	-3.2437444	$1b_2$	-3.3773436
$1a_2$	-3.2440454	$1b_1$	-3.3776763
$1b_1$	-3.2440448	$1a_2$	-3.3776767
$1a_1$	-3.5141604	$1a_1$	-3.6384515

Table 3. Partial charges for atoms in the 2,1,3-benzofurazan ring alone, and the Cr complex.

atom	charge in SCF		partitioned charge	
	ring	Cr complex	ring	Cr complex
C	5.500	5.703	6.016	6.166
C	5.472	5.614	5.972	6.053
C	5.473	5.683	6.065	6.177
N	6.418	6.552	7.069	7.096
O	7.273	6.725	7.698	7.006
Cr	·	25.703	·	26.807
C	·	5.149	·	5.469
O	·	7.619	·	8.065
C	·	5.100	·	5.440
O	·	7.453	·	7.832
C	·	5.131	·	5.539
O	·	7.496	·	8.006

Table 4. Nuclear quadrupole coupling constants $e^2 q_{ii} Q/h$ $(i = z, y, x)$, asymmetry parameters η, and principle moment axis θ for the nitrogen atom in 2,1,3-benzoxadiazole (*ring*) and in the Cr complex (*ligand*).

	ring	*ligand*
zz	5.417	13.014
yy	-3.129	-12.192
xx	-0.786	0.823
η	0.710	0.874
θ	72	68

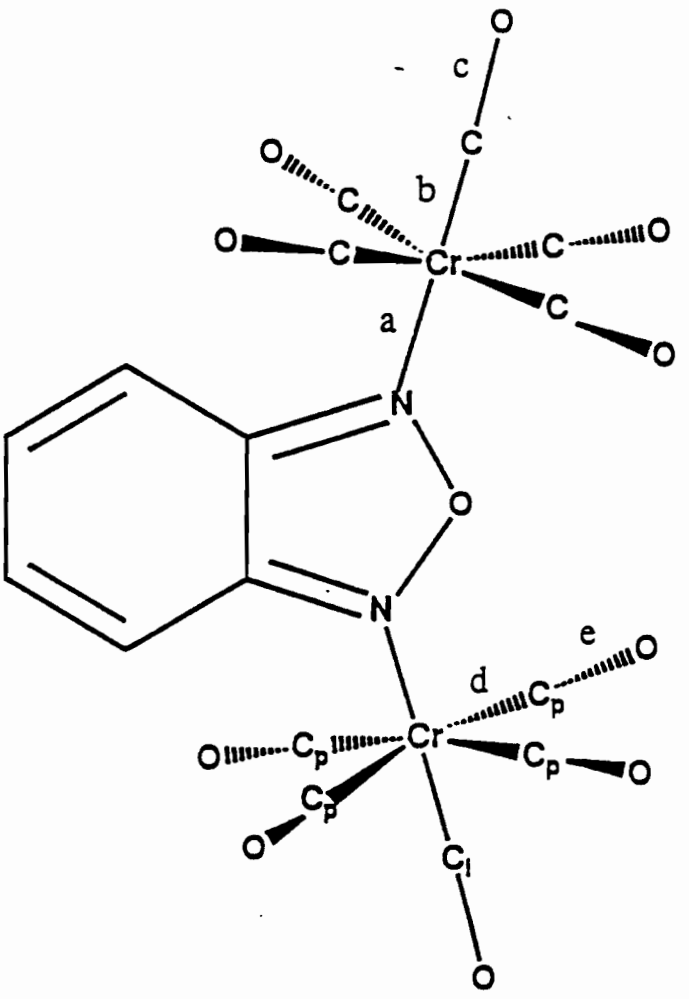

distance	value	angle	value
a	2.14	∠O N Cr	123.4
b	1.84	∠N Cr C_l	180
c	1.15	∠N Cr C_p	88
d	1.90	∠Cr C_p O	180
e	1.14		

Figure 1. Bond distances (Å) and angles for the Cr ligands. The four C_p–O ligands form the corners of a plane twisted 45° with respect to the plane of the benzofurazan ring; the remaining C–O is in the plane of the ring.

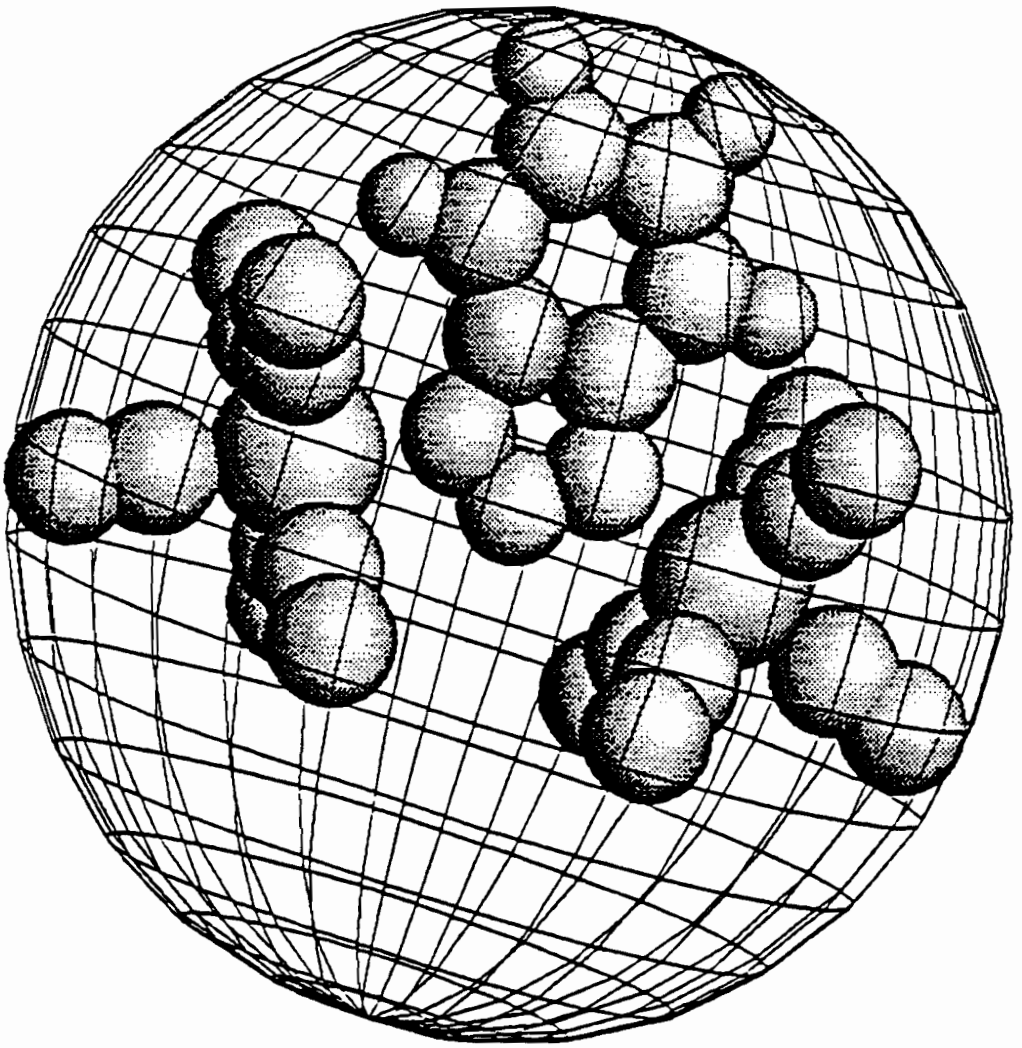

Figure 2. Atomic positions and muffin-tin spheres for 2,1,3-benzoxadiazole$[Cr(CO)_5]_2$. Solid spheres are atoms; the wire-frame represents the outer sphere boundary. Atomic sphere radii are drawn from 0.88 times the Norman criterion.

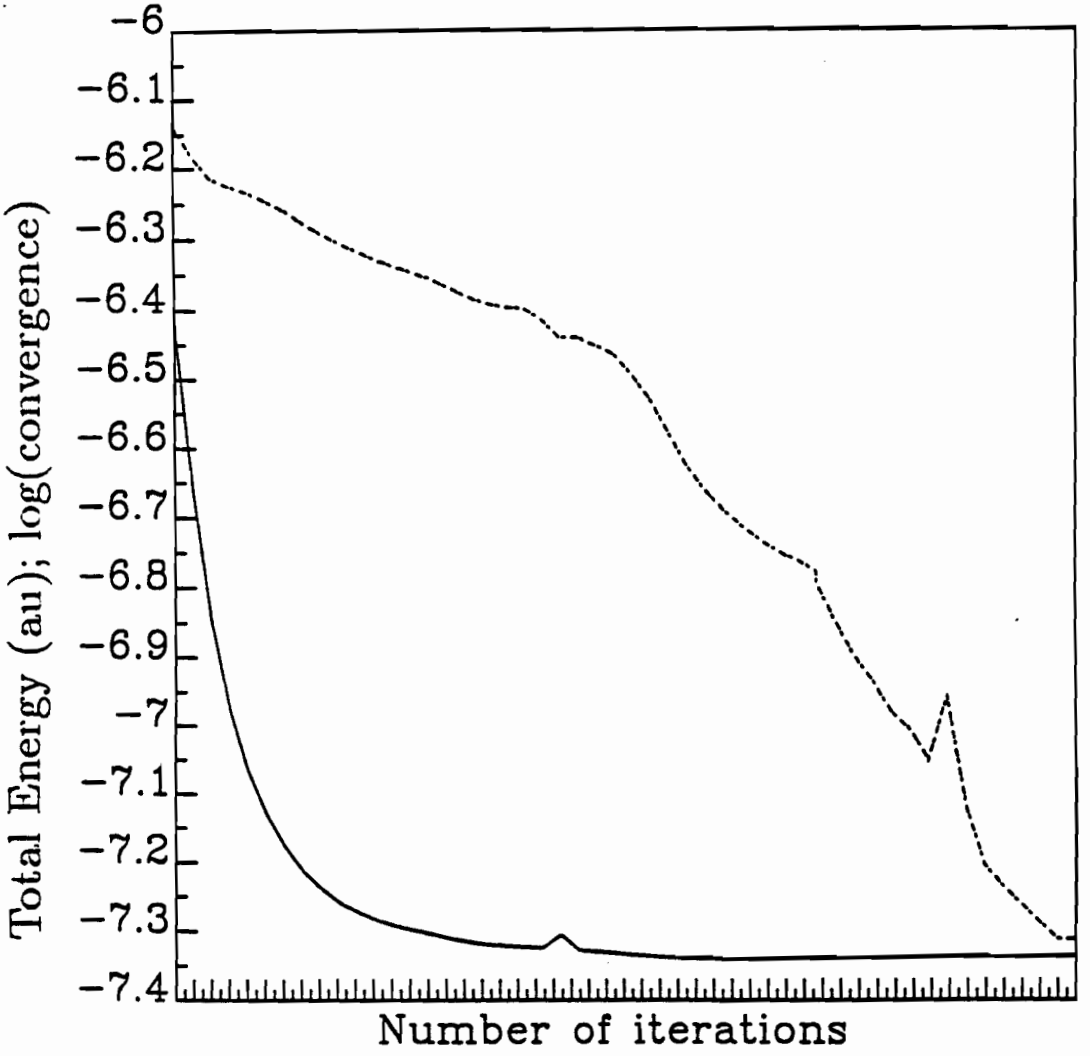

Figure 3. Total energy (au), and logarithm of the convergence factor, versus number of iterations for the SCF procedure for 2,1,3-benzoxadiazole$[Cr(CO)_5]_2$. Only the final digit of the total energy is drawn on the axis. Each tick mark on the horizontal axis represents 5 iterations.

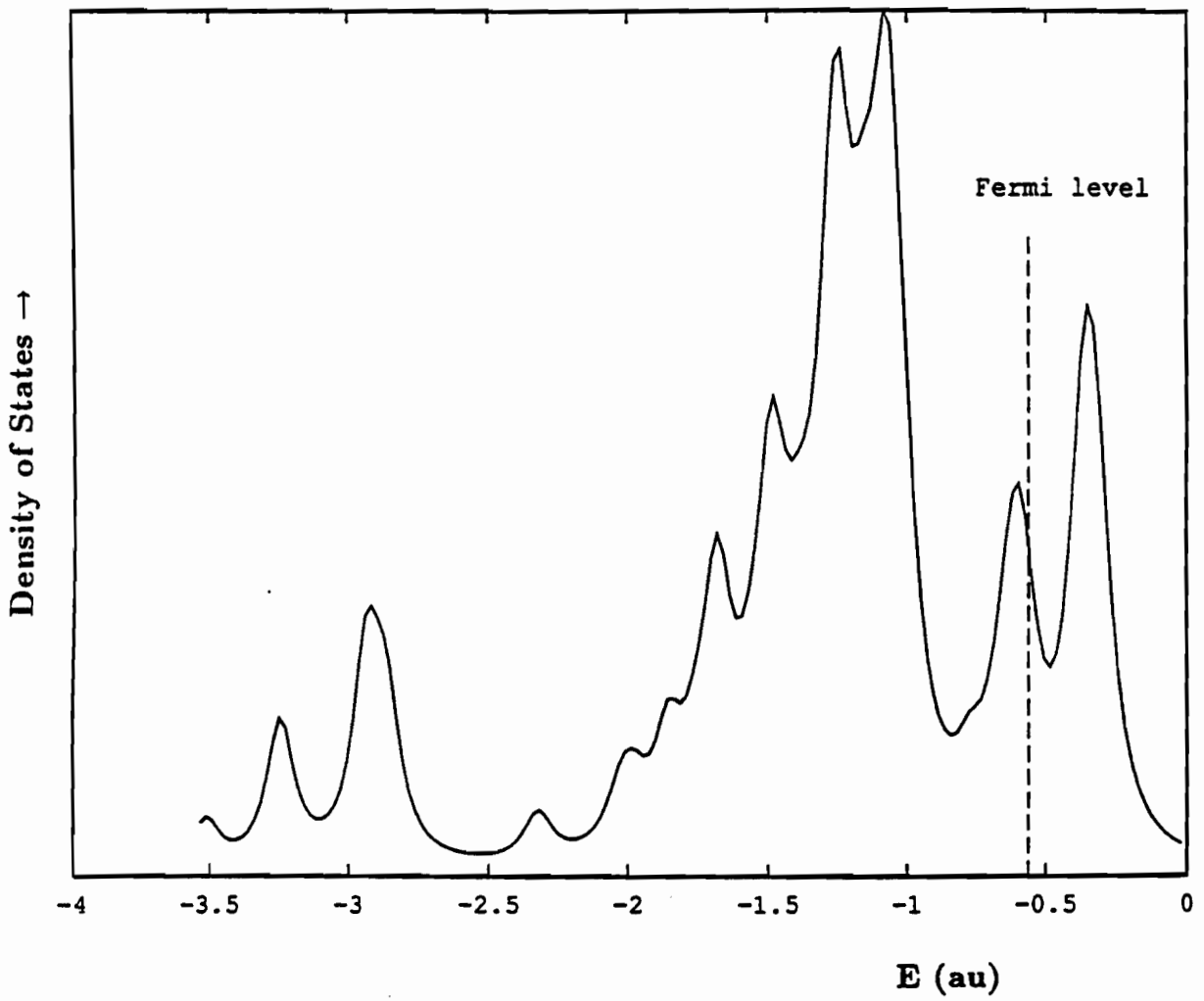

Figure 4. The total density of states versus energy for 2,1,3-benzoxadiazole[$Cr(CO)_5]_2$.

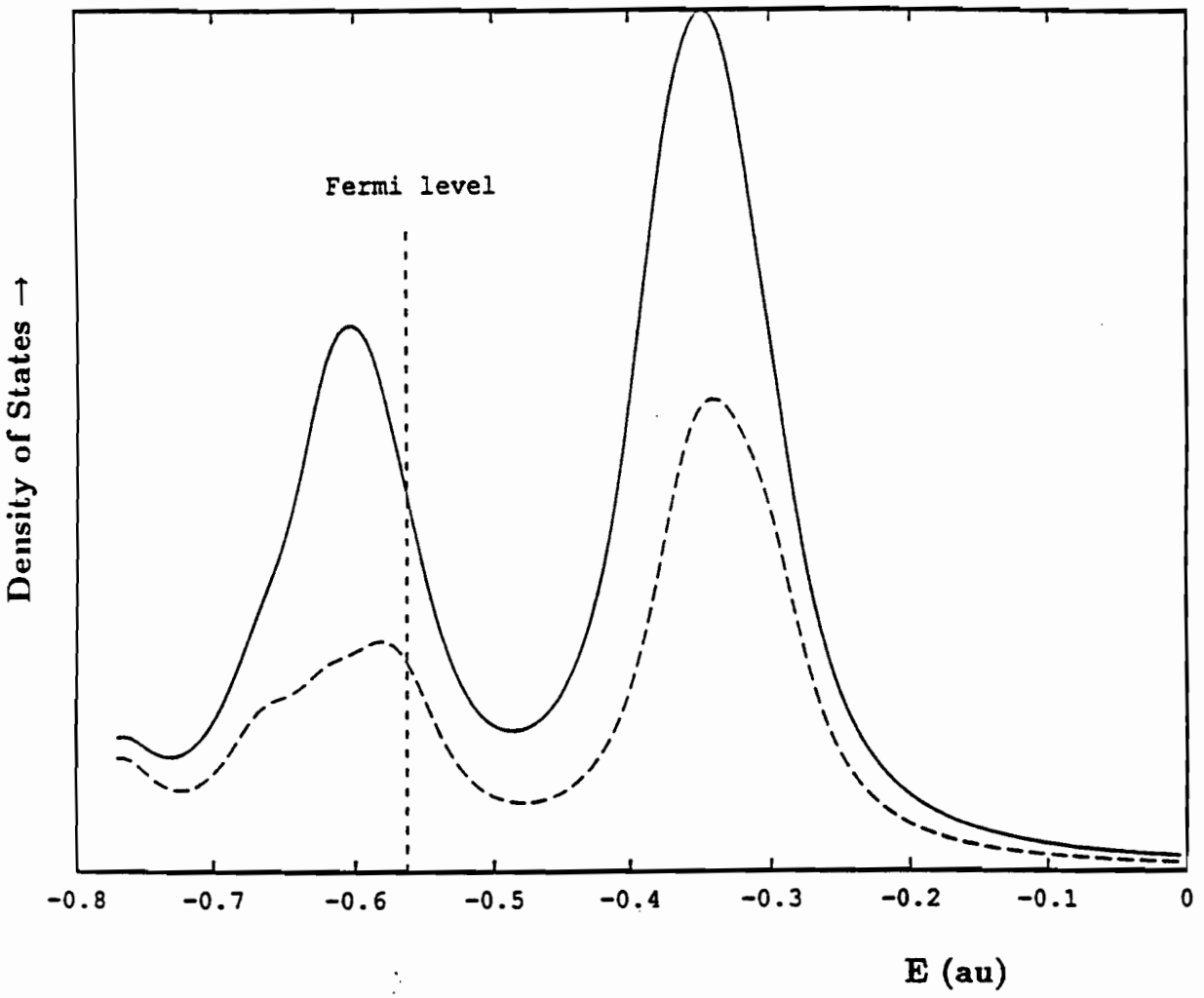

Figure 5. The density of states (DOS) versus energy for the highest occupied and lowest unoccupied bands of 2,1,3-benzoxadiazole$[Cr(CO)_5]_2$. The solid line shows the total DOS; the dotted line below it shows the DOS of the π levels alone.

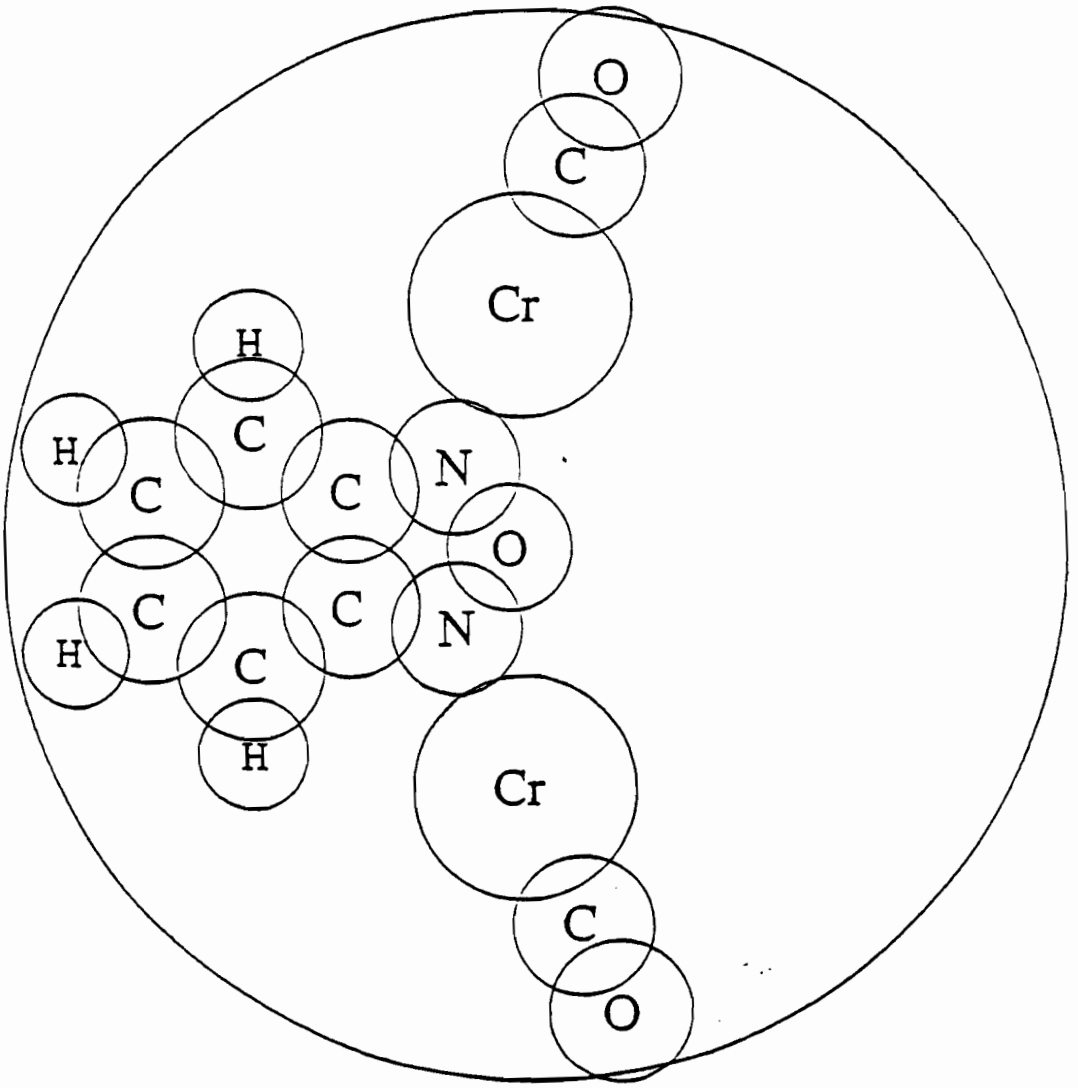

Figure 6. Nuclear positions and muffin-tin sphere radii for 2,1,3-benzoxadiazole$[Cr(CO)_5]_2$ in the molecular plane. The orientation shown here is that used in the following orbital and density figures.

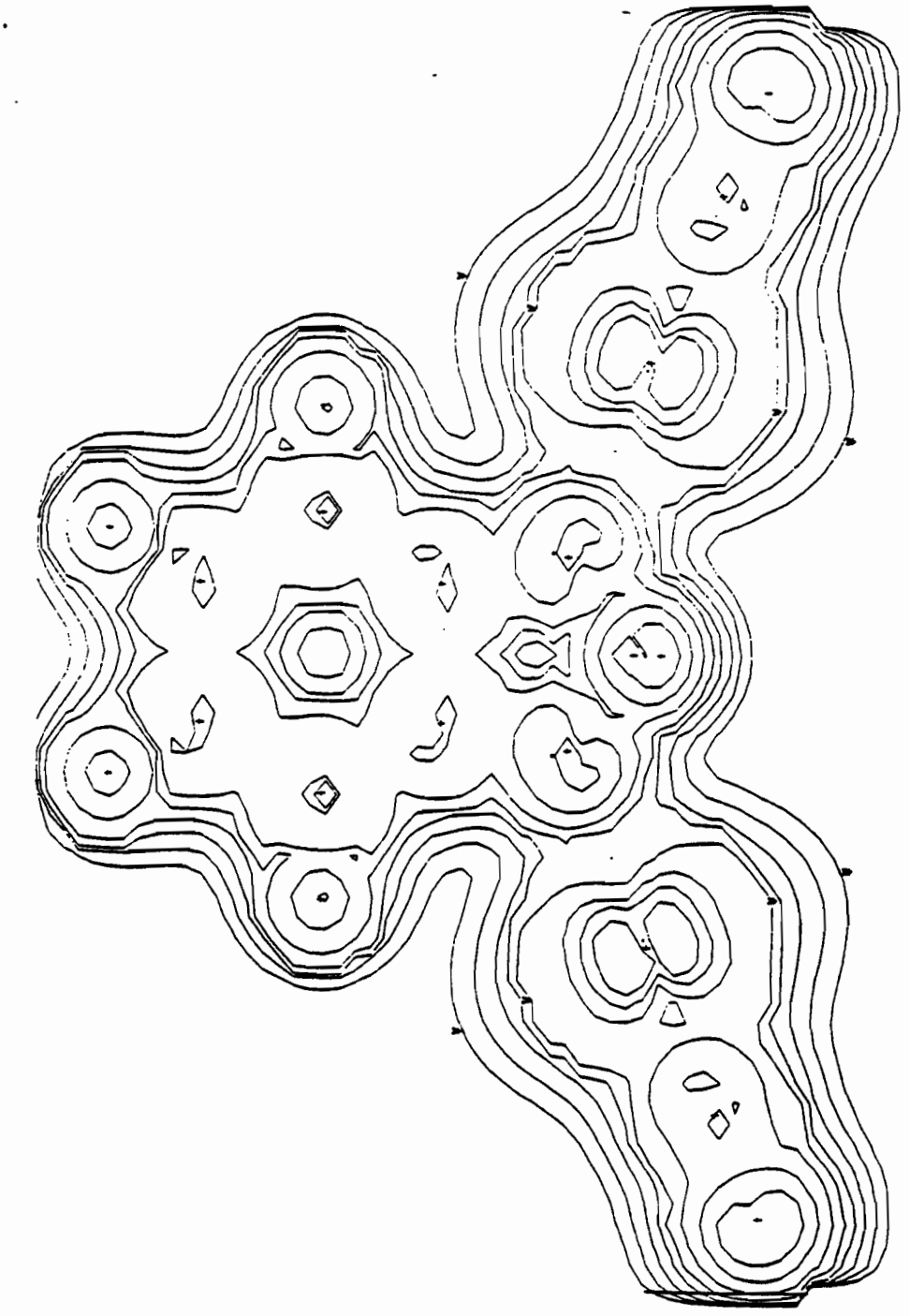

Figure 7a. Total electron density of 2,1,3-benzoxadiazole$[Cr(CO)_5]_2$ in the molecular plane.

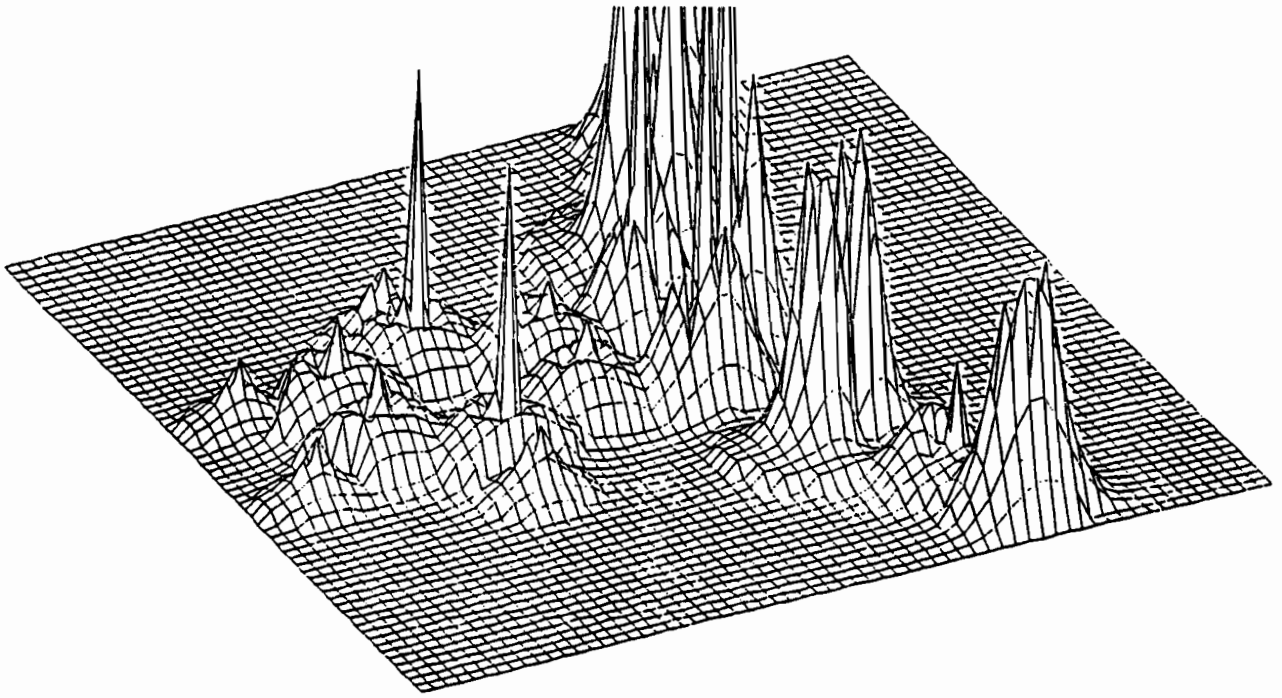

Figure 7b. Total electron density of 2,1,3-benzoxadiazole[$Cr(CO)_5$]$_2$ in the molecular plane; 3-dimensional representation of the same information as Figure 7a.

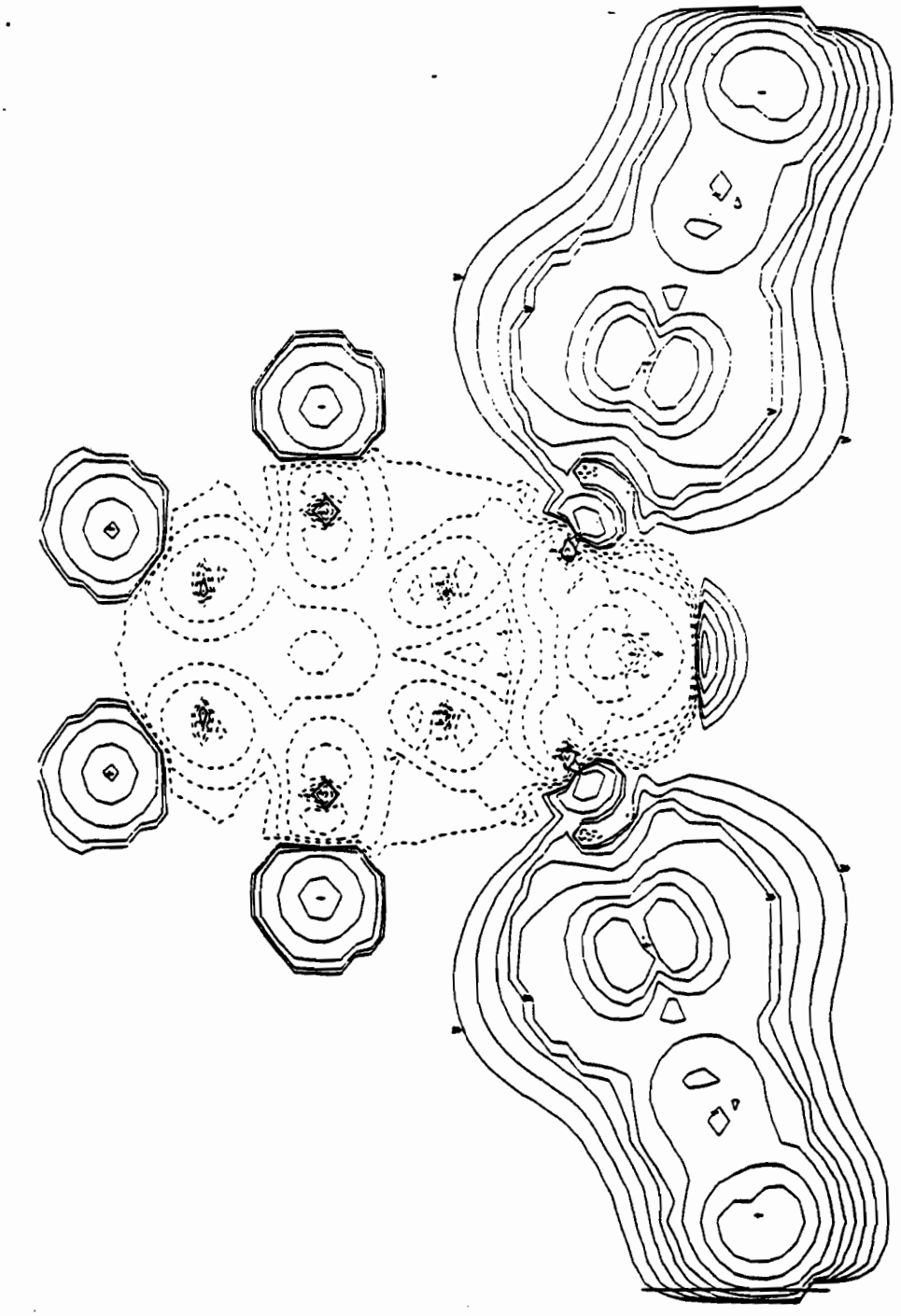

Figure 8a. Total electron density difference, Cr metal complex – isolated heterocycle, in the molecular plane.

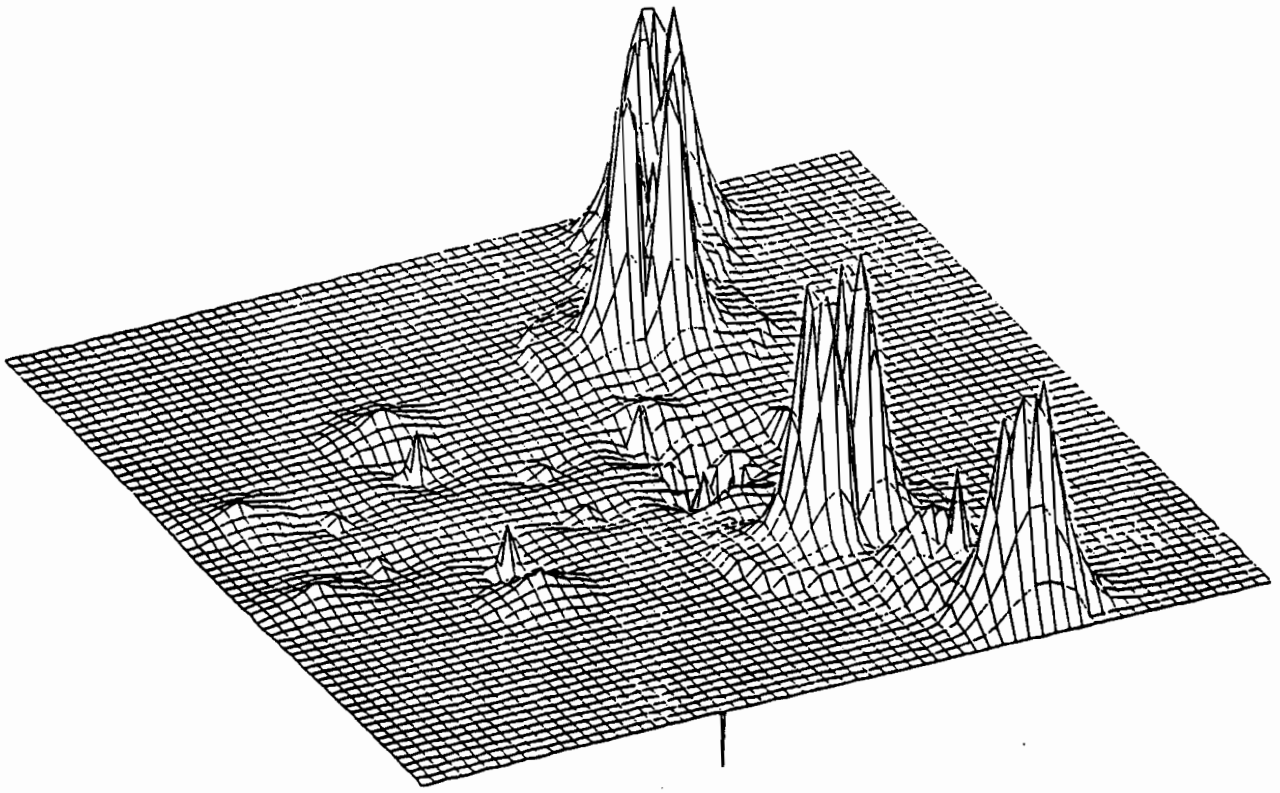

Figure 8b. Total electron density difference, Cr metal complex – isolated heterocycle, in the molecular plane; 3-dimensional representation of the same information as Figure 8a.

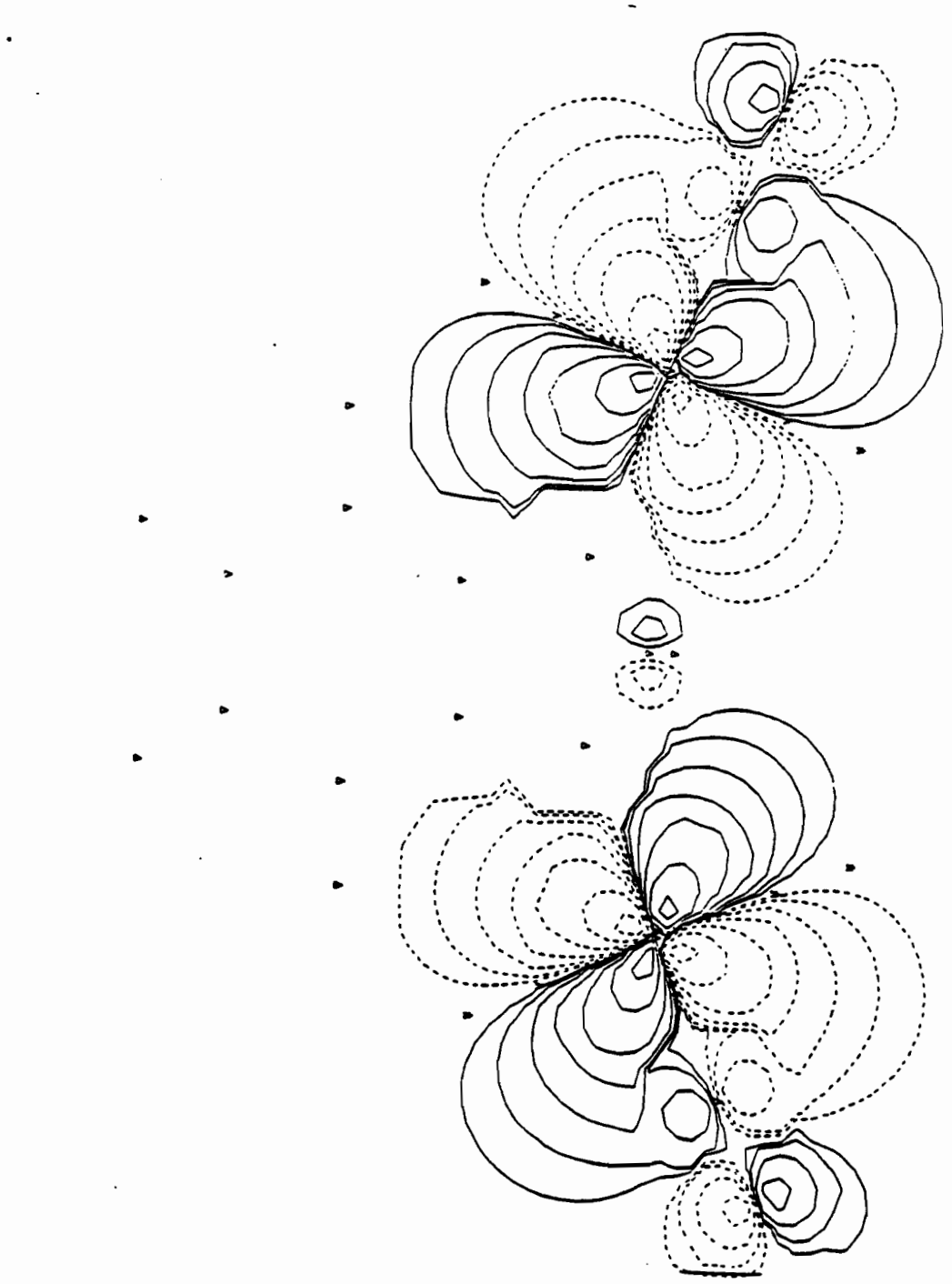

Figure 9. Molecular orbital contours for the $23b_2$ level, in the plane of the molecule.

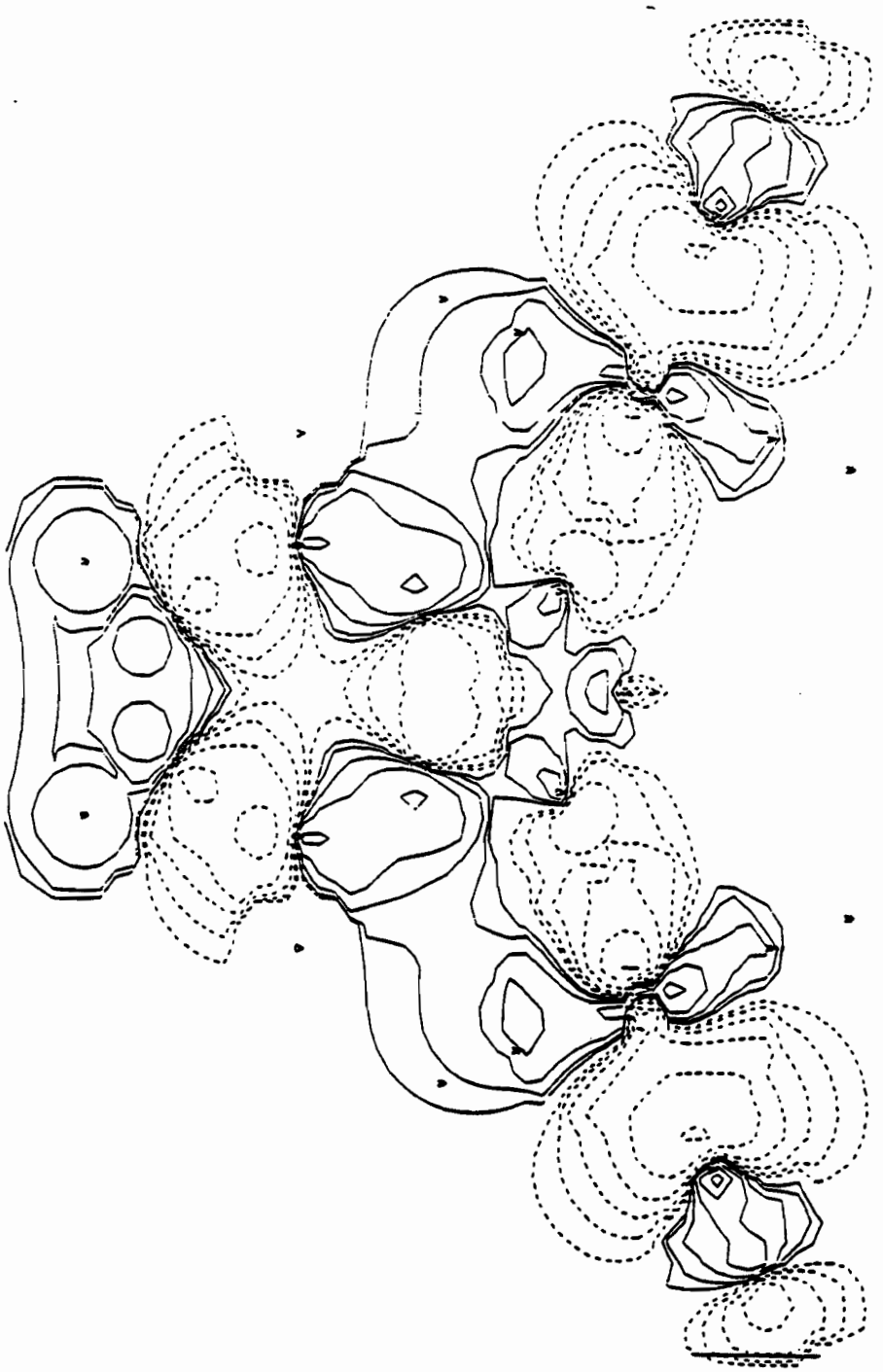

Figure 10. Molecular orbital contours for $14a_1$, in the plane of the molecule.

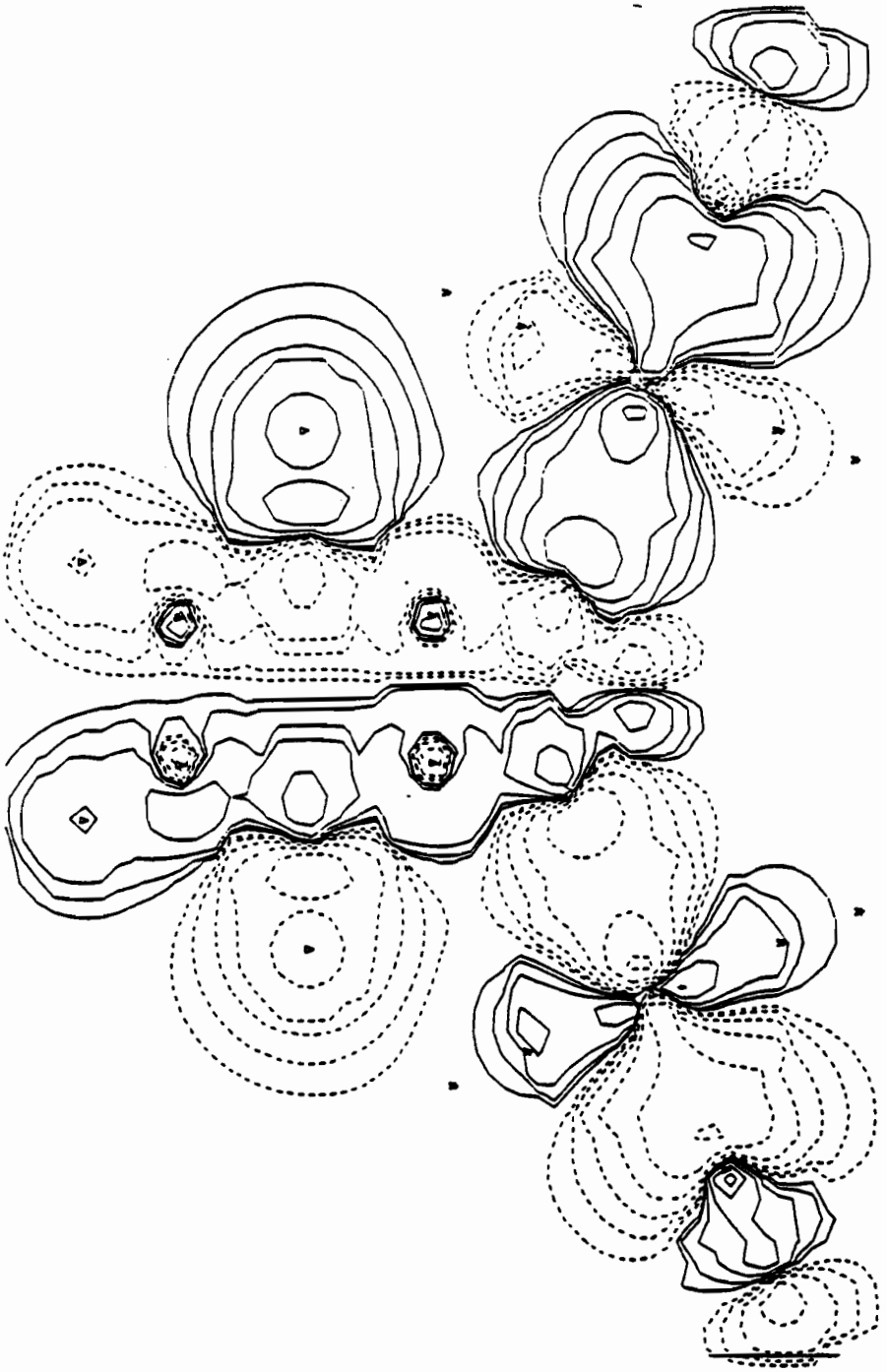

Figure 11. Molecular orbital contours for $13b_2$, in the plane of the molecule.

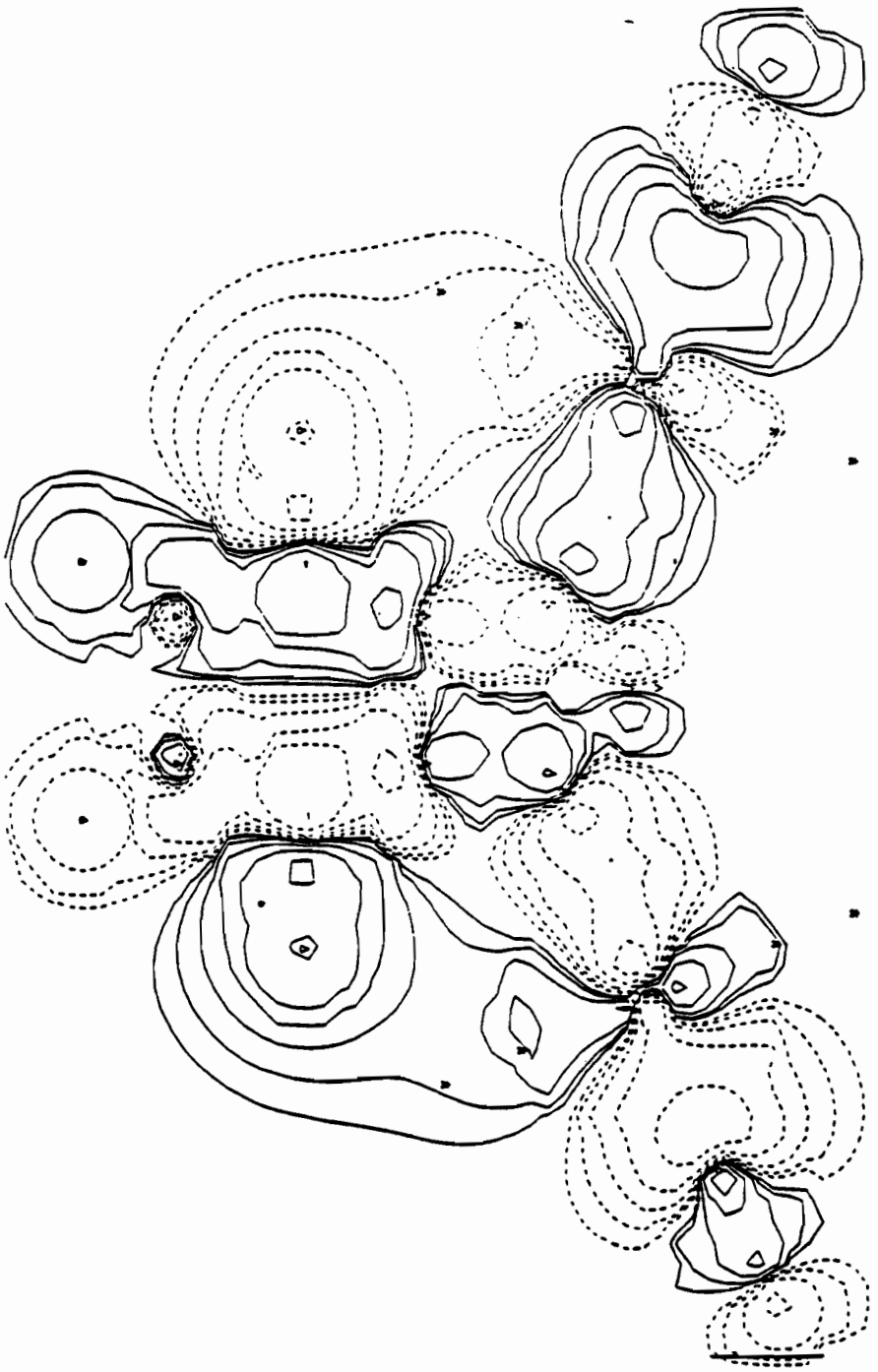

Figure 12. Molecular orbital contours for $12b_2$, in the plane of the molecule.

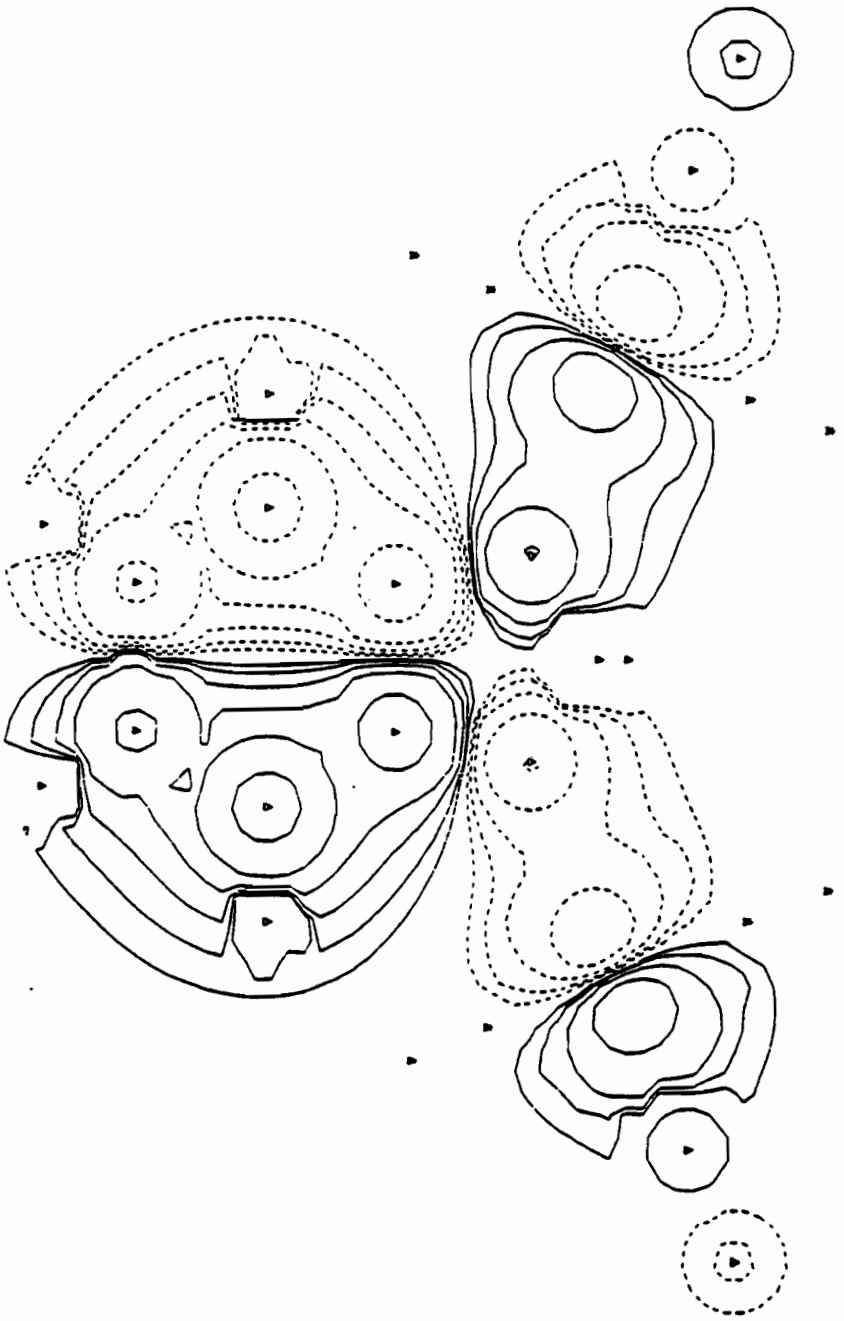

Figure 13. Molecular orbital contours for the $13a_2$ level, 1 au above the plane of the molecule.

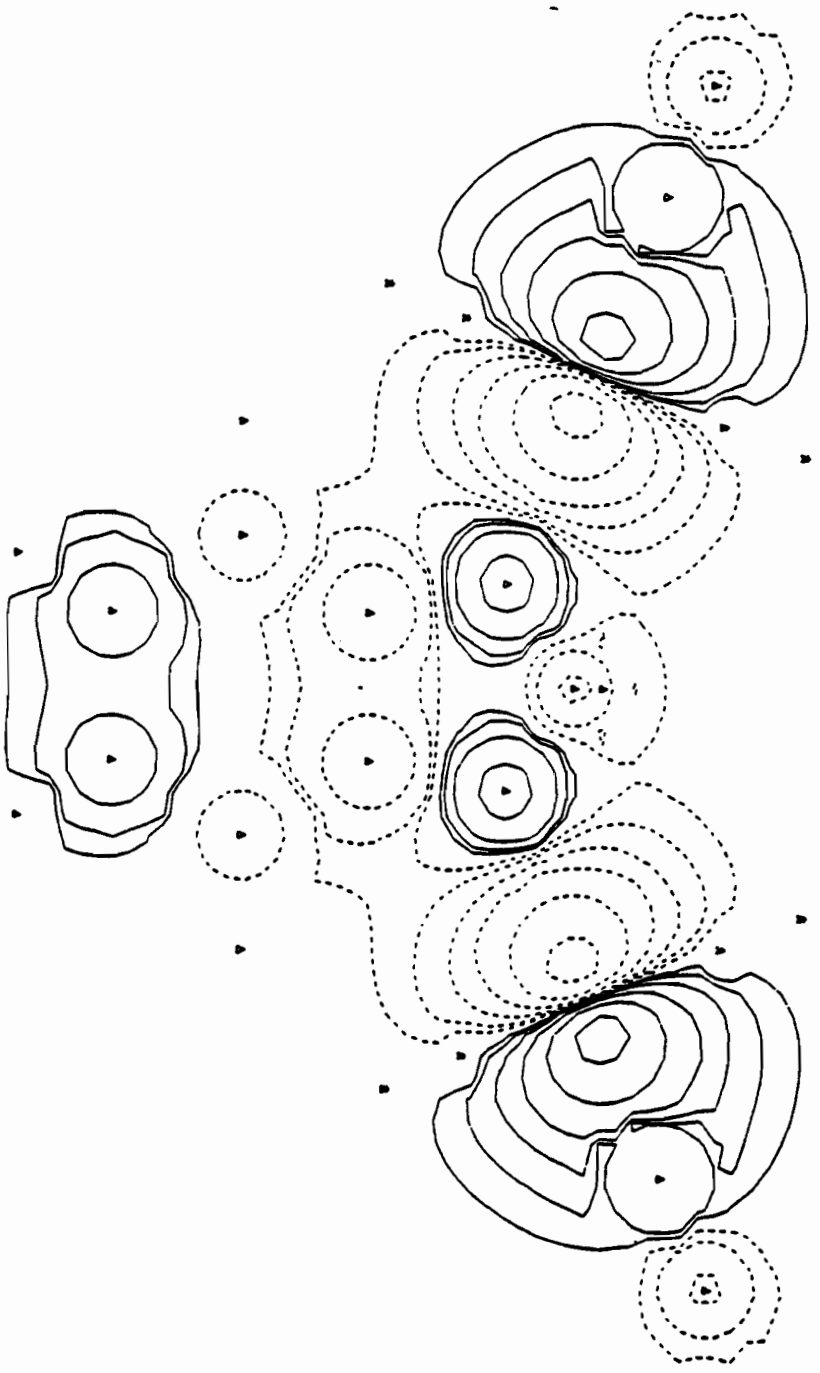

Figure 14. Molecular orbital contours for the $16b_1$ level, 1 au above the plane of the molecule.

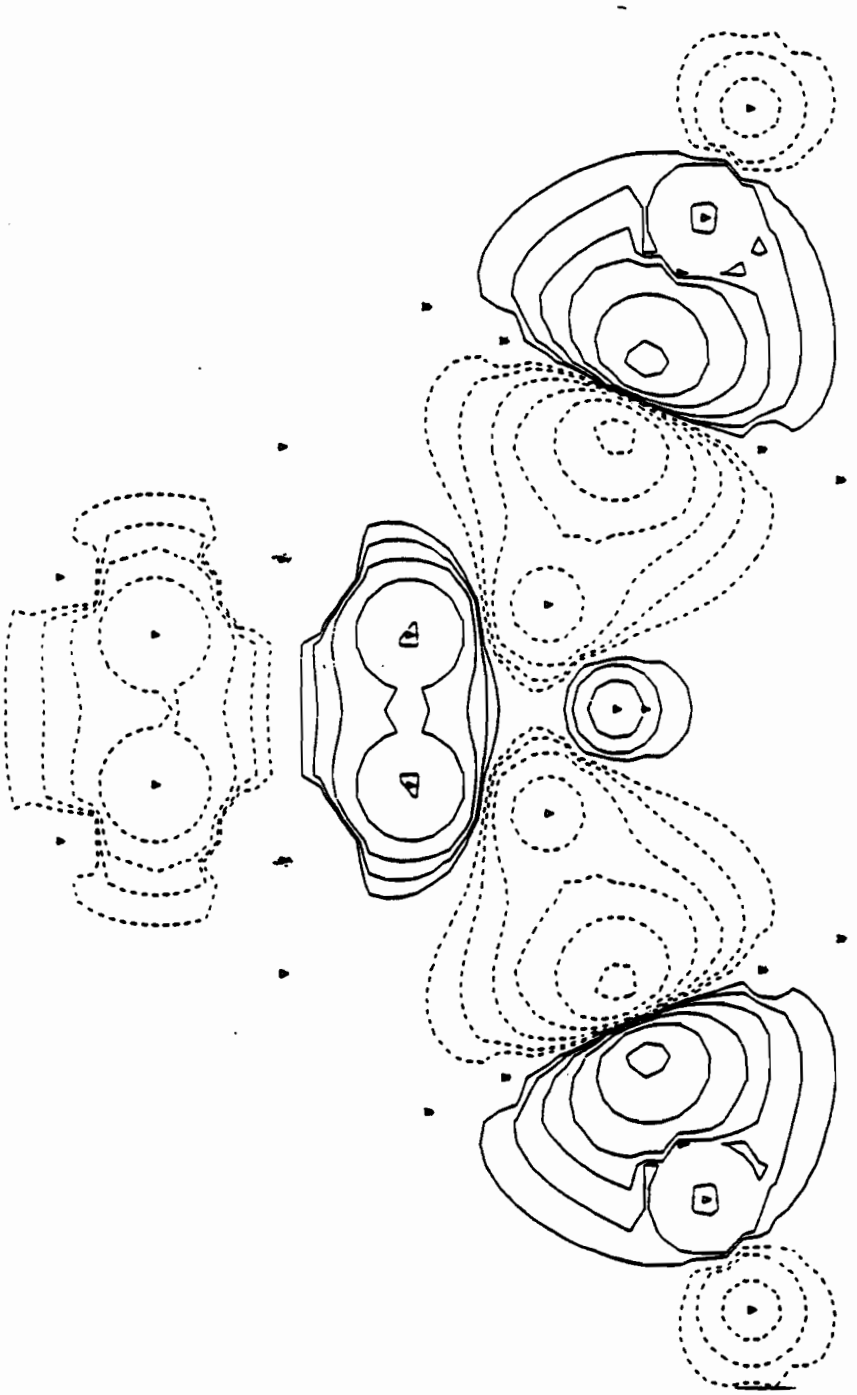

Figure 15. Molecular orbital contours for the $15b_1$ level, 1 au above the plane of the molecule.

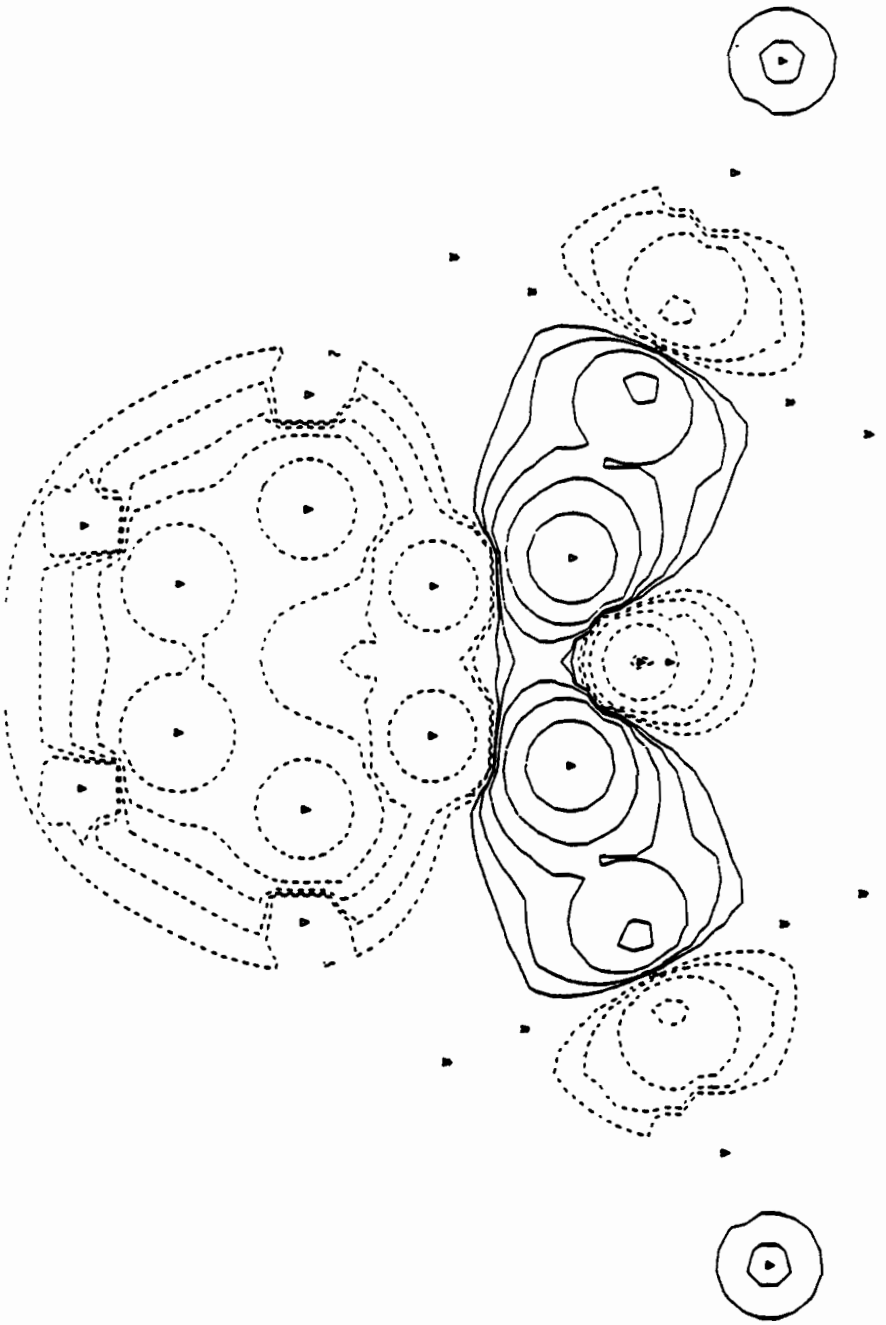

Figure 16. Molecular orbital contours for the $14b_1$ level, 1 au above the plane of the molecule.

References.

Bätzel, V. and R. Boese, 1981, Z. Naturforsch. B **36** , 171

Baerends, E. J. and P. Ros, 1978, Int. J. Quant. Chem. Symp. **12**, 169

Berksoy, E. M. and M. A. Whitehead, 1988, J. Chem. Soc., Faraday Trans. 2 **84**, 1707

Berksoy, E. M. and M. A. Whitehead, 1991, J. Inorg. Chem., in press

Case, D. A. and M. Karplus, 1976, Chem. Phys. Lett. **39**, 33

Case, D. A., M. Cook and M. Karplus, 1980, J. Chem. Phys. **73**, 3294

Case, D. and M.Cook, 1981, Program XASW, *Quantum Chemistry Program Exchange Bulletin*, **1**, 98

Feldhoff, U., F. Grevels, R. P. Kreher, K. Angermund, C., 1986, Chem. Ber., **119**, 1919

Guo, Y., M. C. Wrinn and M. A. Whitehead, 1989, Phys. Rev. A **40**, 6685

Hoffman, R., 1988, Rev. Mod. Phys. **60**, 601

Kaim, W. and S. Kohlmann, 1985, Inorg. Chim. Acta **101**, L21

Kaim, W., S. Kohlmann, S. Ernst, B. Olbrich-Deussner, C. Bessenbacher and A. Schulz, 1987, J. Organomet. Chem. **321**, 215

Kaim, W., S. Kohlmann, A. J. Lees and M. Zulu, 1989, Z. anorg. allg. Chem. **575**, 97

Ladik, J. J., 1988, *Quantum Theory of Polymers as Solids* (Plenum Press, New York)

Lucken, E. A. C., 1969, *Nuclear Quadrupole Coupling Constants* (Academic Press. London, 1969)

Palmer, M. H. and M. F. Kennedy, 1978, J. Mol. Struct. **43**, 33

Raimes, S., 1972, *Many Electron Theory* (North-Holland, Amsterdam)

Ries, W., I. Bernal, M. Quast and T. A. Albright, 1984, Inorg. Chim. Acta. **83**, 5

Salahub, D. R., 1978, J. Chem. Soc., Chem. Commun. **9**, 385

Vosko, S. H., L. Wilk and M. Nusair, 1980, Can. J. Phys. **58**, 1200

Wrinn, M. C. and M. A. Whitehead, 1990, J. Chem. Soc., Faraday Trans. **86**, 889

Wrinn, M. C. and M. A. Whitehead, 1991, submitted for publication

Zulu, M. M. and A. J. Lees, 1988, Inorg. Chem. **27**, 1139

I.4 *Molecular Calculations: the LCAO Method*

I.4.1 Introduction and Background

The Hartree-Fock approximation to the time-independent Schrödinger equation

$$H\Psi = E\Psi \tag{1}$$

formulates the N-body wavefunction Ψ as a single determinant of molecular wavefuncions ψ:

$$\Psi(\mathbf{r}_1, \mathbf{r}_1, \ldots, \mathbf{r}_N) = \sqrt{N!} \begin{vmatrix} \psi_i(\mathbf{r}_1) & \psi_j(\mathbf{r}_1) & \ldots & \psi_k(\mathbf{r}_1) \\ \psi_i(\mathbf{r}_2) & \psi_j(\mathbf{r}_2) & \ldots & \psi_k(\mathbf{r}_2) \\ \vdots & \vdots & \ddots & \vdots \\ \psi_i(\mathbf{r}_N) & \psi_j(\mathbf{r}_N) & \ldots & \psi_k(\mathbf{r}_N) \end{vmatrix} \tag{2}$$

(Szabo and Ostlund, 1989).

The Linear Combination of Atomic Orbitals (LCAO) method replaces the ith molecular wavefunction, $\psi_i(\mathbf{r})$, by a summation over atomic functions:

$$\psi_i(\mathbf{r}) = \sum_p^m c_{pi}\chi_p(\mathbf{r}) \tag{3}$$

where the c_{pi} are coefficients to be determined, and the $\chi_p(\mathbf{r})$ are usually Gaussian or Slater functions (Saluhub, 1987). The practical origins of the LCAO method are Hall (1951) and Roothaan (1951), who showed that this substitution, followed by a variational treatment of the total energy E, reduced the Hartree-Fock equations to a system of coupled linear equations

$$FC = SC\epsilon \tag{4}$$

where F is the Fock operator matrix, C is the matrix of coefficients c_{pi}, S is the matrix of overlap integrals between the $\chi_p(\mathbf{r})$, and ϵ is the matrix of one-electon energies ϵ_i (Hehre *et al.*, 1986).

Equation (4) is solved by making the Fock operator Hermitian with the transform

$$F' = S^{-\frac{1}{2}} F S^{-\frac{1}{2}} \tag{5}$$

which yields the eigenvalue equation

$$F' C' = \epsilon C' \tag{6}$$

After solution of (6), the coefficients c_{pi} which correspond to operator F are recovered by the transform

$$C = S^{-\frac{1}{2}} C' \tag{7}$$

(Starzak, 1989); the elements of C are used to construct a new potential term in the Fock operator, and the process is iterated until self-consistency is achieved (i.e. the change in C between iterations falls below an arbitrary, preset threshold).

The Fock matrix elements $F_{\mu\nu}$ are made up of one- and two-electron integrals:

$$F_{\mu\nu} = H_{\mu\nu} + \sum_{\lambda\sigma}^{N} P_{\lambda\sigma} \left\{ (\mu\nu|\lambda\sigma) - \frac{1}{2}(\mu\lambda|\nu\sigma) \right\} \tag{8}$$

where $H_{\mu\nu}$ describees the interaction of a single electron in the field of the atomic nuclei, and the terms after the summation describe the two-electron interactions:

$$P_{\lambda\sigma} = \sum c_{\lambda i} c_{\sigma i} \tag{9}$$

are the density matrix elements, which are summed over all occupied states;

$$(\mu\nu|\lambda\sigma) = \int \chi_\mu(\mathbf{r}) \chi_\nu(\mathbf{r}) \frac{1}{|\mathbf{r} - \mathbf{r}'|} \chi_\lambda(\mathbf{r}') \chi_\sigma(\mathbf{r}') \, d\mathbf{r}' \, d\mathbf{r} \tag{10}$$

are the Coulomb repulsion integrals, and

$$(\mu\lambda|\nu\sigma) = \int \chi_\mu(\mathbf{r}) \chi_\lambda(\mathbf{r}) \frac{1}{|\mathbf{r} - \mathbf{r}'|} \chi_\nu(\mathbf{r}') \chi_\sigma(\mathbf{r}') \, d\mathbf{r}' \, d\mathbf{r} \tag{11}$$

are the "exchange" integrals.

An LCAO program using Gaussian type orbitals (GTO) was modified by Sambe and Felton (1974) and later Dunlap *et al.* (1979a, 1979b, 1986) to include a local density approximation (LDA) to the exchange integrals:

$$< \chi(\mathbf{r})|v_{ex}|\chi(\mathbf{r}) >= c \int \chi(\mathbf{r})\rho^{\frac{1}{3}}(\mathbf{r})\chi(\mathbf{r})\, d\mathbf{r} \tag{12}$$

This LCGTO-LDA program used Hermite-Gaussian functions for the atomic basis $\chi(\mathbf{r})$. Hermite-Gaussian (HG) functions differ from the more standard Cartesian Gaussians by including the derivative in the functional form; a HG centred at point at point **A** is

$$f(n, a, \mathbf{r}_A) = a^{\frac{n}{2}}\, H_{n1}[a^{\frac{1}{2}}x_{\mathbf{A}}]\, H_{n2}[a^{\frac{1}{2}}y_{\mathbf{A}}]\, H_{n3}[a^{\frac{1}{2}}z_{\mathbf{A}}]e^{\alpha r^2} \tag{13}$$

where, for example,

$$H_{n1}[a^{\frac{1}{2}}x_{\mathbf{A}}] = (-1)^{n_1}\, e^{a^{\frac{1}{2}}x_{\mathbf{A}}}\, \frac{d^{n_1}}{dx^{n_1}}\, e^{-ax_{\mathbf{A}}^2}, \tag{14}$$

$$\mathbf{r}_A = x - A_x, \tag{15}$$

and

$$n = n_1 + n_2 + n_3 \tag{16}$$

(Živković, 1968).

Further details of the LCGTO-LDA program are given in the following section, **I.4.3.**

References.

Dunlap, B. I., J. W. D. Connolly and J. R. Sabin, 1979a, J. Chem. Phys. **71**, 3396

Dunlap, B. I., J. W. D. Connolly and J. R. Sabin, 1979b, J. Chem. Phys. **71**, 4993

Dunlap, B. I. and M. Cook, 1986, Int. J. Quant. Chem. **29**, 767

Hall, G. G., 1951, Proc. Roy. Soc. (London), **A205**, 541

Hehre, W. J., L. Radom, P. Schleyer and J. A. Pople, 1986, *Ab Initio Molecular Orbital Theory* (Wiley, New York)

Roothaan, C. C. J., 1951, Rev. Mod. Phys. **23**, 69

Salahub, D. R., 1987, in *Ab Initio Methods in Quantum Chemistry II (Advances in Chemical Physics, Vol. LXIX)*, edited by K. P. Lawler (Wiley, New York), p. 447

Sambe, H. and R. H. Felton, 1974, J. Chem. Phys. **62**, 1122

Starzak, M. E., 1989, *Mathematical Methods in Chemistry and Physics* (Plenum Press, New York)

Szabo, A. and N. S. Ostlund, 1989, *Modern Quantum Chemistry* (McGraw-Hill, New York)

Živković, T. and Z. B. Maksić, 1968, J. Chem. Phys. **49**, 3083

I.4.3 The Effect of Correlation and the Orbital Dependent Generalized-Exchange on the Equilibrium Geometry of the H_2O Molecule in the LCGTO-LDA Method.

Abstract

An orbital dependent generalized exchange was implemented as a post-SCF correction term within the LCGTO-LDA methodology. Equilibrium geometries of H_2O were calculated with and without a VWN correlation functional. The role of relaxation was examined by comparing result from a post-SCF correlation correction ("unrelaxed"), and the result from the correlation in the one-electron Hamiltonian; the relaxed and unrelaxed results were nearly identical. The orbital dependent correction terms improved significantly the predicted bond length and angle compared with the simple LDA calculation, but increased the force constant $f_{\theta\theta}$, making it further from experiment.

Introduction

Within the Kohn-Sham (1963) theory with the local-density-approximation (LDA), the exchange energy is a functional of the total electron density $\rho(\mathbf{r})$:

$$E_x = -c \int [\rho(\mathbf{r})]^{\frac{4}{3}} \, d\mathbf{r} \tag{1}$$

in atomic units, where

$$c = \frac{3}{4}\left(\frac{6}{\pi}\right) \tag{2}$$

Functionals which depend on orbital densities ρ_i are outside the Kohn-Sham theory. The Coulomb and exchange self-interaction energies do not exactly cancel in the Kohn-Sham LDA, and the self-interaction-correction (SIC) to this failure yields an additional, orbital-dependent energy term (Perdew and Zunger, 1981):

$$E_{SIC} = \sum_{i\sigma} \left\{ -\frac{1}{2} \int \frac{\rho_{i\sigma}(\mathbf{r})\rho_{i\sigma}(\mathbf{r}')}{|\mathbf{r}-\mathbf{r}'|} \, d\mathbf{r} \, d\mathbf{r}' + \mathrm{c} \int [\rho_{\mathrm{i}}(\mathbf{r})]^{\frac{4}{3}} \, \mathbf{dr} \right\} \tag{3}$$

where $\rho_{i\sigma}$ refers to the density of the ith orbital of spin σ.

This SIC Hamiltonian does not posses unitary transform invariance – the individual ρ_i (though not their sum ρ) are not invariant, so their energy contribution and the total energy are sensitive to the particular choice of basis, symmetry orbitals, localized orbitals or other hybrids.

The conventional approach in molecular LDA ignores the self-interaction problem, and assumes that the exactly-calculated Coulomb self-interaction terms will cancel the exchange self-interaction to sufficient accuracy. Besides Perdew and Zunger, Harrison (1983, 1987) showed the importance of SIC in predicting atomic properties such as electron affinities. A series of small-molecule calculations (Pederson *et al.*, 1984, 1985; Heaton *et al.*, 1987; Guo and Whitehead, 1991) exploited the lack of invariance by finding the basis which minimizes the energy; for the SIC, a localization transform maximizes the negative integrals over the ρ_i functional.

Another orbital-dependent Hamiltonian was introduced by Manoli and Whitehead (1988a,b,c), who derived a Generalized Exchange (GX) Hamiltonian from density-matrix and limiting case arguments. The GX exchange energy is

$$E_x[\rho(\mathbf{r})] = \int \rho(\mathbf{r}) \left\{ U_{ex}(\mathbf{r}) \right\} d\mathbf{r} \tag{4}$$

where

$$U_{i,ex}^{GX}(\mathbf{r}) = -9c\,\alpha^{lim} \frac{\rho_\sigma(\mathbf{r}) + B_1 \rho_{i\sigma}(\mathbf{r})}{[\rho_\sigma(\mathbf{r}) + B_2 \rho_{i\sigma}(\mathbf{r})]^{\frac{2}{3}}} \tag{5}$$

and the constants α^{lim}, B_1 and B_2 are determined by the choice of Fermi hole model.

Because there are orbital-dependent terms of opposing signs in the exchange and SIC expressions, a localization transform will not in this case have such a large influence on the total energy as in equation (2); the GX-SIC Hamiltonian could be described as less non-invariant than the the simple SIC case.

In this work, the GX-SIC was implemented into a linear combination of Gaussian-type orbitals local density approximation (LCTGTO-LDA) molecular program as an additive correction to the LDA energy. Additive energy corrections are a standard feature in Hartree-Fock *ab initio* programs, typically as a perturbation expansion term to provide correlation energy (e.g. MP2 corrections). An LDA correlation functional has been used as a post-SCF correction to Hartree-Fock calculations (Clementi *et al.*, 1990). To investigate the differences between correlation energies as post-SCF corrections, an unrelaxed correlation energy, and as an intrinsic part of the SCF procedure by inclusion in the one-electron Hamiltonian, a relaxed correlation energy, calculations were performed in both ways with a Vosko-Wilk-Nusair (1985) (VWN) correlation functional.

The H_2O molecule was used as a test case, to calculate both the equilibrium geometry and force constant $f_{\theta\theta}$. Water is a well-studied system in theoretical chemistry; calculations span more than half a century: Van Vleck (1933) performed a vibrational analysis with a model potential; Yamaguchi (1980) did a large-basis *ab initio* calculation of vibrational frequencies; Zhao (1990) did a rigorous, correlated (MP4) study. Within the Local Density Functional approach, MS-Xα calculations were done by Connolly (1972), Mitzdorf (1975) and Baerends (1975), but geometry optimization was not possible due to the muffin-tin potentials used in the MS-Xα method. Krijn (1988) and Versluis (1989) have both performed water optimizations with a Slater-orbital version of the LCAO-LDA method.

Computational Details

The Linear Combination of Gaussian Type Orbitals, with the Local Density Approximation (LCGTO-LDA) program of Sambe (1974) and Dunlap (1979a,b) uses an auxiliary set of Gaussian functions to fit the density in both the exchange integrals. Four-centre Coulomb integrals

$$< i|V_C|j > = \int \chi_i(\mathbf{r}) \left\{ \int \frac{\sum_k \chi_k(\mathbf{r}') \sum_l \chi_l(\mathbf{r}')}{|\mathbf{r} - \mathbf{r}'|} \, d\mathbf{r}' \right\} \chi_j(\mathbf{r}) \, d\mathbf{r} \tag{6}$$

$$= \int \chi_i(\mathbf{r}) \left\{ \int \frac{\rho(\mathbf{r}')}{|\mathbf{r} - \mathbf{r}'|} \, d\mathbf{r}' \right\} \chi_j(\mathbf{r}) \, d\mathbf{r} \tag{7}$$

are estimated by fitting the density $\rho(\mathbf{r}')$ to an a set of functions $f_m(\mathbf{r}')$ which comprise the charge fitting basis:

$$\rho(\mathbf{r}') \simeq \sum_m a_m f_m(\mathbf{r}') \tag{8}$$

The $f_m(\mathbf{r}')$ are often chosen as a subset of the orbital basis, to minimize the number of primitives used in the calculation.

There are two possible integration schemes to calculate the total Coulomb energy: over both orbital and fitting bases (a three-centre, single-fit quantity),

$$U_C = \sum_{i,j} < i|V_C|j > \tag{9}$$

$$\tilde{U}_C \simeq \sum_{i,j} c_i c_j \int \chi_i(r) \left\{ \int \frac{\sum_m a_m f_m(\mathbf{r})}{|\mathbf{r} - \mathbf{r}'|} \, d\mathbf{r}' \right\} \chi_j(\mathbf{r}) \, d\mathbf{r} \tag{10}$$

or over the fitting basis entirely (a two-centre, doubly fit quantity),

$$U_C = \int \frac{\rho(\mathbf{r})\rho(\mathbf{r}')}{|\mathbf{r} - \mathbf{r}'|} d\mathbf{r}' \, d\mathbf{r} \tag{11}$$

$$\tilde{\tilde{U}}_C \approx \int \frac{\sum_m a_m f_m(\mathbf{r}) \sum_n a_n f_n(\mathbf{r}')}{|\mathbf{r} - \mathbf{r}'|} \, d\mathbf{r}' \, d\mathbf{r} \tag{12}$$

In practice, to minimize the error due to fitting, the total Coulomb energy U_C is calculated as a combination of the two schemes (Dunlap, 1979):

$$U_C = 2\tilde{U}_C - \tilde{\tilde{U}}_C \tag{13}$$

The charge fitting itself is carried out by minimizing

$$D = \int (\rho(\mathbf{r}) - \tilde{\rho}(\mathbf{r}))^2 \, d\mathbf{r} \tag{14}$$

subject to the normalization constraint

$$\int \tilde{\rho}(\mathbf{r}) \, d\mathbf{r} = \sum_i a_i \int f_i(\mathbf{r}) \, d\mathbf{r} = N \tag{15}$$

where N is the total number of electrons in the system.

The coefficients a_k are formally determined by the relation

$$\mathbf{a} = \mathbf{S}^{-1}(\mathbf{t} + \lambda \mathbf{n}) \tag{16}$$

where

$$n = \int f_i(\mathbf{r}) \, d\mathbf{r} \tag{17}$$

$$\lambda = \frac{N - \mathbf{n} \cdot \mathbf{S}^{-1} \cdot \mathbf{t}}{\mathbf{n} \cdot \mathbf{S}^{-1} \cdot \mathbf{n}} \tag{18}$$

$$t_i = \int \frac{\rho(\mathbf{r}) f_i(\mathbf{r}')}{|\mathbf{r} - \mathbf{r}'|} \, d\mathbf{r} \, d\mathbf{r}' \tag{19}$$

$$S_{ij} = \int \frac{f_i(\mathbf{r}) f_j(\mathbf{r}')}{|\mathbf{r} - \mathbf{r}'|} \, d\mathbf{r} \, d\mathbf{r}' \tag{20}$$

The fitting procedure requires that values of $\rho(\mathbf{r})$ be selected on a grid of points. Dunlap (1986) and Jones (1988) have investigated the "noise" associated with three-dimensional grid choices, and found the grid noise below that from other considerations, such as basis set choice. The H_2O molecule investigated in this work used

about 400 points in the fitting grid; a grid slice in the molecular plane is in Figure 1.

Coulomb self-interaction integrals arise from (1) and (1a) when $i = j = k = l$:

$$< ii||ii >= \int \chi_i(\mathbf{r}) \left\{ \int \frac{\chi_i(\mathbf{r}')\chi_i(\mathbf{r}')}{|\mathbf{r} - \mathbf{r}'|} \, d\mathbf{r}' \right\} \chi_i(\mathbf{r}) \, d\mathbf{r} \tag{21}$$

For the case of non-orthogonal basis functions (e.g. Hermite-Gaussian), the situation is more complicated; the number of self-interaction integrals over primitive functions (i.e. the orbital and fitting basis functions) is larger than implied by equation(10). In terms of the molecular wavfunctions $u_i(\mathbf{r})$:

$$u_i(\mathbf{r}) = \sum_m c_m^i \chi_m^i(\mathbf{r}), \tag{22}$$

the Coulomb self interaction integrals are

$$U_C^{SI} = \sum_i \int u_i(\mathbf{r}) \left\{ \int \frac{\rho_i(\mathbf{r}')}{|\mathbf{r} - \mathbf{r}'|} \, d\mathbf{r}' \right\} u_i(\mathbf{r}) \, d\mathbf{r} \tag{23}$$

$$= \sum_i \int \sum_m c_m^i \chi_m^i(\mathbf{r}) \left\{ \int \frac{\rho_i(\mathbf{r}')}{|\mathbf{r} - \mathbf{r}'|} \, d\mathbf{r}' \right\} \sum_m c_m^i \chi_m^i(\mathbf{r}) \, d\mathbf{r} \tag{24}$$

where

$$\rho_i(\mathbf{r}') = u_i(\mathbf{r}) u_i(\mathbf{r}) \tag{25}$$

$$= \sum_m c_m^i \chi_m^i(\mathbf{r}) \sum_n c_n^i \chi_n^i(\mathbf{r}) \tag{26}$$

Note that cross terms $\chi_m^i \chi_n^i$ are included; $\rho_i(\mathbf{r}')$ is not simply the sum of all $\chi_m^i \chi_m^i$ products.

A self-interaction corrected (SIC) Coulomb energy would be written

$$U_C^{SIC} = \sum_{i,j} < i|V_C|j > - U_C^{SI} \tag{27}$$

Alternatively, the self-interaction is removed by not allowing an electron to interact with its own density. Rewriting the total density as the sum of all the orbital densities:

$$\rho(\mathbf{r}) = \sum_{i}^{occupied} \rho_i(\mathbf{r}), \tag{28}$$

and inserting this into equation (9),

$$U_C = \sum_i \int \frac{\sum_i \rho_i(\mathbf{r}) \sum_j \rho_j(\mathbf{r}')}{|\mathbf{r} - \mathbf{r}'|} d\mathbf{r}' \, d\mathbf{r} \tag{29}$$

$$= \int \frac{\sum_i \rho_i(\mathbf{r}) \sum_{j \neq i} \rho_j(\mathbf{r}')}{|\mathbf{r} - \mathbf{r}'|} d\mathbf{r}' \, d\mathbf{r} + \sum_i \int \frac{\rho_i(\mathbf{r}) \rho_i(\mathbf{r}')}{|\mathbf{r} - \mathbf{r}'|} d\mathbf{r}' \, d\mathbf{r} \tag{30}$$

The second term in (30) is the self-interaction contribution; its cancellation is thus effected by

$$U_C^{SIC} = U_C - \sum_i \int \frac{\rho_i(\mathbf{r}) \rho_i(\mathbf{r}')}{|\mathbf{r} - \mathbf{r}'|} d\mathbf{r}' \, d\mathbf{r} \tag{31}$$

$$= U_C - U_C^{SI} \tag{32}$$

To apply the fitting procedure (8) to either of equations (24) or (32), it is necessary to fit $\rho_i(\mathbf{r}')$ in a manner analogous to equation (8):

$$\rho_i(\mathbf{r}') \simeq \sum_m a_m^{SI} f_m(\mathbf{r}') \tag{33}$$

By using the same fitting basis $f_m(\mathbf{r}')$ for $\rho_i(\mathbf{r}')$ as for the total charge $\rho(\mathbf{r}')$, the calculation of new integrals is avoided.

SIC integrals, like their total charge density counterparts, can be calculated in either a singly or doubly fit manner; integral values over the primitives will be identical to those of equations (10) and (12), respectively.

If the fitting procedure is sufficiently accurate, we should find

$$\tilde{U}_C = \tilde{\tilde{U}}_C \tag{34}$$

and

$$\tilde{U}_C^{SIC} = \tilde{\tilde{U}}_C^{SIC} \quad ; \tag{35}$$

these identities provide a useful way to verify whether programming has been done correctly.

The orbital-dependent GX terms (equation 5) were implemented with a procedure similar to that for the SIC.

The Dunning-Huzinaga 9s/5p basis set was used on oxygen.

Results and Discussion

Each one-electron level, in an orbital-density dependent theory, experiences a different potential in the one-electron Fock equations. To show the difference between the GX potentials and the conventional local density approximation (LDA), the potential difference LDA–GX is plotted in Figures 2 and 3 for the water $1a_1$ and $1b_2$ levels, respectively, in the plane of the molecule. Two choices of Fermi hole model are shown: the GWB (for Gopinathan, Whithead and Bogdanovic (1976)), which approximates the Fermi hole shape as a linear function, and the FEL (for free electron limit), a rigorous description for the electron gas case.

The GWB and FEL models give nearly identical potential-difference plots for the $1a_1$, showing a much larger potential value compared to LDA in the region of the oxygen lone pair; the FEL is about 20% larger than the GWB. For the $1b_1$, the character is very different between the two models; the FEL again raises the potential in the O lone pair region, end reduces it, compared to LDA, in the region between the oxygen and the two hydrogen atoms. GWB, in contrast, shows a smaller difference to LDA (the magnitude of the GWB peak in Figure 3 is less than one-third that of the FEL), and of a very different character: the difference is centred on the oxygen nucleus, and there is no reduction in potential along the O–H bonds.

For the other occupied levels, FEL was consistently larger than GWB; as between the $1a_1$ and $1b_1$, FEL maintained a consistent structure with respect to LDA. For the quantitative portion of this work, only the FEL potential was used.

Because energy gradients were not available in this version of the LCGTO-LDA program, equilibrium geometries were found by calculating many points on a potential surface, and fitting those values to a polynomial in E, r and θ. Force constants $f_{\theta\theta}$ were found by fitting the available data to the expression (Szabo and Ostlund, 1989)

$$E(r_1, r_2, \theta) = E_{eqm} + \frac{1}{2} f_{rr} \left\{ (r_1 - r_{eqm})^2 + (r_2 - r_{eqm})^2 \right\} + \frac{1}{2} f_{\theta\theta} r_{eqm}^2 (\theta - \theta_{eqm})^2 \quad (36)$$

Values of the total energy at each point, and the resulting predicted values of r, θ_{eqm} and $f_{\theta\theta}$ are in Tables 1 through 4.

Table 1 compares the results of an exchange-only LDA calculation, a post-SCF correlation correction (LDA + VWN), an "exchange only" value that is derived from a calculation converged with VWN correlation in the one-electron equations but omitted from the final energy, and a self-consistent VWN correlation result (LDA/VWN). The unrelaxed (LDA + VWN) and relaxed (LDA/VWN) correlation results give identical geometries and essentially identical force constants, despite a consistent difference in the total energies. The self-consistent correlation has shifted the energy surface downward by a few millihartrees with respect to the post-SCF, but retained the minima and and shape. The VWN predicted bond length of 0.985 $\AA$ is closer to the experimental value of 0.958, but the VWN predicted bond angle of 107.2° is much further from the experimental value of 104.5° than is the LDA value of 105.5°. Finally, the VWN correlation improves the highly exaggerated LDA value of 2.538 md/$\AA$ for $f_{\theta\theta}$; the correlated value of 0.834 is much closer to the experimental value of 0.69 (Wilson, 1980).

Table 2 shows the results for GX as a post-SCF correction; the SCF was converged on the LDA Hamiltonian. The LDA values are repeated from Table 1, for comparison. GX results with no SIC are also shown, to show the magnitude of the SIC energy for this case: GX total energies are shifted downward by more than 1 hartree by the spurious Coulomb and exchange self-interaction energy.

The geometry predicted by the LDA+GX+SIC calculation is very good: 0.969 $\AA$ for the O–H bond distance, and 104.4° for the angle. The force constant is too high by a factor of 2, but is much better than the LDA result.

The results from adding both the GX-SIC and the VWN correlation to the converged SCF results are in Table 3. The correlation energy brings both the LDA and GX-SIC value for r_{eqm} closer to experiment, but the prediction for θ moves further from experiment. The GX-SIC θ value, however, is more stable than the LDA; it changes by 0.6°, while the LDA changes by 1.7°. The force constant $f_{\theta\theta}$ are lowered for both the LDA and GX-SIC, with the LDA moving closer to experiment. The GX-SIC $f_{\theta\theta}$ value is more stable with regard to correlation.

The geometries for LDA and GX-SIC from relaxed (converged on VWN) correlation calculations, Table 4, show no change from the unrelaxed.

The relative shapes and positions of the energy wells for both LDA and GX-SIC, for this correlated case, are in Figure 4. The O–H bond distance was held fixed at the experimental value of 0.958 for the curve in Figure 4; this caused the GX-SIC to lie at a higher absolute energy than the LDA, but the qualitative features of the graph resemble those shown in Table 4: the equilibrium bond angle is closer to experiment in the GX-SIC case; the steeper parabola around the minimum corresponds to the larger force constant.

Conclusion

Including a correlation functional in the SCF convergence procedure gave geometry results for water no different from using correlation as a post-SCF correction. The nonlocal, orbital-density dependent GX-SIC exchange functional significantly improved the equilibrium geometry predictions for water, and stablized the results with respect to electron correlation. Though this study examined only one molecule, with one basis set, the results suggest that further investigation into a molecular GX-SIC functional is required.

Table 1. Total energies (-au), equilibrium geometry and force constant $f_{\theta\theta}$ for H_2O by several schemes. Columns 1 and 2: values converged on the LDA exchange only; columns 3 and 4: values converged on the VWN correlation functional.

θ	r_{OH}(au)	LDA	LDA+VWN	LDA exch-only	LDA/VWN
100	1.78	75.22523986	75.88789091	75.22478847	75.88864027
100	1.81	75.22893844	75.89086372	75.22849117	75.89162139
100	1.84	75.23150047	75.89270586	75.23105661	75.89347127
100	1.87	75.23254487	75.89301273	75.23210122	75.89378268
100	1.91	75.22658917	75.89216168	75.23221432	75.89293673
105	1.78	75.22766744	75.89028466	75.22721942	75.89103637
105	1.81	75.23089916	75.89278328	75.23045218	75.89354004
105	1.84	75.23248239	75.89361704	75.23203511	75.89437764
105	1.87	75.23352540	75.89393508	75.23307513	75.89469686
105	1.91	75.23327463	75.89272041	75.23282039	75.89348407
110	1.78	75.22822271	75.89078004	75.22778250	75.89153890
110	1.81	75.23110495	75.89292777	75.23066304	75.89368885
110	1.84	75.22554354	75.89363235	75.23210752	75.89439228
110	1.87	75.23147979	75.89349478	75.23269527	75.89425275
110	1.91	75.23272216	75.89211401	75.23226097	75.89286905
$r_{eqm}(\AA)$		0.992	0.985	0.996	0.985
θ_{eqm}		105.5	107.2	107.4	107.2
$f_{\theta\theta}$		2.538	0.837	0.695	0.834

Table 2. Total energies (-au), equilibrium geometry and force constant $f_{\theta\theta}$ for H_2O by several schemes. Energies were converged using the LDA exchange only; no correlation is included.

θ	r_{OH}(au)	LDA	LDA + GX	LDA+GX+SIC
100	1.78	75.22523986	76.79551052	75.74610589
100	1.81	75.22893844	76.79641971	75.74880201
100	1.84	75.23150047	76.79621857	75.75011042
100	1.87	75.23254487	76.79442158	75.74845722
100	1.91	75.22658917	76.79083315	75.74485511
105	1.78	75.22766744	76.79725963	75.74767457
105	1.81	75.23089916	76.79783154	75.75053469
105	1.84	75.23248239	76.79677455	75.75035553
105	1.87	75.23352540	76.79502633	75.74900715
105	1.91	75.23327463	76.79121435	75.74511596
110	1.78	75.22822271	76.79901053	75.74746714
110	1.81	75.23110495	76.79934537	75.74990236
110	1.84	75.22554354	76.79813014	75.74883752
110	1.87	75.23147979	76.79609245	75.74672288
110	1.91	75.23272216	76.79221873	75.74243524
$r_{eqm}(\AA)$		0.992		0.969
θ_{eqm}		105.5		104.4
$f_{\theta\theta}$		2.538		1.424

Table 3. Total energies (-au), equilibrium geometry and force constant $f_{\theta\theta}$ for H_2O by several schemes. Energies were converged using the LDA exchange only, but the VWN correlation energy was calculated and added to the total.

θ	r_{OH}(au)	LDA	LDA + GX	LDA+GX+SIC
100	1.78	75.88789091	77.45816157	76.40875694
100	1.81	75.89086372	77.45834499	76.41072729
100	1.84	75.89270586	77.45742396	76.41131581
100	1.87	75.89301273	77.45488944	76.40892508
100	1.91	75.89216168	77.45033592	76.40435788
105	1.78	75.89028466	77.45987685	76.41029179
105	1.81	75.89278328	77.45971566	76.41241881
105	1.84	75.89361704	77.45790921	76.41149019
105	1.87	75.89393508	77.45543601	76.40941683
105	1.91	75.89272041	77.45066013	76.40456174
110	1.78	75.89078004	77.45960433	76.41067723
110	1.81	75.89292777	77.45921397	76.41239654
110	1.84	75.89363235	77.45726940	76.41062570
110	1.87	75.89349478	77.45451692	76.40782057
110	1.91	75.89211401	77.44971068	76.40263560
$r_{eqm}(\AA)$		0.985		0.963
θ_{eqm}		107.2		105.0
$f_{\theta\theta}$		0.837		1.004

Table 4. Total energies (-au), equilibrium geometry and force constant $f_{\theta\theta}$ for H_2O by several schemes. Energies were converged using the VWN exchange-correlation functional.

θ	r_{OH}(au)	LDA	LDA + GX	LDA+GX+SIC
100	1.78	75.88864027	77.46128645	76.40923343
100	1.81	75.89162139	77.46147065	76.41119791
100	1.84	75.89347127	77.46054946	76.41177703
100	1.87	75.89378268	77.45800941	76.40935653
100	1.91	75.89293673	77.45344747	76.40474533
105	1.78	75.89103637	77.46301997	76.41080022
105	1.81	75.89354004	77.46285591	76.41291740
105	1.84	75.89437764	77.46104434	76.41196650
105	1.87	75.89469686	77.45856169	76.40986000
105	1.91	75.89348407	77.45377388	76.40495682
110	1.78	75.89153890	77.46276694	76.41122351
110	1.81	75.89368885	77.46237118	76.41292817
110	1.84	75.89439228	77.46041490	76.41112228
110	1.87	75.89425275	77.45764993	76.40828036
110	1.91	75.89286905	77.45282681	76.40304332
$r_{eqm}(\AA)$		0.985		0.962
θ_e		107.2		105.1
$f_{\theta\theta}$		0.834		1.001

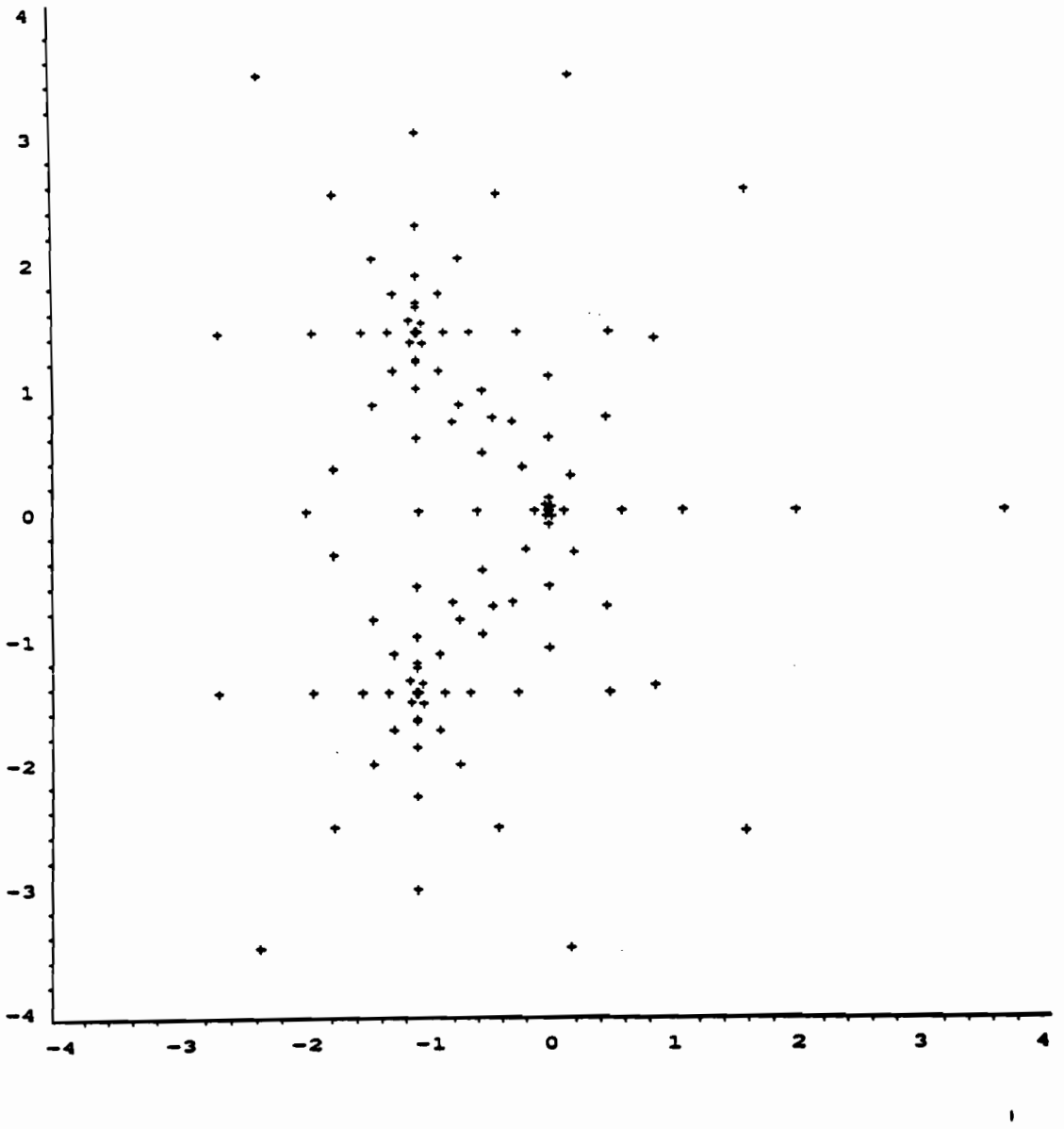

Figure 1. Grid points where the density $\rho(\mathbf{r})$ is calculated for fitting to an auxiliary set of Gaussian functions, in the LCGTO-LDA method. Points shown are in the plane of the H_2O molecule; the oxygen atom is at the 0,0 position, with the two hydrogen atoms to the left. Axes are in bohr atomic units.

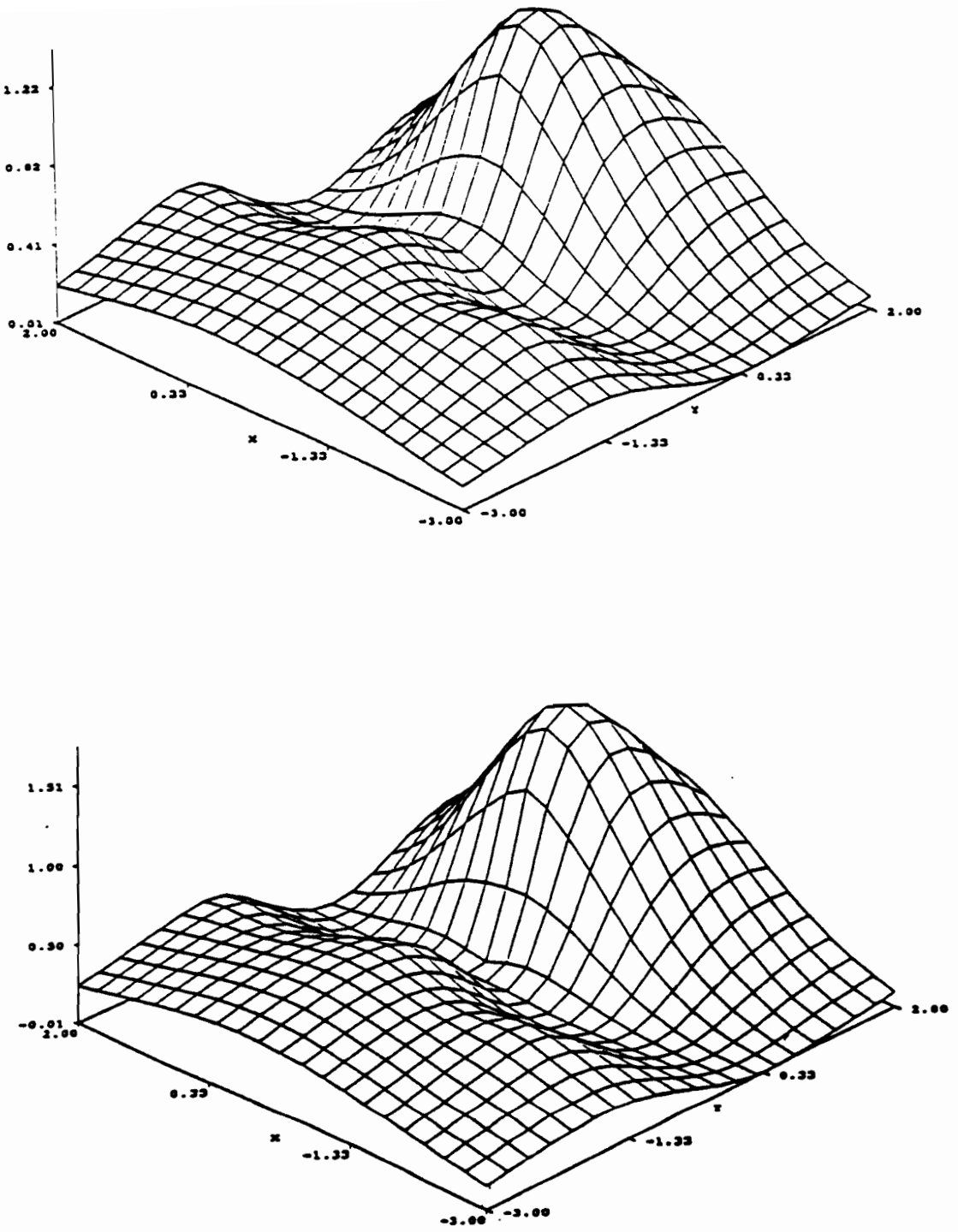

Figure 2. Difference in exchange potential, LDA – GX, in the plane of the the H_2O molecule, for the $1a_1$ orbital. Molecular orientation in the plane is as Figure 1: the oxygen is at 0,0, with hydrogen atoms in the foreground; the vertical dimension is the value of potential difference. The GWB Fermi hole is used in the top graph, and FEL Fermi hole below; bohr atomic units.

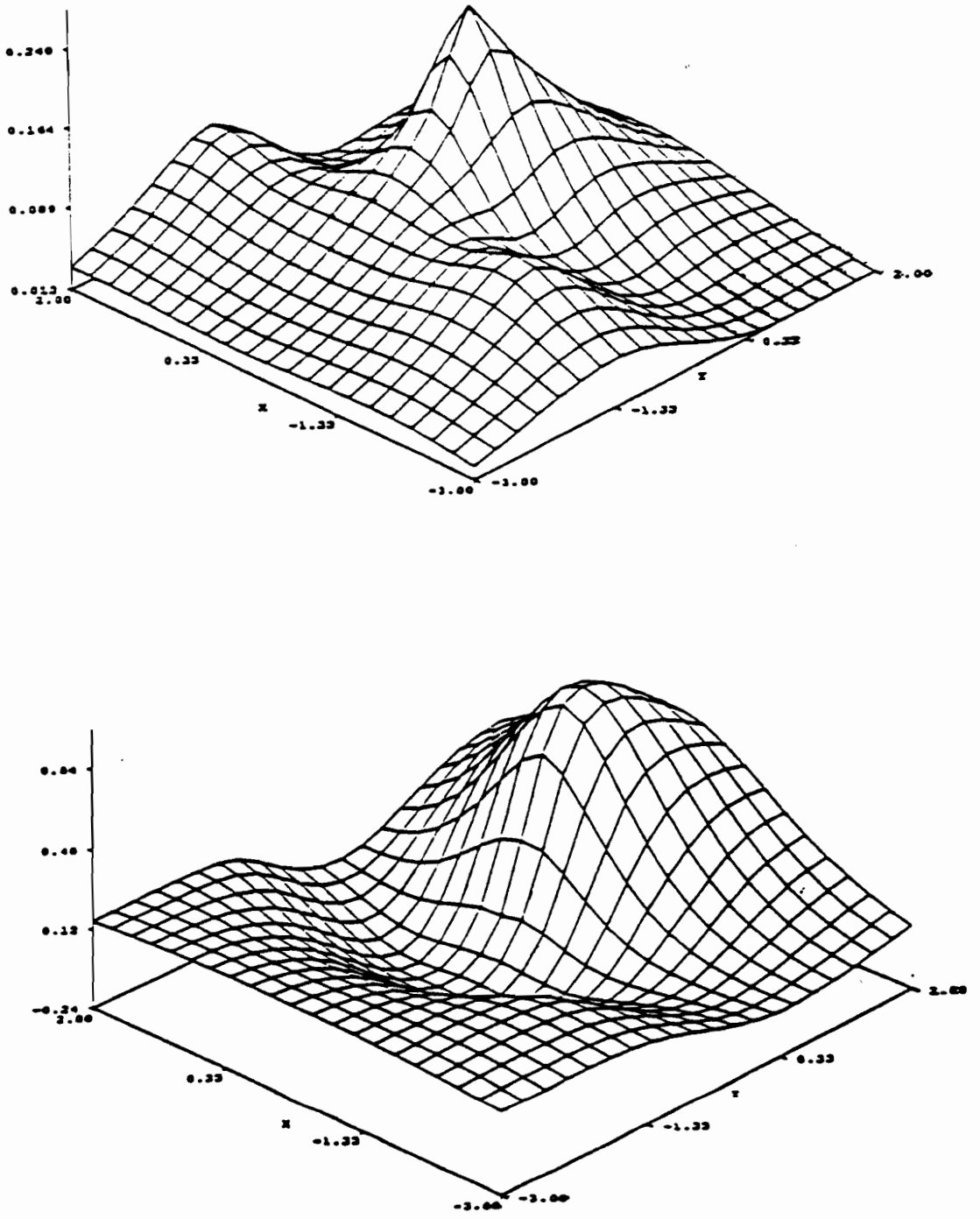

Figure 3. Difference in exchange potential, LDA – GX, in the plane of the the H_2O molecule, for the $1b_1$ orbital. Molecular orientation in the plane is as Figure 1: the oxygen is at 0,0, with hydrogen atoms in the foreground; the vertical dimension is the value of potential difference. The GWB Fermi hole is used in the top graph, and FEL Fermi hole below; bohr atomic units.

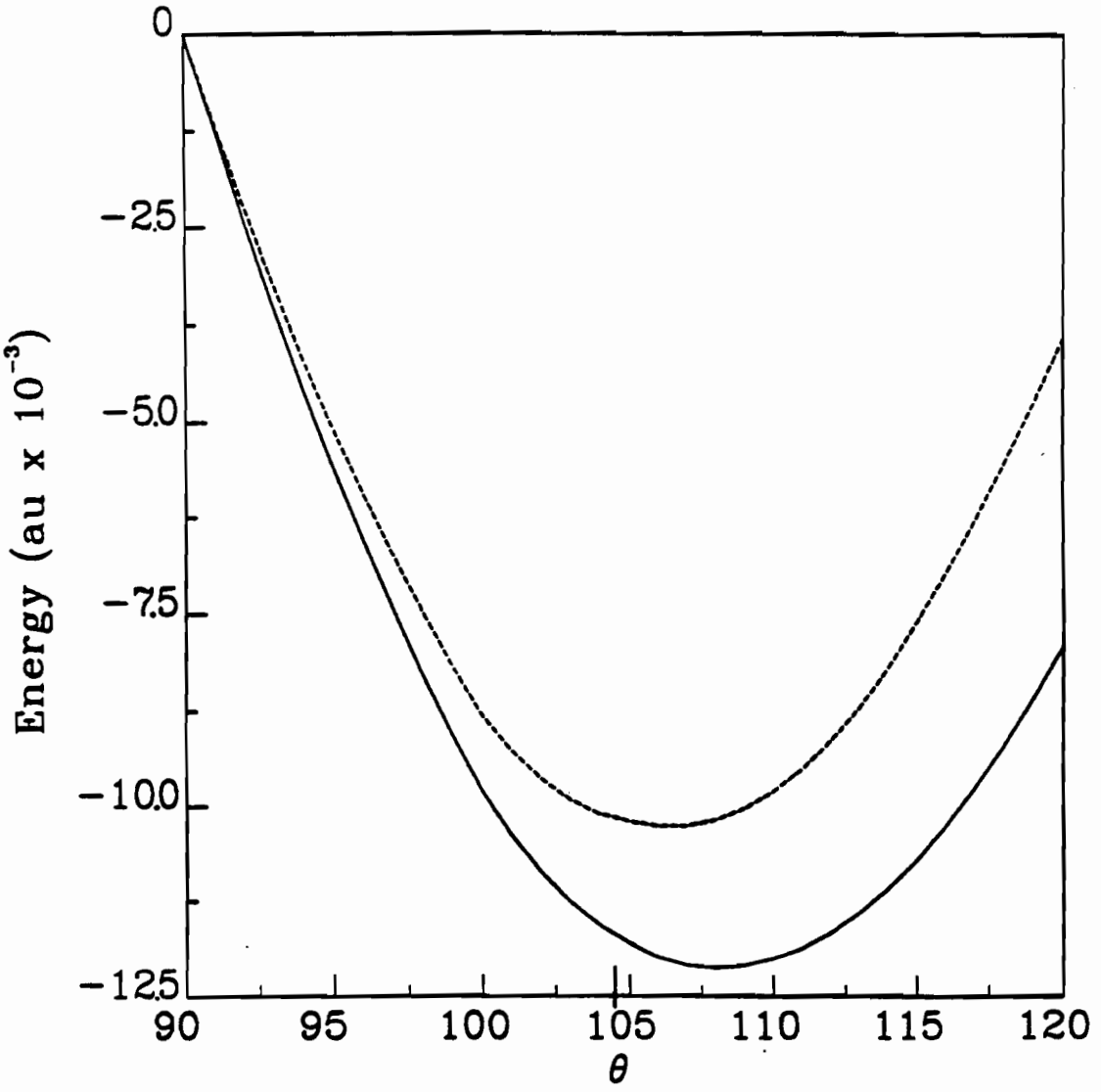

Figure 4. Energy versus bond angle for H_2O, O–H bond length fixed at experimental value. The solid line is the LDA result, dashed line is GX-FEL. The experimental bond angle, 104.5°, is marked with an additional tic on the θ axis.

References.

Baerends, E. J. and P. Ros, 1975, Chem. Phys. **8**, 412

Clementi, E., 1990, *MOTECC-90* (ESCOM, Leiden)

Connolly, J. W. D. and J. R. Sabin, 1972, J. Chem. Phys. **56**, 5529

Dunlap, B. I., J. W. D. Connolly and J. R. Sabin, 1979a, J. Chem. Phys. **71**, 3396

Dunlap, B. I., J. W. D. Connolly and J. R. Sabin, 1979b, J. Chem. Phys. **71**, 4993

Dunlap, B. I. and M. Cook, 1986, Int. J. Quant. Chem. **29**, 767

Guo, Y. and M. A. Whitehead, 1991 in press

Gopinathan, M. S., M. A. Whitehead and R. Bogdanovic, 1976, Phys. Rev. A **14**, 1

Harrison, J., R. Heaton and C. Lin, 1983, J. Phys. B. **16**, 2079

Harrison, J., 1987, J. Chem. Phys. **86**, 2849

Heaton, R., M. Pederson and C. Lin, 1987, J. Chem. Phys. **86**, 258

Jones, R. S., J. W. Mintmire and B. I. Dunlap, 1988, Int. J. Quant. Chem. Symp. **22**, 77

Kohn, W. and L. J. Sham, 1965, Phys. Rev. **140**, A1133

Krijn, M. P. C. M. and D. Feil, 1988, J. Chem. Phys. **89**, 5787

Manoli, S. D. and M. A. Whitehead, 1988a, Phys. Rev. A **38**, 639

Manoli, S. D. and M. A. Whitehead, 1988b, Phys. Rev. A **38**, 3187

Manoli, S. D. and M. A. Whitehead, 1988c, Collect. Czech. Chem. Commun. **53**, 2279

Mitzdorf, U., 1975, Theoret. Chim. Acta **37**, 129

Pederson, M. R., R. A. Heaton and C. C. Lin, 1983, J. Chem. Phys. **80**, 1972

Pederson, M. R., R. A. Heaton and C. C. Lin, 1984, J. Chem. Phys. **82**, 2688

Perdew, J. P. and A. Zunger, 1981, Phys. Rev. B **23**, 5048

Sambe, H. and R. H. Felton, 1974, J. Chem. Phys. **62**, 1122

Schiff, L., 1968, *Quantum Mechanics*, (McGraw-Hill, New York)

Szabo, A. and Neil S. Ostlund, 1989, *Modern Quantum Chemistry*, (McGraw-Hill, New York)

Van Vleck, J. H. and P. C. Cross, 1933, J. Chem. Phys. **1**, 357

Versluis, L., 1989, Ph.D. thesis (University of Calgary)

Vosko, S. H., L. Wilk and M. Nusair, 1980, Can. J. Phys. **58**, 1200

Yamaguchi, Y. and H. F. Schaefer III, 1980, J. Chem. Phys. **73**, 2310

Zhao, Y. and J. S. Francisco, 1990, Chem. Phys. Lett. **167**, 285

I.5 *Appendix: the Adiabatic Convergence Technique*

I.5.1 Introduction

To calculate ionization potentials (IP) within the local density functional (LDF) framework, it is customary to remove half an electron from the level of interest, then repeat the SCF procedure until convergence is achieved. In cases where the system is difficult to converge, as in section I.3.6 of this thesis, it was found to be advantageous to approach the half-electron state by small increments of charge from the converged, fully-occupied state. This "adiabatic" approach in convergence space can result in fewer overall iterations to achieve solution; in some negative ion cases, it proved to be the only way to reach self-consistency.

LDF calculations of negative ions of the Noble gases and the actinide series had never been succesful, since the calculation would not converge; the stability of these ions, and their electron affinities, could not be predicted. The adiabatic convergence technique was able to induce convergence on the complete Noble gas series, and actinides, for the first time, predicting some of them to be stable; the details of the technique, and the results, are in the following paper.

Recently a similar approach to SCF convergence of negatively-charged systems has been reported:* converge first with artificially increased nuclear charges, which contract and stabilize the excess electron charge, then slowly return the charges to their proper values.

* Harrell Sellers, NCSA, private communication

Electron affinities for rare gases and some actinides from local-spin-density-functional theory

Yufei Guo,* M. C. Wrinn, and M. A. Whitehead
Theoretical Chemistry Group, Department of Chemistry, McGill University, 801 Sherbrooke Street West, Montreal, Quebec, Canada H3A 2K6
(Received 21 June 1989)

The negative ions of the rare gases (He, Ne, Ar, Kr, Xe, and Rn) and some actinides (Pu, Am, Bk, Cf, and Es) have been calculated self-consistently by the generalized exchange local-spin-density-functional theory with self-interaction correction and correlation. The electron affinities were obtained as the differences between the statistical total energies of the negative ions and neutral atoms; the electron affinities were positive around several millirydbergs. Consequently, the negative ions are predicted stable for the rare gases and actinides.

I. INTRODUCTION

Theoretical calculation and experimental measurement of the electron affinities for atoms have attracted attention,[1-3] because the electron affinity not only leads to an understanding of the microscopic electron structure, but also leads to an understanding of the stability of macroscopic matter.[4] The negative ions of the alkaline-earth and rare-gas elements have long been thought unstable. But, recently Fischer *et al.*[5] reported a positive electron affinity for the alkaline-earth element Ca from a multiconfiguration Hartree-Fock (MCHF) calculation including a relativistic shift correction (RSC). This prediction was confirmed in an elegant experiment by Pegg *et al.*[6] Vosko *et al.*[7] found the negative ions of other alkaline-earth elements Sr^-, Ba^-, and Ra^- stable by a Hartree-Fock (HF) calculation with RSC and correlation energy functional when the negative ion electron configurations were ns^2np ($n=5$, 6, and 7) but not when the configurations were $(n-1)dns^2$. The prediction of stable negative ions for the alkaline-earth elements was supported by Guo and Whitehead[8] using a self-interaction corrected generalized exchange local-spin-density-functional (LSD-GX-SIC) calculation[9] and a corrected statistical exchange LSD-GX[10] calculation with relativistic and correlation corrections.[11,12] The agreement between the predicted electron affinities in HF and LSD-GX theories was excellent. Recently, Sen *et al.*[13] presented the electron affinities of actinides in several self-interaction corrected quasirelativistic approximate density-functional theories.[14,15] Some of the actinide results were missing because there was no convergence for some negative ions.

The probability that stable negative ions exist for the rare gases has been investigated theoretically and experimentally. Kuyatt *et al.*,[16] calculated electron affinities within ±0.03 eV for the rare gases from resonances observed in the elastic scattering of electrons. Zollweg[17] estimated negative electron affinities for the rare gases by horizontal analysis. In contrast the excited state of the rare-gas negative ions are predicted to be stable experimentally and theoretically with respect to the excited state of the corresponding neutral atoms.[17-21] The electron affinity is 0.51 eV from He ($1s2s\,^3S$) to He^- ($1s2s^2\,^2S$).

The present work considers calculation of the electron affinities for the rare gases and some actinide elements which were not previously considered.[8,13] The LSD-GX-SIC and quasirelativistic LSD-GX-SIC theories with Gopinathan-Whitehead-Bogdanovic[22] (GWB) Fermi-hole exchange parameters and Vosko-Wilk-Nusair[11] (VWN) correlation energy functional are used.[8,9,15]

II. ADIABATIC CONVERGENCE TECHNIQUE

Starting with the converged potential of the neutral atom from a Herman-Skillman[23] calculation and the electron configuration for the corresponding negative ion, neither gave converged values for any of the rare gases, nor for the actinides. The converged potential deviates too much from the real negative ion potential to be able to bind to an extra electron. However, starting with the converged potential and the electron configuration of the neutral atom, 10% of an electron was added in each following iteration until a total of one electron was included in the extra orbital; for the rare gases, convergence was then achieved from this negative-ion state. In the SCF processes of actinide negative ions, adding 10% electron in the extra orbital in the following each iteration turned out to be too big for the SCF process to stabilize. In order to increase the occupation number of the extra orbital slowly and stop the increase smoothly, the function 0.051×1.05^{-i} in which i is the iteration number was used to add the new fractional electron in the first 81 iterations. This slow, adiabatic change from the neutral atom allows the system to remain in its ground state. The mixture factor was chosen to be 0.25 for the negative ions of the rare gases, so that 75% of electron density from the $(i-1)$th iteration and 25% of electron density from the ith iteration were combined together and used to calculate the new potential for the $(i+1)$th iteration. The mixture factor for the actinide elements was reduced to 0.05 for the negative ions. The SCF was then performed until the differences of the wave functions be-

TABLE I. The negative of one-electron eigenvalues (in rydbergs) of the extra electrons for the negative ions of rare gases.

Z	nl	LSD-GX-SIC	QR-LSD-GX-SIC
2 He	2s	0.007 38	0.007 38
10 Ne	3s	0.008 05	0.008 06
18 Ar	4s	0.008 62	0.008 65
36 Kr	5s	0.009 04	0.009 19
54 Xe	6s	0.009 16	0.009 57
86 Rn	7s	0.009 32	0.010 90

TABLE III. The negative of one-electron eigenvalues (in rydbergs) of the extra electrons for the negative ions of some actinides.

Z	nl	LSD-GX-SIC	QR-LSD-GX-SIC
94 Pu	6d	0.0710	0.002 88
95 Am	6d	0.0682	0.002 91
97 Bk	6d	0.0473	0.002 97
98 Cf	6d	0.0369	0.002 99
99 Es	6d	0.0267	0.002 99

tween the ith and the $(i+1)$th iterations were less than 10^{-8}.

III. RESULTS AND DISCUSSION

The existence of the stable negative ions of atoms in nature is mainly caused by the quantum effect; because of the negative contribution of the exchange-correlation effect of the electrons to the energy functional, the neutral system (neutral atom) can bind an extra electron and form a stable system. The contribution of the nuclear attraction to forming the stable system is very small because each electron partially screens the nucleus from all other electrons. Furthermore, the exchange-correlation potential is approximately proportional to the electron number, so that the exchange-correlation effect increases with the number of electrons. The Coulomb repulsion between electrons, of course, increases with the total number of electrons. The exchange-correlation effect competes with the Coulomb repulsion; if the exchange correlation is bigger than the Coulomb repulsion, the negative ion is stable.

Table I lists the negative of the one-electron eigenvalues of the extra orbitals for the negative ions of rare gases in the LSD-GX-SIC theory, both nonrelativistic and quasirelativistic (QR). The GWB exchange parameters and the VWN energy correlation functional were employed in both cases. Table II gives the corresponding electron affinities. These tables show (i) that all the negative ions of the rare gases are stable, the electron affinities being several millirydbergs. The stability of these negative ions is caused by the correlation between the extra electron and all the other electrons. The Coulomb repulsion is much bigger than the exchange-only effect. Consequently the exchange-only term is not responsible for binding the extra electron for these elements; (ii) the relativistic effect of the electrons increases the binding energy and the electron affinity. This is the reverse of the relativistic contribution to the negative ions of the alkaline-earth elements[8] in which the relativistic effect decreases the binding energies; (iii) the binding energies and electron affinities increase with atomic number, because the increase in the exchange-correlation effect is greater than the increase in the Coulomb repulsion as the number of electrons increases.

Tables III and IV summarize the results of some actinide elements for which no converged results had previously been obtained.[8,13] Therefore the present results are compared with the estimated values obtained by energy extrapolation analysis.[24] Table III shows the one-electron eigenvalues of negative ions for some actinide elements. The numbers decrease in absolute value with the occupation number of the $5f$ orbitals in the LSD-GX-SIC theory, excluding the relativistic effect. When the relativistic effect is included the extra-electron eigenvalues are almost constant for these negative ions. The electron affinities for these actinide atoms are summarized in Table IV and compared with the estimated values. The relativistic effect binds the extra electron for the neutral system and forms a stable negative ion, even if there is no contribution from the correlation correction. The present prediction of the stability for the negative ions of these actinide elements is opposite to that by the energy-extrapolation analysis[24] in which the estimated uncertainty is ± 0.022 Ry in the results. Previously,[8] the electron affinities have been calculated for the electron configuration $5f^N7s^2$ ($N=7$, 10, 11, and 12 for Pu^-, Bk^-, Cf^-, and Es^-, respectively) and yielded negative electron affinities. Consequently the extra electrons in these negative ions favor the $6d$ orbital and not the $5f$ orbital.

TABLE II. Electron affinities (in rydbergs) for the rare gases calculated by LSD-GX-SIC and QR-LSD-GX-SIC theories with VWN correction.

	Configuration		LSD-GX-SIC		QR-LSD-GX-SIC	
Z	Atom	Ion	No correlation	VWN	No correlation	VWN
2 He	$1s^2$	$1s^22s^1$	−0.0029	0.0054	−0.0029	0.0054
10 Ne	$2p^6$	$2p^63s^1$	−0.0035	0.0061	−0.0035	0.0061
18 Ar	$3p^6$	$3p^64s^1$	−0.0040	0.0071	−0.0040	0.0071
36 Kr	$4p^6$	$4p^65s^1$	−0.0043	0.0079	−0.0043	0.0081
54 Xe	$5p^6$	$5p^66s^1$	−0.0043	0.0082	−0.0043	0.0091
86 Rn	$6p^6$	$6p^67s^1$	−0.0045	0.0085	−0.0038	0.0126

TABLE IV. Electron affinities (in rydbergs) for some actinides calculated by LSD-GX-SIC and QR-LSD-GX-SIC theories with VWN correction.

Z	Configuration Atom	Ion	LSD-GX-SIC No correlation	LSD-GX-SIC VWN	QR-LSD-GX-SIC No correlation	QR-LSD-GX-SIC VWN	Extrapolated[a]
94 Pu	$5f^6 7s^2$	$5f^6 6d^1 7s^2$	0.0068	0.0596	0.0180	0.0272	−0.022
95 Am	$5f^7 7s^2$	$5f^7 6d^1 7s^2$	0.0036	0.0564	0.0195	0.0178	−0.022
97 Bk	$5f^9 7s^2$	$5f^9 6d^1 7s^2$	−0.0165	0.0386	0.0094	0.0154	−0.022
98 Cf	$5f^{10} 7s^2$	$5f^{10} 6d^1 7s^2$	−0.0253	0.0303	0.0088	0.0140	−0.022
99 Es	$5f^{11} 7s^2$	$5f^{11} 6d^1 7s^2$	−0.0340	0.0217	0.0061	0.0108	−0.022

[a]Estimated values, Ref. 24.

The reliability of the present relativistic correction is shown by Table V which lists the relativistic energy contributions to the *ns*, *np*, and $(n-1)d$ electron removal energies, ΔE_{rel}(QR), in the QR-LSD-GX-SIC theory and compares these with the ΔE_{rel} obtained by the $(2J+1)$ weighted Dirac-Fock (DF) results, ΔE_{rel}(DF), and the ΔE_{rel} from the relativistic perturbed HF theory, ΔE_{rel}(pert), for the alkaline metals[25,26] and the elements in group IIIB.[7] Table V shows that the QR-LSD-GX-SIC theory slightly overestimates the relativistic contribution to the *ns* electron removal energies, except for Fr $(6p^6 7s^1)$ and slightly underestimated the relativistic contribution to the *np* and $(n-1)d$ electrons except Sc $(4s^2 4p^1)$. The agreement between the relativistic contributions in QR-LSD-GX-SIC and DF is comparable with that in the HF theory including RSC and the DF theory.

The relativistic contribution to the removal energy for the 7*s* orbital of Fr, 0.0357 Ry, is overestimated in this theory, compared to the Dirac-Fock value of 0.0180 Ry. To check whether this contribution came strictly from the quasirelativistic effect, the Fr calculations [i.e., Fr $(6p^6 7s^1)$ and Fr^+ $(6p^6)$] were repeated without any VWN correlation energy functional; the 7*s* removal energy in that case was 0.0358 Ry. Thus the deviation of the removal energy for the 7*s* orbital in the QR-LSD-GX-SIC and Dirac-Fock theories is not caused by the correlation energy functional. The overestimation may be caused by the underlying 4*f* orbital, which strongly affects the 7*s* removal energy in the QR-LSD-GX-SIC theory for Fr; study of the interaction between the *f* and *s* orbitals is needed.

In contrast with Fr, the electron affinity of Rn, for which the negative ion is of the same electron configuration, is probably overestimated by the QR-LSD-GX-SIC theory, but its value should be bigger than 0.0085 Ry because of the positive contribution of relativistic effect to the removal energy of ns^1 orbital.

TABLE V. Comparison of the QR-LSD-GX-SIC relativistic energy contributions to the *ns*, *np*, and $(n-1)d$ electron removal energies with the DF and perturbation calculation in DFT (in rydbergs).

Elements	ΔE_{rel} (QR)[a]	ΔE_{rel} (DF)		E_{rel} (pert)[a]
ns electron				
K $(3p^6 4s^1)$	0.0013	0.0010[b]	0.0011[c]	
Rb $(4p^6 5s^1)$	0.0053	0.0040	0.0041	
Cs $(5p^6 6s^1)$	0.0107	0.0094	0.0078	
Fr $(6p^6 7s^1)$	0.0357		0.018	
np electron				
Sc $(4s^2 4p^1)$	−0.0011	−0.0010[d]	−0.0010[d]	−0.0012
Y $(5s^2 5p^1)$	−0.0030	−0.0034	−0.0034	−0.0032
La $(6s^2 6p^1)$	−0.0058	−0.0058	−0.0058	−0.0054
Ac $(7s^2 7p^1)$	−0.0121	−0.0152	−0.0152	−0.0116
$(n-1)d$ electron				
Sc $(3d^1 4s^2)$	−0.0134	−0.0140	−0.0140	−0.0136
Y $(4d^1 5s^2)$	−0.0295	−0.0316	−0.0316	−0.0310
La $(5d^1 6s^2)$	−0.0547	−0.0590	−0.0590	−0.0572
Ac $(6d^1 7s^2)$	−0.1166	−0.1324	−0.1324	−0.1222

[a]This work.
[b]Reference 25.
[c]Reference 26.
[d]Reference 7.
[e]Reference 7.

The present results for the rare gases and some actinides show that their negative ions are still stable, even when the relativistic correction to the electron removal energy is overestimated for the rare gases and underestimated for the actinides as in the QR-LSD-GX-SIC theory, except for the negative ions of Bk, Cf, and Es with electron configurations $5f^N7s^2$. Further investigation of the stability for the negative ions of the rare gases and actinides is needed experimentally and using perhaps the MCHF method[5] or the multiconfiguration Dirac-Fock (MCDF) method, and the convergence technique which was so successful in the present work.

ACKNOWLEDGMENTS

This research was supported by the Natural Science and Engineering Research Council of Canada.

---

*Permanent address: Department of Applied Physics, National University of Defense Technology, Changsha, Hunan, People's Republic of China.

[1]H. Hotop and W. C. Lineberger, J. Phys. Chem. Ref. Data 4, 539 (1975); 14, 731 (1985).
[2]J. G. Harrison, J. Chem. Phys. 86, 2849 (1987).
[3]C. F. Fischer, Phys. Rev. A 39, 963 (1989).
[4]E. H. Lieb, Phys. Rev. A 29, 3018 (1984).
[5]C. F. Fischer, J. B. Lagowski, and S. H. Vosko, Phys. Rev. Lett. 59, 2263 (1987).
[6]D. Pegg, J. S. Thompson, R. N. Compton, and G. D. Alton, Phys. Rev. Lett. 59, 2267 (1987).
[7]S. H. Vosko, J. B. Lagowski, and I. L. Mayer, Phys. Rev. A 39, 446 (1989).
[8]Y. Guo and M. A. Whitehead, Phys. Rev. A 40, 28 (1989).
[9]S. Manoli and M. A. Whitehead, Phys. Rev. A 34, 4269 (1986); 38, 630 (1988).
[10]Y. Guo and M. A. Whitehead (unpublished).
[11]S. H. Vosko, L. Wilk, and M. Nusair, Can. J. Phys. 58, 1200 (1980).
[12]H. Stoll, C. M. E. Pavlidou, and H. Preuss, Theor. Chim. Acta 49, 143 (1978).
[13]K. D. Sen and P. Politzer (private communication).
[14]L. A. Cole and J. P. Perdew, Phys. Rev. A 25, 1265 (1982).
[15]Y. Guo and M. A. Whitehead, Phys. Rev. A 38, 3166 (1988).
[16]C. E. Kuyatt, J. A. Simpson, and S. R. Mielczarek, Phys. Rev. 138, A385 (1965).
[17]R. J. Zollweg, J. Chem. Phys. 50, 4251 (1969).
[18]A. V. Bunge and C. F. Bunge, Phys. Rev. A 19, 452 (1979).
[19]K. T. Chung, Phys. Rev. A 22, 1341 (1980).
[20]C. A. Nicolaides, Y. Komninos, and D. R. Beck, Phys. Rev. A 24, 1103 (1981).
[21]C. F. Bunge, M. Galán, R. Jáuregui, and A. V. Bunge, Nucl. Instrum. Methods 202, 299 (1982).
[22]M. S. Gopinathan, M. A. Whitehead, and R. Bogdanovic, Phys. Rev. A 14, 1 (1976).
[23]F. Herman and S. Skillman, *Atomic Structure Calculations* (Prentice-Hall, Englewood Cliffs, NJ 1963).
[24]S. G. Bratsch and J. J. Lagowski, Chem. Phys. Lett. 107, 136 (1984).
[25]A. Savin, P. Schwerdtfeger, H. Preuss, H. Silberback, and H. Stoll, Chem. Phys. Lett. 98, 226 (1983).
[26]S. Fraga, J. Karwowski, and K. M. S. Saxena, *Handbook of Atomic Data* (Elsevier, Amsterdam, 1976).

II. *PCILO: Perturbative Configuration Interaction over Localized Orbitals*

II.1.1 Introduction

The Perturbative Configuration Interaction over Localized Orbitals (PCILO) method calculates a zeroth-order approximation to the electronic ground state by solving Hall-Roothaan equations for molecular orbitals strictly localized to a bond. The "bond" in this instance corresponds to the traditional chemical representation of bonds and electron lone pairs. Delocalization and correlation energy are added to this description through terms in the perturbation expansion.

The original form of PCILO (Diner *et al.*, 1969a, 1969b; Jordan *et al.*, 1969; Malrieu *et al.*, 1969) used Epstein-Nesbet partitioning of the Hamiltonian, and solved the Hall-Roothaan equations with the semiempirical CNDO/2 Hamiltonian (Pople and Beveridge, 1970), and was limited at first to 2nd order in the perturbation. It was later extensively modified by Cullen and Zerner (1982). This version of PCILO, and its results, has been the subject of several reviews (Leroy and Peeters, 1975; Malrieu, 1977; Pulmann, 1977).

For this work, the more recent implementation of Boca and Pelikan was used (Boca *et al.*, 1975; Boca and Pelikan, 1978, 1980; Boca, 1980). This version of the theory uses the Moller-Plesset Hamiltonian partitioning, where the zeroth order Hamiltonian is the Hartree-Fock Hamiltonian (Szabo and Ostlund, 1989). Boca and Pelikan added the INDO Hamiltonian (Pople and Beveridge, 1970), and extended the perturbation series to 3rd order.

Recognized by both groups as a potential influence but left unresolved was the influence on the choice of hybridization in the atomic orbitals used to construct the localized molecular orbitals. In the following paper, the issue of hybridization

References

Boca, R., P. Pelikan and L. Valko, 1975, Chem. Phys. **11**, 229

Boca, R. and P. Pelikan, 1978, Theor. Chem. Acta **50**, 11

Boca, R. and P. Pelikan, 1980, Int. J. Quant. Chem. **18**, 1361

Boca, R., 1980, QCPE **14**, 390

Cullen, J. M. and M. C. Zerner, 1982, Int. J. Quant. Chem. **22**, 497

Diner, S., J. P. Malrieu, P. Claverie, 1969a, Theor. Chem. Acta **13**, 1

Diner, S., J. P. Malrieu, F. Jordan and M. Gilbert, 1969b, Theor. Chem. Acta **15**, 100

Jordan, F., M. Gilbert, J. P. Malrieu and U. Pincelli, 1969, Theor. Chem. Acta **15**, 211

Leroy, G. and D. Peeters, 1975, in *Localization and Delocalization in Quantum Chemistry, Vol. 1* (Reidel, Dordrecht), p. 207

Malrieu, J. P., P. Claverie and S. Diner, 1969, Theor. Chem. Acta **13**, 18

Malrieu, J. P., 1977, in *Semiempirical Methods of Electronic Structure Calculation, Modern Theoretical Chemistry, Vol. 7* (Plenum Press, New York), p. 69

Pople, J. A. and D. L. Beveridge, 1970, *Approximate Molecular Orbital Theory* (McGraw-Hill, New York)

Pulmann, B., 1977, in *Advances in Quantum Chemistry, Vol. 19*, (Academic Press, New York), p.251

Szabo, A. and N. S. Ostlund, 1989, *Modern Quantum Chemistry* (McGraw-Hill, New York)

Journal of Molecular Structure (Theochem), 137 (1986) 197—205
Elsevier Science Publishers B.V., Amsterdam — Printed in The Netherlands

PCILO: PROBLEMS IN PREDICTING VALID STRUCTURE

M. C. WRINN and M. A. WHITEHEAD

Chemistry Department, McGill University, 801 Sherbrooke St. West, Montreal, Quebec H3A 2K6 (Canada)

(Received 25 February 1985)

ABSTRACT

The localized orbitals from CNDO/2 and CNDO/BW calculations were used to generate hybridized atomic orbitals (HAO) for PCILO. The final third-order predicted bond lengths in PCILO showed poorer agreement with experiment than did the initial zero order calculation. No correlation was found between the quality of the HAO and the equilibrium-geometry predictions of PCILO. There is, therefore, doubt as to the validity of structures predicted by PCILO up to third order.

INTRODUCTION

The PCILO method [1—8] for calculating molecular total energies is used by organic and biochemists to decide among possible conformations of a molecule. The method is computationally economic, and gives better results than either force field or extended Hückel calculations [9].

PCILO uses a basis of molecular orbitals $|i>$, localized to a bond:

$$|i> = b_{i\mu}|\mu> + b_{i\nu}|\nu>$$

$$|i^*> = b_{i\nu}|\mu> - b_{i\mu}|\nu>$$

where $|i^*>$ is the antibonding localized molecular orbital (LMO), μ and ν are hybridized atomic orbitals (HAO),

$$|\mu> = \sum_{\alpha}^{A} a^{A}_{\mu,\alpha}\chi^{A}_{\alpha}$$

from the atomic basis χ_α on atom A. The hybridization coefficients $a^{A}_{\mu,\alpha}$ have to be determined before starting the calculation; they are input to the PCILO program.

The zero- and higher-order energies, at least to 3rd-order, depend on the choice of the coefficients $a^{A}_{\mu,\alpha}$ [10]. For the version of the PCILO program used here [11], the $a^{A}_{\mu,\alpha}$ have been obtained previously by the EMOA [12] (extended maximum overlap approximation) procedure, and from *sp* hybridization. However, PCILO calculations done with these hybrids have given bond-length predictions further from experimental values than do the

0166-1280/86/$03.50

starting 0th-order approximations [7]. To investigate the effect on this behavior of the choice of hybridization, another approach was taken to generate the coefficients.

In this work, the $a^{A}_{\mu,a}$ were obtained from localized semi-empirical CNDO SCF calculations. The CNDO/BW [13] theory gives good predictions of experimental bond lengths, and its molecular orbitals have a well-established localizability [14, 15]. CNDO/2 calculations were also used, for comparison. If these coefficients improved the PCILO results for small molecules, they could be transferred to larger systems [16].

METHOD

A series of small organic molecules were calculated by the CNDO/BW (with Z_H = 1.0 or 1.2) and CNDO/2 methods, with geometries fixed at the experimental equilibrium values. The compounds were ethane, ethyl chloride, methylamine, methanol, hydrazine, formaldehyde and carbon monoxide. The wavefunctions were localized by the Ruedenberg method [17], which maximizes the sum, D, of orbital self-repulsion energies:

$$D = \sum_{n} (\phi_n^2 | \phi_n^2)$$

Gopinathan and Narasimhan's [18] program was used and iterated until the difference in D between successive calculations was less than 10^{-4} eV. The localized wavefunctions were truncated to remove the small remaining delocalization, and orthonormalized with a Löwdin procedure [19]. Ethane wavefunctions are given in Table 1 to illustrate the procedure.

TABLE 1

Hybridization coefficients of C—H and C—C bonds in ethane: (a) localized CNDO/BW1.2 wavefunctions; (b) the same wavefunctions after truncation and orthogonalization

Atom	C—H				C—C			
	s	p_x	p_y	p_z	s	p_x	p_y	p_z
(a) C	0.388834	−0.275736	0.477588	−0.212569	0.399436	0.000000	0.000000	0.581817
C	0.018689	0.020945	−0.036282	−0.012665	0.399436	0.000000	0.000000	−0.581817
H	0.008580				0.025426			
H	0.008580				0.025426			
H	0.038621				0.025426			
H	0.702571				0.025426			
H	0.031568				0.025426			
H	0.031568				0.025426			
(b) C	0.492538	−0.408249	0.707107	−0.301229	0.521745	0.000000	0.000000	0.853101
C	0.000000	0.000000	0.000000	0.000000	0.521745	0.000000	0.000000	−0.853101
H	0.000000				0.000000			
H	0.000000				0.000000			
H	1.000000				0.000000			
H	0.000000				0.000000			
H	0.000000				0.000000			
H	0.000000				0.000000			

RESULTS

The resulting coefficients from each method (CNDO/BW 1.0, 1.2 and CNDO/2), and for comparison the EMOA and *sp* hybridizations, are given in Table 2 for methylamine. These coefficients were used in PCILO, and the bond lengths were varied to give an energy minimum. Hydrogen atoms were fixed at their experimental bond distances and angles. The bond lengths for both E_0 and 3rd-order corrected ($E_0 + E_2 + E_3$) energy minima are shown in Table 3. The total energies for each scheme at zero and third order, along with the CNDO/2 SCF total energies, are shown in Table 4.

DISCUSSION

Comparing the bond lengths in Table 3 to the experimental values shows the 3rd-order result to be worse than 0th-order in almost every case (34 of 35; the exception, *sp* hybridization for N_2H_4, moves only 0.005 Å toward experiment), in keeping with previously reported results [7]. For the purely sigma-bonded molecules, 3rd-order results always give bonds shorter than 0th-order, which was close to experiment. For the two compounds with pi bonds, where the 0th-order bond length is larger than the experimental one, the 3rd-order makes the bond length larger.

The CNDO/2 approximations were used in the PCILO Hamiltonian, therefore it is possible that the perturbation results will converge toward the CNDO/2 SCF results. Table 3 includes the SCF equilibrium bond lengths. The five sigma-bonded molecules do indeed move toward the SCF value, regardless of HAO choice, but CH_2O and CO move away. Other workers have used the CNDO/BW Hamiltonian in PCILO, and report results that sometimes move toward, and sometimes away from the SCF result [23].

The three different sets of $a^A_{\mu,\alpha}$ generated from localized CNDO wavefunctions thus all yield the same behaviour of PCILO: the 3rd-order predictions are further from experimental values than the 0th-order. This suggests that this behaviour is independent of the choice of hybridization. However, small differences in the HAO (the similarities between the different coefficients in Table 2 for methylamine is typical of all cases) do lead to different bond lengths in a variable way. For example, Fig. 1a shows the minimum energies, E, and the corresponding bond lengths, r, for each order of perturbation and each set of HAO for ethane. The zero-order energies and distances are very similar, and by third order have become nearly identical; this molecule is insensitive to HAO choice. By contrast, hydrazine is quite sensitive; Fig. 1b shows considerable variation in the zero-order N—N distance, and these variations, though reduced, are not eliminated by third order.

Inspection of Fig. 1 shows that the second-order mono-electronic term, the delocalization energy, dominates the equilibrium bond length predictions, and that third-order terms have almost no influence. This was found to be true in all seven molecules, regardless of the sensitivity to HAO.

TABLE 2

Hybridization coefficients for carbon and nitrogen in methylamine for five different schemes

Method	s	p_x	p_y	p_z
Carbon				
CNDO/BW 1.2	0.438897	−0.011468	0.020305	0.898235
	0.524172	0.815379	0.001975	−0.245757
	0.507589	−0.409181	0.708815	−0.269267
	0.524372	−0.409385	−0.705099	−0.245507
CNDO/BW 1.0	0.424531	0.000775	0.019386	0.905206
	0.523821	0.815414	0.001411	−0.246394
	0.514629	−0.409233	0.708561	−0.256179
	0.529662	−0.409425	−0.705382	−0.232949
CNDO/2	0.486453	−0.007396	0.013098	0.873578
	0.507182	0.816616	−0.000214	−0.275508
	0.498791	−0.408050	0.706791	−0.291804
	0.507285	−0.408140	−0.707301	−0.275333
EMOA	0.426945	0.007909	−0.013989	0.904135
	0.519816	0.816081	0.000735	−0.252592
	0.526663	−0.408586	0.707704	−0.234174
	0.519744	−0.408665	−0.706370	−0.252785
sp	0.500000	0.000000	0.000000	0.866025
	0.500000	0.816497	0.000000	−0.288675
	0.500000	−0.408248	0.707107	−0.288675
	0.500000	−0.408248	−0.707107	−0.288675
Nitrogen				
CNDO/BW 1.2	0.465239	−0.051383	0.090897	−0.879005
	0.424871	0.374768	0.773916	0.282998
	0.424895	−0.856330	0.077928	0.283004
	0.650002	0.351580	−0.621867	0.259174
CNDO/BW 1.0	0.457939	0.005110	0.085489	0.884852
	0.435703	0.383695	0.756609	0.300805
	0.465511	−0.848648	0.065934	0.242386
	0.619480	0.364075	−0.644893	0.260398
CNDO/2	0.509966	−0.025409	0.044950	−0.858644
	0.457462	0.394641	0.738762	0.298692
	0.457467	−0.836466	0.042792	0.298692
	0.566910	0.379390	−0.671103	0.290340
EMOA	0.521984	0.065052	−0.115077	−0.842650
	0.572281	0.480318	0.587219	0.311389
	0.572281	−0.750807	−0.108720	0.311388
	0.269299	0.448722	−0.793795	0.309864
sp	0.500000	0.000000	0.000000	−0.866025
	0.500000	0.408248	0.707107	0.288675
	0.500000	−0.816497	0.000000	0.288675
	0.500000	0.408248	−0.707107	0.288675

TABLE 3

Equilibrium bond distances in A for 0th-order (r_0) and 3rd-order (r_3) PCILO calculations with various HAO. Hydrogen atoms are fixed at experimental positions

Molecule	Expt.[a]	CNDO/2 SCF[b]	EMOA		*sp*		CNDO/2		CNDO/BW1.0		CNDO/BW1.2	
			r_0	r_3	r_0	r_3	r_0	r_3	r_0	r_3	r_0	r_3
CH_3—CH_3	1.534	1.468	1.534	1.494	1.539	1.496	1.531	1.494	1.538	1.496	1.532	1.494
CH_3—CH_2Cl	1.594	1.462	1.530	1.490	1.539	1.494	1.532	1.492	1.537	1.493	1.532	1.492
CH_3—NH_2	1.474	1.409	1.453	1.430[c]	1.459	1.434	1.457	1.433	1.474	1.434	1.470	1.438
CH_3—OH	1.427	1.374	1.393	1.385	1.401	1.392	1.411	1.396	1.422	1.406	1.420	1.400
NH_2—NH_2	1.449	1.336	1.359	1.354	1.346	1.349	1.366	1.357	1.389	1.365	1.386	1.364
H_2C=O	1.208	1.248	1.263	1.268[d]	1.260	1.274	1.266	1.277	1.273	1.280	1.272	1.280
C≡O	1.128	1.191	1.183	1.216[e]	1.165	1.195	1.183	1.203	1.193	1.208	—	—

[a] Ref. 20. [b] The SCF results here differ slightly from those of Pople and Beveridge [21], where the hydrogen bond distances and angles were optimised. [c] The K parameter in the EMOA method for the C—N bond was not included in the PCILO program. The K value used, 104.3359, was determined by optimising it to the experimental binding energy of CH_3NH_2 [22]. [d] Ref. 11, test input. [e] Ref. 7.

TABLE 4

Molecular total energies, in −eV, for both experimental and minimum-energy bond distances, at zero- and third-order PCILO calculations for five different HAO. The SCF results are included for comparison

Molecule		CNDO/2 SCF	EMOA		*sp*		CNDO/2		CNDO/BW 1.0		CNDO/BW 1.2	
			E_0	E_3	E_0	E_3	E_0	E_3	E_0	E_3	E_0	E_3
CH_3—CH_3	Exp.	511.841	510.170	513.037	510.343	513.091	510.398	513.111	510.363	513.102	510.396	513.107
	Min.	512.039	510.170	513.112	510.344	513.158	510.398	513.183	510.364	513.170	510.396	513.182
CH_3—CH_2Cl	Exp.	930.625	923.822	928.064	925.403	928.772	925.930	928.949	925.903	929.002	925.984	929.034
	Min.	931.370	924.004	928.535	925.554	929.207	926.117	929.403	926.060	929.442	926.173	929.491
CH_3—NH_2	Exp.	614.064	611.640	614.582[a]	612.779	615.235	612.866	615.300	612.589	615.205	612.614	615.774
	Min.	614.273	611.665	614.689	612.798	615.329	612.884	615.394	612.589	615.271	612.623	615.280
CH_3OH	Exp.	776.918	773.375	776.623	775.683	777.900	775.894	778.034	775.761	777.983	775.799	778.005
	Min.	777.095	773.451	776.733	775.733	777.981	775.912	778.096	775.763	778.026	775.802	778.052
NH_2—NH_2	Exp.	715.216	713.751	716.196	713.293	716.053	713.743	716.192	713.113	715.956	713.262	716.009
	Min.	716.038	714.328	716.782	714.101	716.714	714.249	716.746	713.366	716.405	713.548	716.473
H_2C=O	Exp.	730.127	726.215	730.379	728.504	731.476	728.519	731.490	728.395	731.445	728.412	731.447
	Min.	730.306	726.540	730.799	728.855	731.960	728.942	732.012	728.928	732.019	728.930	732.017
C≡O	Exp.	681.396	678.426	*	679.567	682.797	681.364	673.586	681.150	683.522	—	—
	Min.	681.964	*	*[b]	677.768	683.417	681.884	684.392	681.827	684.405	—	—

[a]See footnote (c) of Table 3. [b]The E_0 energy reported here is the electronic energy given in ref. 7, less the calculated core repulsion energy. There is no defined way to choose K parameters for multiple bonds, and no K values for CO have been reported.

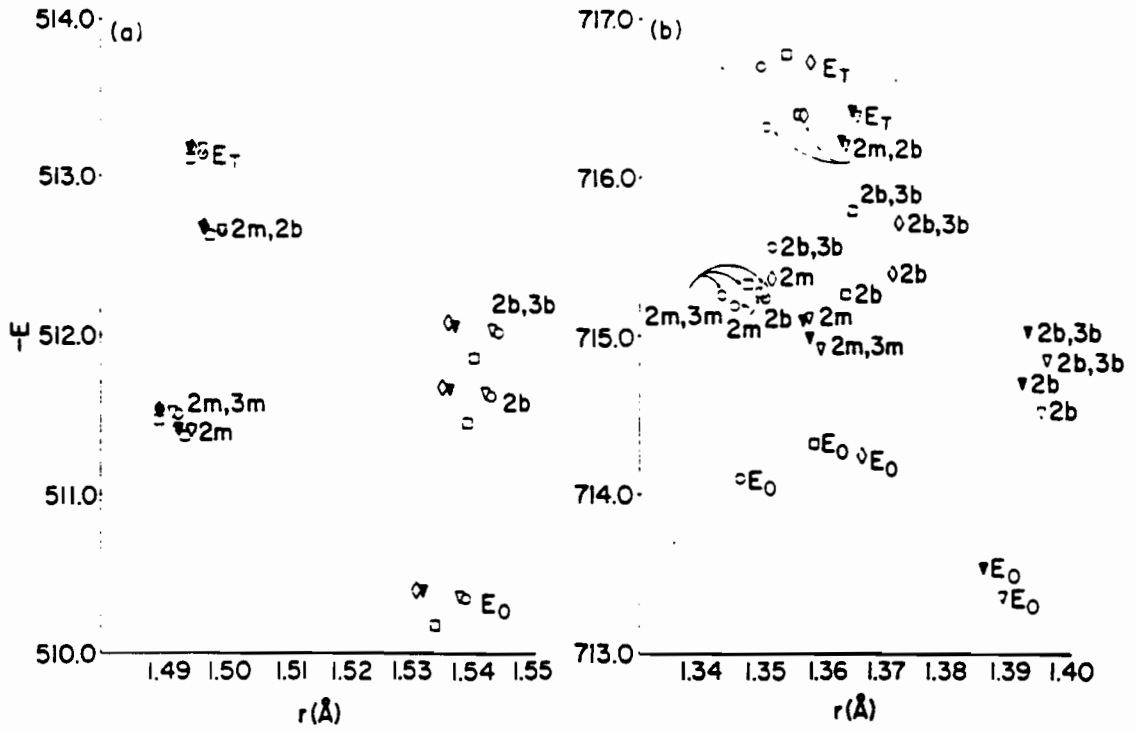

Fig. 1. The total energy, $-E$ (in eV), versus the bond distance, r (in Å), for various orders of PCILO total energies. (a) CH_3—CH_3; (b) NH_2—NH_2. The symbols indicate the energy minimum at the given order, i.e., 2m, 2b is the minimum of $E_0 + E_2^m + E_2^b$, where m and b indicate mono- and bi-electronic terms; E_T is the minimum of $E_0 + E_2 + E_3$. Five different HAO schemes are represented: (□) EMOA, (○) *sp*, (◇) CNDO/2, (▽) CNDO/BW 1.0 and (▼) CNDO/BW 1.2.

The CNDO/2-generated coefficients gave the lowest zero-order energy for six of the seven molecules tested; CNDO/BW ($Z_H = 1.2$) coefficients gave the lowest E_0 in the other case, CH_3CH_2Cl. However, these CNDO/2 HAO were not the best choice in terms of matching either experimental or SCF bond lengths; for CH_3OH, for example, the EMOA third-order bond distance was closest to SCF, while the CNDO/BW ($Z_H = 1.0$) third-order was closest to experiment.

To test the quality of the localization in the Ruedenberg scheme, a percentage of delocalization, d, is calculated:

$$d = (1 - \int \psi^2_{\mathrm{TLMO}}\, d\tau) \times 100$$

where ψ_{TLMO} is the truncated localized molecular orbital before normalization or Löwdin orthogonalization. In the present CNDO method [24]

$$d = (1 - \sum_i C^2_{i_{\mathrm{TLMO}}}) \times 100$$

The values of d for the CNDO/2, BW1.0 and BW1.2 orbitals are given in Table 5.

There is no correlation between the size of d and the bond length

TABLE 5

Percent delocalization, d, and bond distances for nonorthogonal coefficients

Molecule	Expt. (Å)	CNDO/2			CNDO/BW1.0			CNDO/BW1.2		
		d	r_0	r_3	d	r_0	r_3	d	r_0	r_3
CH_3–CH_3	1.534	3.18	1.534	1.454	2.70	1.524	1.549	3.93	1.524	1.534
CH_3–CH_2Cl	1.594	3.77	1.534	1.430	3.75	1.524	1.744	4.86	1.514	1.694
CH_3–NH_2	1.474	2.92	1.402	1.419	2.51	1.464	1.549	3.43	1.459	1.499
CH_3–OH	1.427	2.54	1.387	1.377	2.58	1.417	1.432	3.56	1.412	1.407
NH_2–NH_2	1.449	2.92	1.359	1.329	3.48	1.379	1.479	5.27	1.369	1.459
H_2C=O	1.208	1.74	1.263	1.258	2.89	1.253	1.198	3.55	1.268	1.228

predictions in Table 3. In some cases, an intermediate or a higher value of d corresponds to a better prediction; in others each hybridization converges to the same value.

The literature suggests using nonorthogonal wavefunctions to improve localized molecular orbital theory results [25—28]. These wavefunctions are not appropriate to perturbation theory, because the number of 2nd-, 3rd- and higher-order terms proliferates. However, if the ψ_{TLMO} are normalized, they are very close to orthogonal; they overlap more than 99% with the orthogonalized orbitals ($\langle\psi_{nonorth}|\psi_{orth}\rangle$). Consequently, inserting them into PCILO should lead to only small errors. The bond length predictions for these nonorthogonalized coefficients are included in Table 5. As with the orthogonalized coefficients, there is no pattern of better agreement with experiment.

CONCLUSION

In the discussion, the quality of results were judged by their relation to experimental values. This may seem inappropriate, given that the PCILO was constrained to a CNDO/2 Hamiltonian. However, the aim of this study was twofold: to test whether a set of HAO coefficients derived from experimental geometries could move the PCILO results closer to experimental values, and to test the stability of PCILO calculations with regard to different HAO input. For the former, experimental values are clearly pertinent. For the stability investigation, they serve as reference points.

Though the differences in bond lengths between the various HAO are small, they can lead to significant cumulative effects in large structures (e.g., antibiotics [29]); the final conformation will, therefore, depend on which HAO are chosen.

Unfortunately, there is no unique way to choose among the HAO, neither the quality of the wavefunction defined by the lowest E_0 in PCILO, nor the measure of the localization of the starting SCF wavefunction, can reliably predict the equilibrium-geometry behavior at third-order. This

sensitivity to hybridization is reported to diminish once 4th-order is included [10, 30], but the bond lengths will still diverge farther from experiment than the 0th-order calculation, consequently there is no guarantee that the final predicted structure will correlate with the experimental structure desired.

ACKNOWLEDGEMENTS

This research was supported by the NSERC (Canada). The McGill Computing Centre provided facilities (Amdahl 5850).

REFERENCES

1 S. Diner, J. P. Malrieu, P. Claverie and F. Jordan, Chem. Phys. Lett., 2 (1968) 301.
2 S. Diner, J. P. Malrieu and P. Claverie, Theor. Chim. Acta, 13 (1969) 1.
3 J. P. Malrieu, P. Claverie and S. Diner, Theor. Chim. Acta, 13 (1969) 18.
4 S. Diner, J. P. Malrieu, F. Jordan and M. Gilbert, Theor. Chim. Acta, 15 (1969) 100.
5 F. Jordan, M. Gilbert, J. P. Malrieu and U. Pincelli, Theor. Chim. Acta, 15 (1969) 211.
6 J. P. Malrieu, in Modern Theoretical Chemistry, Vol. 7, Semiempirical Methods of Electronic Structure Calculation, Plenum, New York, 1977, Chap. 3, p. 69—104.
7 R. Boca and P. Pelikan, Theor. Chim. Acta, 50 (1978) 11.
8 R. Boca and P. Pelikan, Int. J. Quantum Chem., 18 (1980) 1361.
9 B. Pulmann, Adv. Quantum Chem., 10 (1977) 251.
10 J. M. Cullen and M. C. Zerner, Int. J. Quantum Chem., 22 (1982) 497.
11 R. Boca, QCPE, 14 (1980) 390.
12 R. Boca, P. Pelikan and L. Valko, Chem. Phys., 11 (1975) 229.
13 R. J. Boyd and M. A. Whitehead, J. Chem. Soc., Dalton Trans., 1 (1972) 73.
14 T. J. Tseng and M. A. Whitehead, J. Comput. Chem., 3 (1982) 552.
15 T. J. Tseng and M. A. Whitehead, J. Chem. Soc., Faraday Trans. 2: 79 (1983) 37.
16 G. Leroy and D. Peeters, in Localization and Delocalization in Quantum Chemistry, Vol. 1, Reidel, Dordrecht, Holland, 1975, p. 207—221.
17 C. Edmiston and K. Ruedenberg, Rev. Mod. Phys., 35 (1963) 457.
18 M. S. Gopinathan and P. T. Narasimhan, Mol. Phys., 22 (1971) 473.
19 B. C. Carlson and J. M. Keller, Phys. Rev., 105 (1957) 102.
20 Tables of Interatomic Distances, The Chemical Society, London, 1965.
21 J. A. Pople and D. L. Beveridge, Approximate Molecular Orbital Theory, McGraw-Hill, New York, 1970.
22 S. W. Benson, Thermochemical Kinetics, Wiley, New York, 1976.
23 R. Lochmann, Th. Weller and H.-J. Kohler, Int. J. Quantum Chem., 25 (1984) 1055.
24 M. S. Gopinathan and M. A. Whitehead, Can. J. Chem., 53 (1975) 1343.
25 I. D. Petsalakis, G. Theordorkopoulos, C. A. Nicolaides, R. J. Buenker and S. D. Peyerimhoff, J. Chem. Phys., 81 (1984) 3161.
26 P. R. Surjan, Croat. Chem. Acta, 56 (1983) 289.
27 T. K. Bruuck and F. Weinhold, J. Am. Chem. Soc., 101 (1979) 1700.
28 V. Magnasco, G. F. Musso and R. McWeeny, J. Chem. Phys., 47 (1967) 4617.
29 See, for example, L. Cassidei et al., J. Mol. Struct. (Theochem), 86 (1981) 173.
30 M. C. Zerner, private communication, Mt. Ste. Hilaire Conference, Quebec, Canada, November, 1984.

Suggestions for Future Research

1. *MS-LDA*

Organize and implement a Green's function method to remove the need for muffin-tin potentials. As long as the muffin-tin potentials remain, the MS-LDA method has severely limited utility.

Recalculate the 2,1,3-benzoxadiazole$[Cr(CO)_5]_2$ compound and its experimentally known analogues (replace Cr with W, and replace O on the ring with S and Se) with a more suitable method, e.g LCAO-LDA with gradients , to determine equilibrium geometries. Determine why Cr–to–ring bonding is more stable through the N than through Se, but W is more stable coordinated through Se. Can stacked chains of these these compounds be constructed, e.g. $\left(2,1,3\text{-benzoxadiazole}[Cr(CO)_4]\right)_n$? What is the effect on the HOMO-LUMO gap as substituents are changed on either the ring or the metal?

2. *LCAO-LDA*

An orbital-dependent exchange may be an important way to improve the local density approximation. Test this across a wider range of compounds and basis sets. Implement the functional self-consistently, and test the effect on one-electron energies. Investigate a variety of schemes to deal with the non-orthogonal wavefunctions: average the Hamiltonian over all states, or over each irreducible representation if there is point group symmetry; use symmetric (Löwdin) orthogonalization on the eigenvectors before constructing density matrix. Test the dispersion of results between fully-localized and fully-delocalized bases: how wide for SIC alone, and is it narrowed when the GX is included? Does the newer version of GX, the "G-LSD", give improved molecular results? What are the relative merits of orbital versus

gradient corrections in the LDA? Can comparison of orbital Hamiltonians to the exact, Hartree-Fock exchange shed any light on how to systematically improve the LDA?

3. *PCILO*

Replace the semi-empirical CNDO and INDO Hamiltonians; the 2x2 Roothaan equations on each bond can be solved with a Hartree Fock or Local Density method, making irrelevant the hybridization issue studied in this thesis. Investigate the effect of a rigorous zeroth-order Hamiltonian on the CI perturbation series, especially if some correlation is built into the ground state through a Local Density Approximation. Implement energy gradients for geometry optimization; PCILO has the potential, then, to be the fastest quantum chemistry computational method. Modify the method to exploit massively parallel computers; the local, bond-oriented approach of this theory makes it especially suitable to parallel architectures. By mapping one bond to each processor node, such a program could do quantum chemical geometry predictions of molecules with a few thousand atoms.

Statement of Contributions to Original Knowledge

I. *Density Functional Theory*

I.1 Introduction and Background

The demonstration, by using the Hartree-Fock form of the exchange energy density, of a classical approximation present in the GX local density functional.

I.3 *Molecular Calulations: the Multiple-Scattering Method*

The first application of the MS-LDA method, and the first calculation of nuclear quadrupole coupling constants, for heterocycles with nitrogen and one other heteroatom from the series O, S, Se. The systematic comparison, in I.3.3 and I.3.5, of the Xα and VWN exchange-correlation functionals, and of the partial wave basis set size.

I.3.3 The demonstration that differential relaxation in the Slater transition state can profoundly alter the calculated ionization potentials; a common approximation used in LDA methods is therefore not always valid. The demonstration, through density-difference plots, of the effect the VWN correlation functional on charge distribution.

I.3.5 The relationship between terminal heteroatom electronegativities and molecular electronic structure, as shown in orbital populations, ionization potentials, dipole moments, and quadrupole coupling constants. The calculation of first excited states by $\Delta\epsilon$ and transition state methods. The proposed peak assignments for the photoelectron spectrum of the Se compound in this series.

I.3.6 The implementation and testing of a "converged fragment" method in attempt to improve SCF convergence in a difficult system. The use of the adiabatic convergence technique to calculate the Slater transition state ionization potentials. The

description of orbital interactions between the heterocyle and the $Cr(CO)_5$ fragments, and the analysis, using density-of-states, of interaction between the Cr and the empty ring π system. The demonstration, through molecular orbital diagrams, that the heterocycle adopts a benzenoid structure in this complex.

I.4 *Molecular Calculations: the LCAO Method*

I.4.3 The testing, with H_2O computations, of the difference between predicted geometries using the VWN correlation functional as a post-SCF correction term, and including it in the calculation self-consistently. The implementation of the GX orbital-density dependent local density functional into a LCAO molecular program as a post-SCF correction term, and the investigation of its effect, with and without correlation, on the predicted geometry and force constant of water.

I.5 *Appendix: the Adiabatic Convergence Technique*

I.5.2 The technique of SCF convergence to a system in a difficult charge state by starting from the same system in a more-easily-converged state, and changing the charge slowly from one to the other, converging at each stage. In the co-authored paper, the technique was used to converge several negative ions succesfully for the first time. (The remainder of the original work in this paper was done by the principle author, Dr. Yufei Guo)

II. *PCILO: Perturbative Configuration Interaction over Localized Orbitals*

II.1.3 The systematic investigation of the effect of atomic orbital hybridization on the predicted bond length of PCILO up to 3rd order in the perturbation. Two existing hybrid schemes were compared to two new ones (hybridization coefficients produced from localized, truncated, symmetrically- orthogonalized CNDO/2 and CNDO/BW molecular wavefunctions); the hybrid choice proved important.